To the Graduate Council:

I am submitting herewith a thesis written by Robert Bradley Cunningham entitled "Mechanical Design and Integration of a Tracking Fluoroscope System." I have examined the final electronic copy of this thesis for form and content and recommend that it be accepted in partial fulfillment of the requirements for the degree of Master of Science, with a major in Mechanical Engineering.

William R. Hamel
Major Professor

We have read this thesis
and recommend its acceptance:

Richard D. Komistek

G. V. Smith

Accepted for the Council:

Anne Mayhew
Vice Chancellor and
Dean of Graduate Studies

(Original signatures are on file with official student records.)

MECHANICAL DESIGN AND INTEGRATION OF A TRACKING FLUOROSCOPE SYSTEM

A THESIS
PRESENTED FOR THE
MASTER OF SCIENCE
DEGREE
THE UNIVERSITY OF TENNESSEE, KNOXVILLE

ROBERT BRADLEY CUNNINGHAM
AUGUST 2005

To Vanae

ACKNOWLEDGEMENTS

I am grateful to all who have made possible my continued education at The University of Tennessee. Thanks to Dr. Richard D. Komistek for believing in this project and providing the financial means necessary to achieve successful results. I would especially like to thank Dr. William R. Hamel for taking me on so quickly upon my arrival and trusting me with this research. His guidance as a professor, project manager, and mentor has been invaluable to me throughout my time as a graduate student. I would like to express appreciation to my graduate committee, Dr. William R. Hamel, Dr. Richard D. Komistek, and Dr. Gary V. Smith for taking the time to help me through the completion of my thesis. Special thanks to the Mechanical, Aerospace and Biomedical Engineering Department, especially shop personnel Danny Graham, Gary Hatmaker, and Dennis Higdon for their patience, enthusiasm, and support in the fabrication of the Tracking Fluoroscope System. Thanks to all with whom I have worked on this research, Fei Liu, who will continue with the project to complete his PhD., Dr. Sewoong Kim, who helped in the critical beginning stages of control system development, and especially Gabriel R. Preliasco, with whom I spent the majority of my time. Gabriel has become a trusted research partner and a good friend. His support and dedication in developing the control system of the TFS has been invaluable to the success of the project. Finally, thanks to all my family and friends for their continued support.

ABSTRACT

The Tracking Fluoroscope System (TFS) – patent pending serial number 60/606,480 – is a robotic platform designed to follow a patient's natural, uninhibited walking motion and obtain full-range-of-motion x-ray videos of a patient's ankle, knee, or hip. The video data can be used to analyze dynamics within the human body and develop mathematical models of the joints. The TFS can also be used to study artificial implants under various conditions in order to design more effective versions. Similar systems could be used to aid surgeons in artificial implant procedures. Athletic motions could be analyzed to design more effective sports equipment or aid in rehabilitation.

The objective of this thesis is to present the evolution of the mechanical design of the TFS, analyze different strategies for the fluoroscope system, discuss safety concerns, and present future design improvements. Anthropomorphic, geometric, speed, acceleration, inertial, electrical and budgetary constraints have all influenced the mechanical design of the TFS. These issues are presented in detail. The TFS weighs approximately 454 kg, can move at a maximum speed of 2.2 m/s, and operates in close proximity to humans. Therefore, many safety concerns are presented as well as suggestions for future design improvements and alternative applications.

TABLE OF CONTENTS

CHAPTER 1 INTRODUCTION 1

CHAPTER 2 DESIGN PROCESS 3

2.1 Functions and Requirements 3

2.1.1 System Structure 3

2.1.2 Functional Requirements 5

2.1.3 Physical Requirements 7

2.1.4 Safety Requirements 8

2.2 Conceptual Design 9

CHAPTER 3 FINAL DESIGN 13

3.1 MIWD Units 13

3.1.1 MIWD Procurement 16

3.2 X-Z Tables 20

3.2.1 X-Z Table Procurement 21

3.3 Final Frame Design 27

CHAPTER 4 CONTROL SYSTEM 31

4.1 Floor Drive System 31

4.2 Joint Tracking Control 34

4.3 Control Components 34

CHAPTER 5 FLUOROSCOPE SYSTEM 35

5.1 Basic X-Ray Physics 35

5.1.1 Description of X-Ray Tubes 35

5.1.2 Producing X-Rays 37

5.1.3 X-Ray Detection 40

5.1.4 Basic X-Ray Physics Summary 40

5.2 X-Ray Source 40
5.2.1 Specifications 41
5.3 X-Ray Detector 42
5.3.1 Specifications 42
5.3.2 High-Speed Camera with Scintillation Screen 43
5.3.3 Flat Panel Detector 43
5.3.4 X-Ray Detector Summary 45

CHAPTER 6 SAFETY 46
6.1 Fluoroscope Line-of-sight 46
6.2 Measurement Cavity Protection 48
6.2.1 Chassis Protection 48
6.2.2 Joint Tracking Protection 49
6.3 External Protection 50
6.4 Operator Interface, Hardware Protection, and E-Stops 53
6.5 Safety Conclusion 54

CHAPTER 7 FUTURE WORK 55
7.1 Frame Design 55
7.2 Ergonomics 59
7.3 Power Strategy 59
7.4 Fluoroscope 60
7.5 Directional Tracking 61
7.6 Potential TFS Applications 61

CHAPTER 8 CONCLUSION 62

References 64
Appendices 66
Appendix A Additional Material for Chapter 3 67

Appendix B TFS Detailed Drawings 73
Appendix C Additional Material for Chapter 4 104
Appendix D PaxScan® 2520 Digital Detection 108
Appendix E Additional Material for Chapter 7 124

Vita 128

LIST OF TABLES

Table 3.1 MIWD specifications 16

Table 3.2 Weight distribution before and after spacer modification 18

Table 3.3 Max step parameters for 95% prediction intervals for various ages 21

Table 3.4 X-Z table specifications 25

Table 3.5 Frame design constraints 28

Table 5.1 Desired x-ray source specifications 41

Table 5.2 Desired x-ray detector specifications 42

Table A.1 Health statistics of the National Health Survey in 1960-1962 for male 69

Table A.2 Health statistics of the National Health Survey in 1960-1962 for female 70

LIST OF FIGURES

Figure 2.1 TFS coordinate system 4

Figure 2.2 Top views of three cases of subject tracking 5

Figure 2.3 Top view of geometric concept showing ankle and knee setup 10

Figure 2.4 Top view of geometric concept showing hip setup 10

Figure 2.5 Preliminary conceptual TFS design 11

Figure 3.1 Final TFS design with subject positioned for ankle and knee detection 14

Figure 3.2 End-view profile of 76mm x 38mm 80/20® with attached bracket 14

Figure 3.3 Front view of TFS with walking path profile 15

Figure 3.4 Bottom view of TFS 15

Figure 3.5 MIWD Type 15.60.14/85.35.20 17

Figure 3.6 Caster and MIWD subassemblies 19

Figure 3.7 X-Z table terminologies 20

Figure 3.8 Forward displacements of joints relative to trunk displacement 23

Figure 3.9 Vertical displacements of joints relative to initial static height of joints 24

Figure 3.10 X-Z axis linear actuator tables with mass simulation 26

Figure 3.11 Rear view of final TFS assembly 28

Figure 4.1 Platform position error response to PID control 32

Figure 4.2 Kinematic stand-off distance control 33

Figure 5.1 Schematic of a rotating anode x-ray tube 36

Figure 5.2 Characteristic (a) and Bremsstrahlung (b) radiation 38

Figure 5.3 Redlake high-speed camera model MotionXtra HG-LE 44

Figure 5.4 Varian Medical Systems PaxScan® 2520 flat panel detector 44

Figure 6.1 Stationary c-bar style fluoroscope unit 47

Figure 6.2 Possible standoff distance sensor layout and bumper switch layout 49

Figure 6.3 Possible sonar proximity sensor layout and light curtain 53

Figure 7.1 Hip configuration wing support detail 56

Figure 7.2 Temporary wing supports for knee configuration 57

Figure 7.3 X-Z table linear bearing side support 58

Figure A.1 Max walking speeds for 95% prediction interval of various age ranges 68
Figure A.2 Max step frequencies for 95% prediction interval of various age ranges 68
Figure A.3 Max step lengths for 95% prediction interval of various age ranges 69
Figure A.4 Isometric view of final TFS assembly 70
Figure A.5 Ankle configuration and body position 71
Figure A.6 Knee configuration and body position 71
Figure A.7 Hip configuration and body position 72
Figure B.1 Tracking fluoroscope assembly 74
Figure B.2 Carriage assembly 75
Figure B.3 Wing assembly 76
Figure B.4 Rear caster assembly 77
Figure B.5 Rear MIWD assembly 78
Figure B.6 Front caster assembly 79
Figure B.7 Front MIWD assembly 80
Figure B.8 X-ray detector simulation 81
Figure B.9 X-ray tube simulation 82
Figure B.10 Lower shelf 83
Figure B.11 Upper shelf 84
Figure B.12 Lower side shelf 85
Figure B.13 Laser mount 86
Figure B.14 8020 – Part No. 2020 – 20.019 Inches 87
Figure B.15 8020 – Part No. 2020 – 20.239 Inches 88
Figure B.16 8020 – Part No. 2020 – 41.588 Inches 89
Figure B.17 Wing to carriage plate 90
Figure B.18 MIWD & caster mounting angle 91
Figure B.19 Mirror MIWD & caster mounting angle 92
Figure B.20 MIWD & caster mounting plate 93
Figure B.21 Caster mount spacer 94
Figure B.22 Mass simulation base 95
Figure B.23 Mass simulation body bottom 96

Figure B.24 Mass simulation body top 97
Figure B.25 Mass simulation body sides 98
Figure B.26 Mass simulation end 99
Figure B.27 Mass simulation end – no camera 100
Figure B.28 Mass simulation camera base 101
Figure B.29 X-axis to 8020 mounting plate 102
Figure B.30 Transport caster mounting plate 103
Figure C.1 Human position and platform position response to PID control 105
Figure C.2 Motor current response to PID control 105
Figure C.3 Host computer NI PXI 8186 106
Figure C.4 Remote desktop computer 106
Figure C.5 Linksys wireless router 106
Figure C.6 Laser distance feedback device 107
Figure C.7 Driving motor amplifier for MIWD unit 107
Figure C.8 Four of the eight batteries used to supply power to the amplifiers 107
Figure E.1 Temporary wing support for hip configuration 125
Figure E.2 Temporary wing support for ankle configuration 125
Figure E.3 Preliminary conceptual design with stationary lead shielding 126
Figure E.4 TFS conceptual design for an operating table 126
Figure E.5 TFS conceptual design for shoulder analysis 127

NOMENCLATURE

TFS:	Tracking Fluoroscope System.
Fluoroscope:	Comprised of an x-ray source and an x-ray detector. The observed object must be placed between the source and detector.
MIWD:	Motor-In-Wheel-Drive – fully contained unit comprised of a wheel with integrated steering and driving motors.
Omnidirectional:	Capable of moving in any direction.
Trunk:	Subject's body above the waist.
x-z tables:	Two-axis linearly servo-driven table system. The horizontal x-axis is a direct-drive linear motor and the vertical z-axis utilizes a ball screw and rotary motor. Refer to Figure 2.1 for the TFS coordinate system.
fps:	Frames per second
G:	Unit of gravitational acceleration. 2G's = two times gravity.
kg:	Kilograms
m:	Meters
cm:	Centimeters
mm:	Millimeters
kV:	Kilovolts
mA:	Milliamps
m/s:	Meters per second
lp/mm:	Line pairs per millimeter

CHAPTER 1. INTRODUCTION

The Tracking Fluoroscope System (TFS) is a robotic platform designed to follow a subject's natural, uninhibited walking motion and obtain full-range-of-motion x-ray videos of the subject's ankle, knee, or hip. The video data can be used to analyze dynamics within the human body and develop mathematical models of the joints. The TFS can also be used to study artificial implants under various conditions in order to design more effective versions. Similar systems could be used to aid surgeons in artificial implant procedures. Athletic motions could be analyzed to design more effective sports equipment or aid in rehabilitation.

The TFS consists of a metallic framed platform driven by two motor-in-wheel-drive (MIWD) units. Each MIWD consists of a wheel integrated with steering and driving motors. Using two MIWD units mounted on diagonal points of the platform allows for omnidirectional capability. Therefore, the subject is not constrained to a predefined walking path. The platform maintains a set-point distance from the subject using feedback from a laser and a control algorithm stored in an on-board computer. Independently from the motion of the platform, an x-ray source and a detector are servo-driven on respective x-z axis linearly servo-driven actuator tables (x-z tables) to follow the specific motion of the joint. The x-z tables are controlled using error feedback from real-time fluoroscopic images to maintain a "lock" on the center of the joint.

Treadmill systems with stationary fluoroscope units have been used in the past to study videos of the forward walking motion of a patient. However, the dynamics within the human body on a treadmill are completely different than when walking naturally. Also, the range-of-motion which can be viewed when using a stationary fluoroscope system is constrained by the size of the fluoroscope system. The TFS allows for full-range-of-motion videos for the 95^{th} percentile maximum stride length at a maximum walking speed of 2 m/s. In addition, the TFS allows for directional changes and can follow a patient in an arbitrary path.

This thesis will present the evolution of the mechanical design of the TFS including geometric and anthropomorphic constraints, structural considerations, and sizing of all mechanical parts. The x-z tables are sized to move a load of 5 – 9 kg at 2G's acceleration in the x-direction and 1G acceleration in the z-direction. Conventional off-the-shelf x-ray sources and detectors are currently too heavy for the x-z tables. Therefore, strategies for implementing different technology for the fluoroscope system will be explored. In addition, a brief summary of the control system architecture will be presented.

The TFS weighs around 454 kg, has a maximum driving speed of 2.2 m/s, and operates in close proximity to humans. Therefore, multiple safety issues need to be addressed. Finally, this thesis will discuss future possibilities for improving the overall design of the system and present alternative applications utilizing similar tracking concepts.

CHAPTER 2. DESIGN PROCESS

In the beginning stages of designing the TFS, functions and requirements were specified and modified based on conceptual designs, and then finalized. When suitable conceptual designs were finalized, the design process became more detailed. Research was performed for individual components and sub-systems of the TFS and new constraints sometimes required modification of the conceptual designs. This chapter will present the final acceptable and achievable functions and requirements and discuss the process for obtaining a conceptual design of the TFS.

2.1 FUNCTIONS AND REQUIREMENTS

The functions and requirements are divided into four subsections: system structure, functional requirements, physical requirements, and safety requirements. The following sections explain the functions and requirements in detail.

2.1.1 System Structure

General Layout. The TFS is a vehicle platform which does not require tracks or any other lab room modifications to run properly. The subject must feel as comfortable as possible while the TFS is tracking. Therefore, the TFS should maintain the smallest profile possible and still be able to perform all desired functions.

The platform shall maintain a set-point distance from the subject based on error feedback from an on-board laser. Separately, the x-ray source and detector are concentrically servo-driven to track the ankle, knee, or hip through the entire walking motion. The TFS must be capable of holding all on-board equipment including the computer and wireless connection, tracking laser and electronics, batteries, amplifiers, x-z axis linear actuator tables, x-ray source and generator, x-ray detector, and all other associated equipment.

Floor Drive System. The driving and steering system of the TFS shall be capable of smooth accelerations and maximum velocities which depend on the weight and shape of the structure as well as desired maximum walking speeds and anthropomorphic data.

Fluoroscope. The fluoroscope system consists of an x-ray source, generator, x-ray detector, and associated electronics. These components need to be as light and small as possible to maximize the capabilities of the floor drive system and joint tracking system. The x-ray source and detector must be capable of viewing a 150 – 230 mm diameter area centered on ankles, knees, and hips to perform real-time joint tracking.

Joint Tracking System. The current strategy for joint tracking involves concentrically servo-driving the x-ray source and detector based on feedback from the real-time x-ray images. The fluoroscope system shall be servo-driven in the x- and z-directions with maximum stroke lengths and accelerations dependent on anthropomorphic data. Figure 2.1 shows the coordinate system applicable to subsequent chapters in this thesis. The joint tracking system shall be easily adjustable to accommodate ankles, knees, and hips and shall not interfere with the walking motion of the subject.

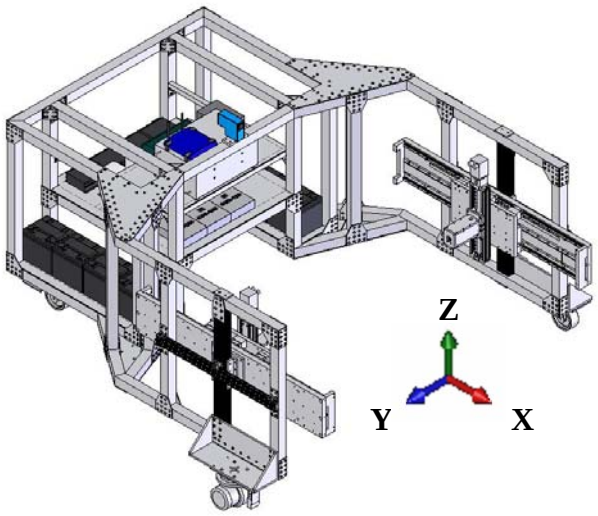


Figure 2.1 TFS coordinate system

Operator and Subject Interfaces. The TFS and operator workstations shall be wirelessly connected so that the TFS workstation is integrated onto the platform while the operator workstation is stationary. The platform design shall be such that the subject feels comfortable and is free to walk naturally.

2.1.2 Functional Requirements

Joint Diagnosis. The TFS shall be capable of tracking ankles, knees, and hips – right and left sides – for walking subjects.

Patient Setup Features. The operator should be able to make preliminary mechanical adjustments to aim the fluoroscope unit at the subject's joint. The operator should be able to view images in real-time if further adjustments are necessary.

Subject Tracking. The TFS shall be designed to accommodate forward, lateral, and arbitrary walking paths to view ankles, knees, and hips as shown in Figure 2.2. The floor drive system should track with minimum velocity variations and maximum smoothness. The physical and motion sensing interface between the subject and the TFS structure shall not disrupt or distort the body and gait characteristics of the subject during walking. For joint motion tracking, the fluoroscope unit should be mounted to an x-z table, which is carried by the platform.

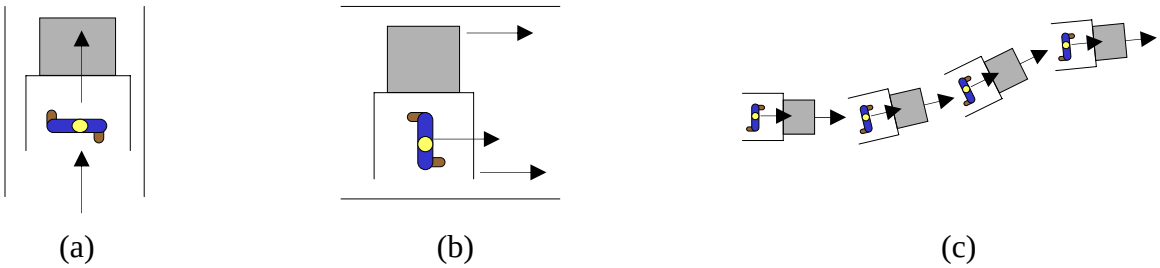


Figure 2.2 Top views of three cases of subject tracking; (a) forward ankle and knee setup, (b) lateral hip setup, and (c) arbitrary walking path

Free Walking Specifications. The platform and x-z tables shall be designed to accommodate free walking rates ranging from 0 m/s to the maximum speed observed in the 95th percentile of healthy female and male subjects walking at normal to fast speeds. This specification was modified throughout the design process.

Originally, the specification stated that the TFS shall accommodate the fastest human running speed of about 10 m/s. However, when sizing components for the floor drive and joint tracking systems, the specification needed to be reduced. Furthermore, if maximum speeds were to be achieved, a variety of additional safety concerns would complicate the system to the point of being cost-prohibitive.

Omnidirectional Floor Operation. The TFS shall be able to perform limited steering maneuvers to track a subject's change in direction. The platform design should accommodate a stationary walking path which could incorporate a few steps or ramps to study the joints under different conditions.

Fluoroscope Interfaces. The x-ray source and detector should be sufficient to capture all the information in which researchers are interested while maintaining excellent resolution. The space between the source and detector should not influence the natural walking motion of the subject either directly or indirectly. The x-ray source and detector line-of-sight shall be "locked" concentrically throughout the tracking process to avoid radiation leakage.

Operator and Subject Interfaces. The operator should be able to view the fluoroscopic images in real-time to be able to make necessary adjustments for optimal results. Subjects shall be able to view the fluoroscopic images in real-time.

Control System. The control system for platform set-point tracking shall be separate from the control system for joint tracking. Chapter 4 presents a brief overview of the TFS control system.

2.1.3 Physical Requirements

Anthropomorphic Data. The TFS shall be designed to facilitate ankle, knee, and hip imaging of subjects ranging from the minimum 5^{th} percentile body dimensions to the maximum 95^{th} percentile body dimensions. The joint tracking servo drives shall be designed to accommodate minimum and maximum stride lengths and minimum and maximum speeds and accelerations of each joint in the x- and z-directions.

Walking Path. The stationary walking path shall be long enough to accommodate six strides of the maximum 95^{th} percentile stride length at the maximum specified walking speed. The path shall be sized to support maximum body width and weight as specified. The walking path should provide inclines and declines of ramps and stairs, should be easy to deploy, and the surface of the path should be a non-slip material.

Passive Setup Features. The mechanical structure of the TFS should be designed such that it can be adjusted to match subject size and stature easily during test setup procedures. The joint tracking system should be designed so that it can be mechanically positioned to fit specific subjects. The fluoroscope, on-board computer, x-z axis tables, support electronics, and drive systems should be fully contained by the TFS platform.

Power. The TFS shall be electrically powered and the supply voltage should not exceed 240VAC, single phase. Any potential exposure to short circuits shall be guarded with ground fault isolators. High power devices shall be separated from low power devices to avoid signal interference. Control cables should be separated as much as possible from power supply cables. The prototype TFS design should utilize a tethered power cord to supply power to AC devices. Future designs should be completely battery powered.

Noise and Vibration. The TFS structure and motion drives shall be designed to minimize noise and vibration emissions which are potentially sensed by the subject or disruptive to image acquisition.

Aesthetics. The TFS prototype shall be designed such that all mechanical features and electrical connections are pleasing to the eye and consistent with common medical equipment standards. The TFS shall be painted or finished for aesthetic consistency. Mechanical drives shall be designed such that lubricants are self-contained within sealed assemblies. The final design should incorporate a thin cover over the chassis which provides safety guarding and is aesthetically pleasing.

Component Weights and Dimensions. The various TFS sub-systems shall be designed such that no single operator needs to lift more than 35 kg during setup procedures, maintenance, or inspection routines. As explained in later chapters, the chosen x-z tables will accommodate weights of 5 – 9 kg. The x-ray source and detector must not exceed this specification if the desired walking speeds are to be achieved. The TFS must be capable of fitting through a standard lab room door to be moved within a building. The TFS geometry shall accommodate the 95^{th} percentile maximum body breadth, joint height, and stride length of a human subject.

2.1.4 Safety Requirements

Chapter 6 describes in more detail the specific safety requirements of the TFS. This section only outlines the general safety requirements as specified before the prototype was designed.

Motion Interlocks. The axes of any electrically driven mechanisms shall have limit sensors which can be used to effect appropriate shutdown operations in response to approaching out-of-range operating conditions. Auxiliary and independent sensor-based interlocks shall detect inappropriate and/or dangerous subject posture or motion, as well as inappropriate platform motion.

Emergency Stops. The TFS operator and subject shall have remote-control emergency stop buttons which completely de-energize all motion drives. The TFS will incorporate

additional E-stops such as magnetic pull-cord and hard-wired buttons integrated onto the platform. All motion drives should hold position on emergency stop commands.

Electrical Power. All University of Tennessee and State of Tennessee standards and practices for electrical power feeds and internal wiring shall be followed.

Fluoroscope Operation. All Tennessee standards and practices for fluoroscope operation apply to the design of the TFS.

Enclosures and Pinch Points. The TFS shall meet or exceed OSHA safety requirements.

2.2 CONCEPTUAL DESIGN

The shape if the TFS depends on a number of specifications. The following section describes the geometric concept of the TFS platform. Before the details of the TFS could be specified, the overall geometric concept of the chassis needed to be conceptualized. The shape of the chassis and capabilities of the TFS depend on the functions and requirements presented in the preceding section.

The functions and requirements of the TFS specify the use of a stationary walking track which would enable the subject to step up or down a couple of stairs or ramps to gain additional dynamic data. To achieve this result, the TFS must be able to "straddle" the walking path such that the machine is always moving on a flat surface while the subject walks on the path.

For ankles and knees, the fluoroscope must be mounted on each side of the joint; for hips, the fluoroscope must be mounted in front of and behind the hip. Figure 2.3 shows a top view of the geometric concept of the TFS for ankle and knee detection setup. Figure 2.4 shows a top view of the geometric concept of the TFS in a hip detection setup.

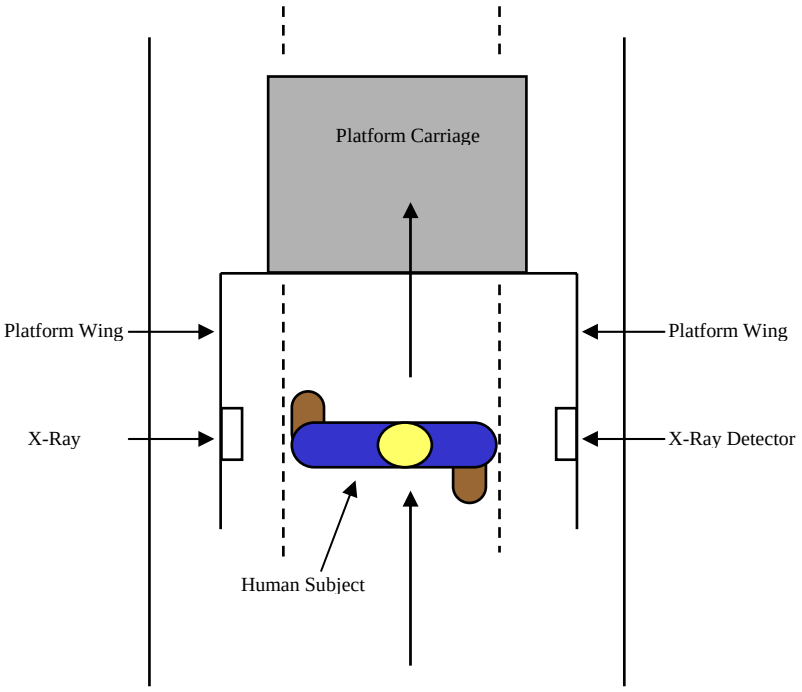


Figure 2.3 Top view of geometric concept showing ankle and knee setup

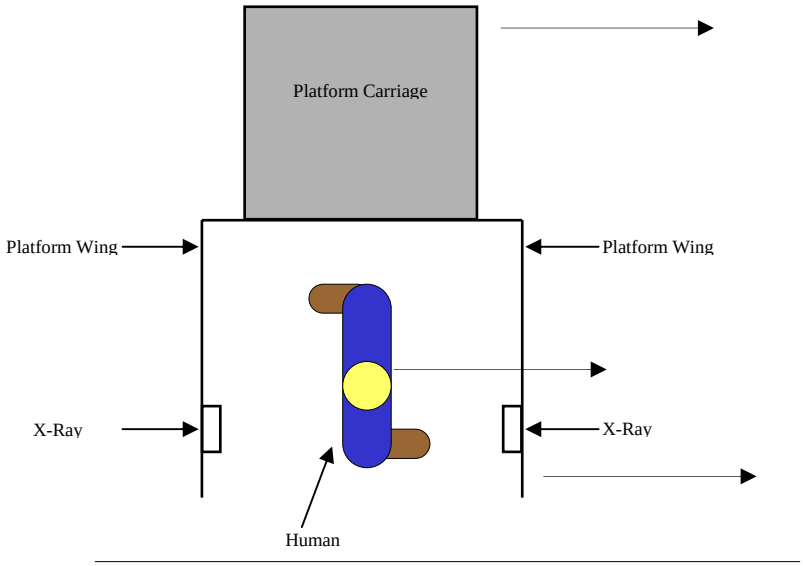


Figure 2.4 Top view of geometric concept showing hip setup

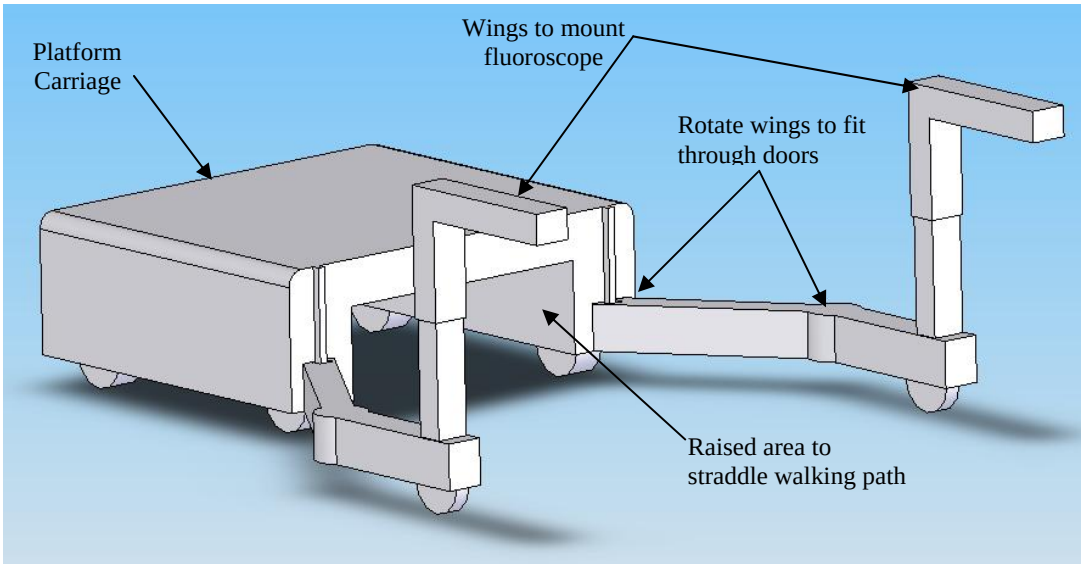


Figure 2.5 Preliminary conceptual TFS design

The TFS should be capable of moving in both directions as shown in Figures 2.3 and 2.4. The subject walks between the wings of the platform so that the fluoroscope has a line-of-sight to either side of the joint. The platform chassis carries the on-board computer, amplifiers, batteries, and any additional electronics or equipment. The x-ray source and detector are mounted on each respective wing. The carriage and wings form one complete unit.

Figure 2.5 shows a preliminary 3D design concept for the TFS structure. As shown, the carriage is small enough to fit through a door and maintains as low a profile as possible. Based on required anthropomorphic data, which will be presented in Chapter 3, the width between the wings must be greater than the width of a typical doorway. Therefore, the wings must either detach from the carriage or swivel inward to fit through a door. The conceptual design in Figure 2.5 shows the swivel concept. In the final design, the wings do not swivel because of a variety of constraints, but they can be removed.

The raised area shown on the carriage is necessary to allow tracking over a walking path in forward translation mode (refer to Figure 2.2(a)). This raised area restricts the design

of the floor drive system because the use of axles and gear boxes is not realistically feasible with such a configuration.

The wings shown in the conceptual design of Figure 2.5 maintain a simple profile. Further investigation into the weight of appropriate x-z tables, as well as the momentum of moving mass, both led to a more robust final design. Similarly, the size of the carriage was increased throughout the design process as the necessary components were chosen. The final design is explained in Chapter 3.

CHAPTER 3. FINAL DESIGN

The final design of the TFS is shown in Figure 3.1. In the beginning stages of the design process, the frame was to be constructed of one solid weldment. Throughout the design process, it became clear that with a first-run prototype, the frame would need to be more adjustable. The frame was designed and built using 51mm x 51mm 80/20® extruded aluminum. The flexibility provided by slotted aluminum extrusion allows for repositioning of shelves and easy mounting of components without the need for major fabrication processes. Figure 3.2 shows an end-view profile of 76mm x 38mm 80/20® with bolts, t-nuts, and a bracket. If the bolts are loosened, the bracket can slide along the length of aluminum extrusion. In the future, when the TFS design has been finalized, tested, and optimized, models may be constructed of solid weldments for material cost savings and added strength. The details of the frame geometry depend on the specifications of the floor driving system, specifications of the x-z tables, all related components, and anthropomorphic data.

3.1 MIWD UNITS

The specifications of the floor drive system of the TFS were presented in Chapter 2. The floor drive system must allow for omnidirectional capability of the platform and enough space to integrate a stationary walking path for forward translation mode (refer to Figure 2.2a). Figure 3.3 shows a front view of the TFS with a profile of the proposed walking path. As shown, the floor drive system can not feasibly integrate axles so each driving wheel must be capable of independent steering and driving. Figure 3.4 shows a bottom view of the TFS. Two MIWD units are mounted on diagonal positions on the frame. Each MIWD is capable of rotating 360º and driving concurrently. The diagonal mounting configuration allows for omnidirectional platform movement and enough space for a walking platform. Free-swivel low-friction casters are mounted on the remaining diagonal points on the platform. If additional MIWD units are desired for future applications, they can be mounted on the existing caster brackets.

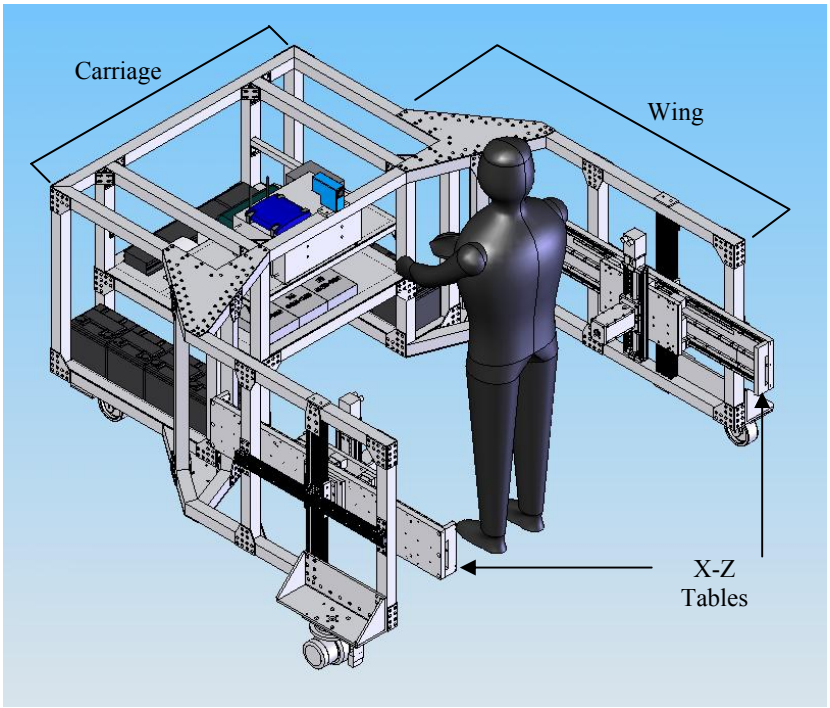


Figure 3.1 Final TFS design with subject positioned for ankle and knee detection

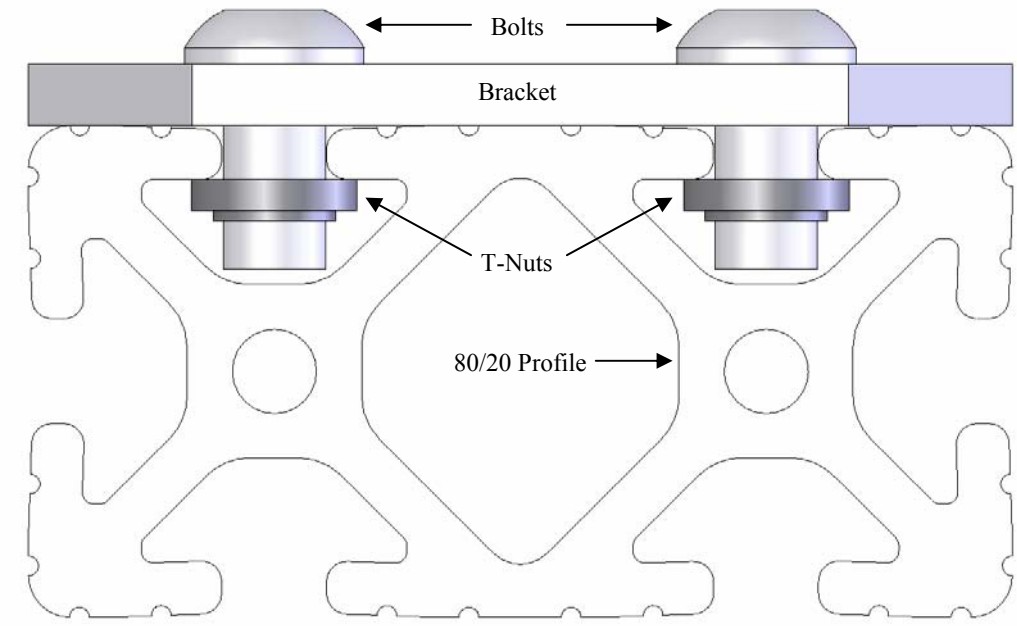


Figure 3.2 End-view profile of 76mm x 38mm 80/20® with attached bracket

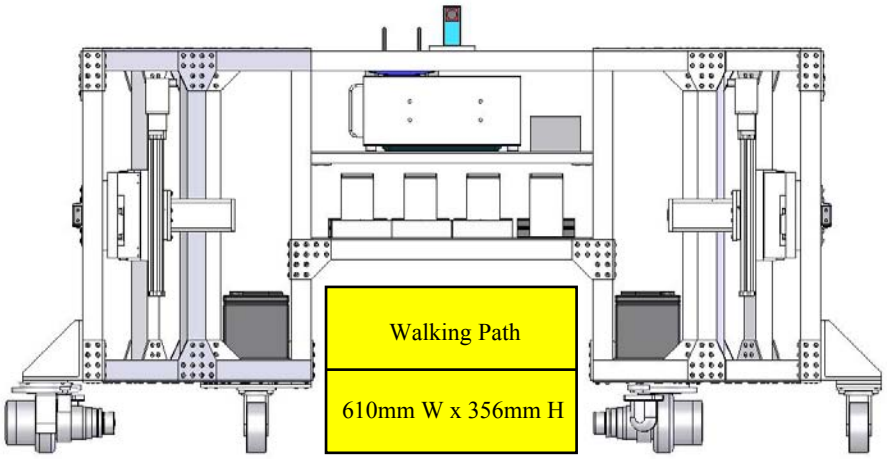


Figure 3.3 Front view of TFS with walking path profile

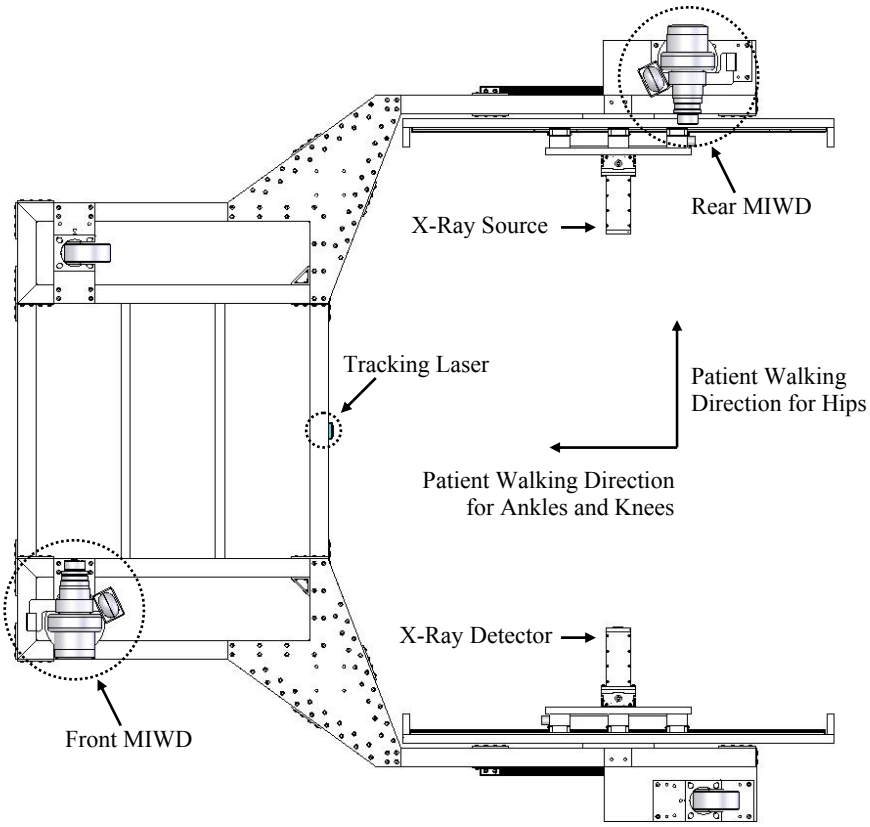


Figure 3.4 Bottom view of TFS

3.1.1 MIWD Procurement

The market was surveyed for manufacturers and vendors of steerable, drivable wheels and only one company was found which could match TFS specifications. Sauer Danfoss is a subsidiary of Schabmuller, who designs and manufactures MIWD units. The only distributor for the MIWDs in North America is Transbotics.

Maximum platform speed was originally specified to be 10 m/s and the final specification ended up being around 2 m/s. The specification was changed because of safety and budgetary reasons. The weight of the final TFS design is around 454 kg. If the TFS were driven to speeds higher than 2 m/s in close proximity to a human subject, multiple safety issues are obvious. Furthermore, comparing models of MIWD units available within a reasonable budget showed that the maximum speed which could be obtained affordably was around 2 m/s. Table 3.1 shows the specifications of the chosen MIWD units and Figure 3.5 shows three different perspective views of the unit.

Table 3.1 MIWD specifications

MIWD Type	15.60.14/85.35.20
Load Capacity	200 kg
Input Voltage	24 V
Electromagnetic Brake	3 Nm
Max RPM	2780 rpm
Max Platform Speed	2.2 m/s
Max Rotation Speed	90° / s
Gear Ratio	9.9
Wheel Diameter	150 mm
Wheel Thickness	50 mm
Encoder (Driving)	1000 ppr
Potentiometer (Steering)	10 kΩ

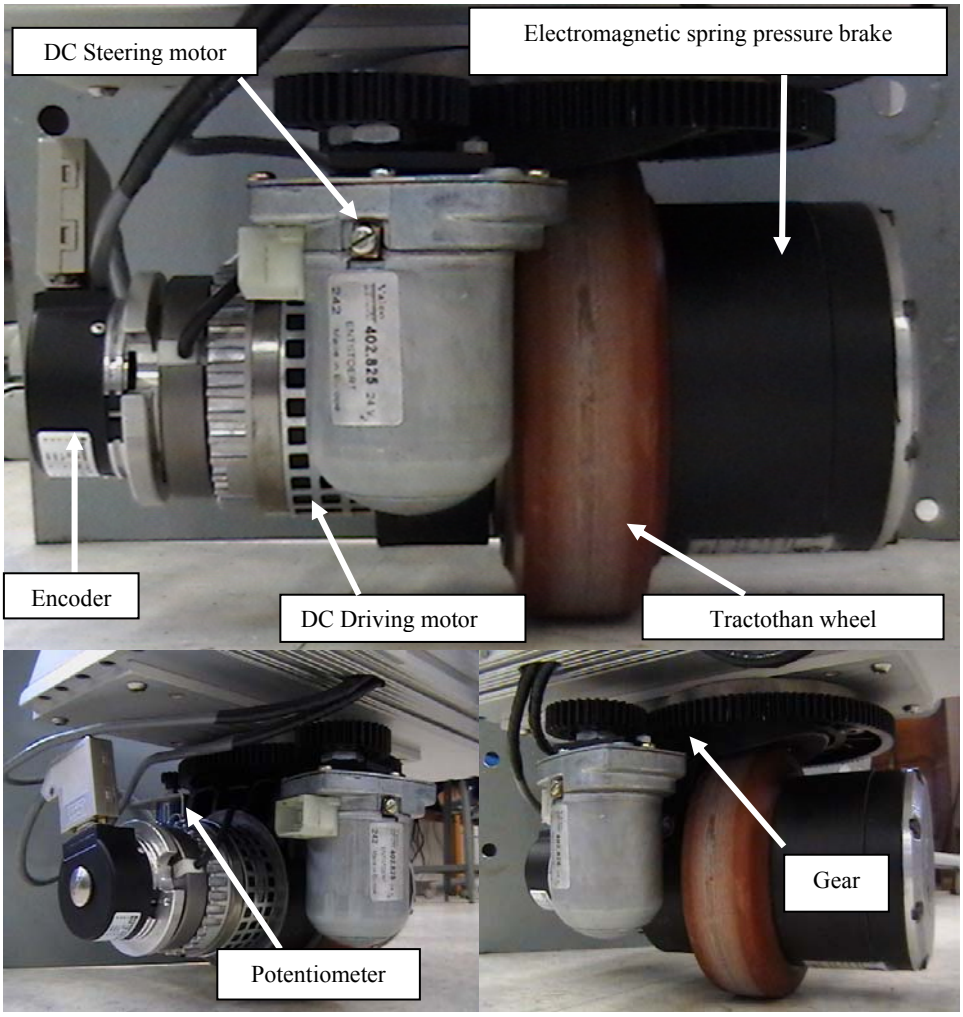


Figure 3.5 MIWD Type 15.60.14/85.35.20

As shown in Figure 3.4, two MIWD units and two low-friction swivel casters are used to support the entire weight of the TFS. The TFS is designed to run on smooth uniform surfaces, eliminating the need for shock absorbers. Due to material fabrication tolerances, more weight was being carried on the casters than on the driving units, resulting in slipping during operation.

The MIWD units and casters are each mounted to a universal caster/MIWD bracket. The brackets are designed to allow for additional MIWD units if they are needed to replace the casters in the future. The vertical dimension of the casters is less than the vertical dimension of the MIWDs. Therefore, spacers are used and mount directly to the caster brackets to level the TFS platform.

To reduce slipping, the spacers were made to be slightly thinner than they were when originally fabricated. This process placed more weight on the MIWDs than on the casters, which resulted in less slipping. Table 3.2 shows the weight distribution before and after modifying the spacers. Figure 3.6 shows the caster and MIWD subassemblies with universal brackets and spacers.

Table 3.2 Weight distribution before and after spacer modification

	Before (kg)	After (kg)
Front Right MIWD	132	138
Front Left Caster	141	135
Rear Right Caster	93	86
Rear Left MIWD	88	95

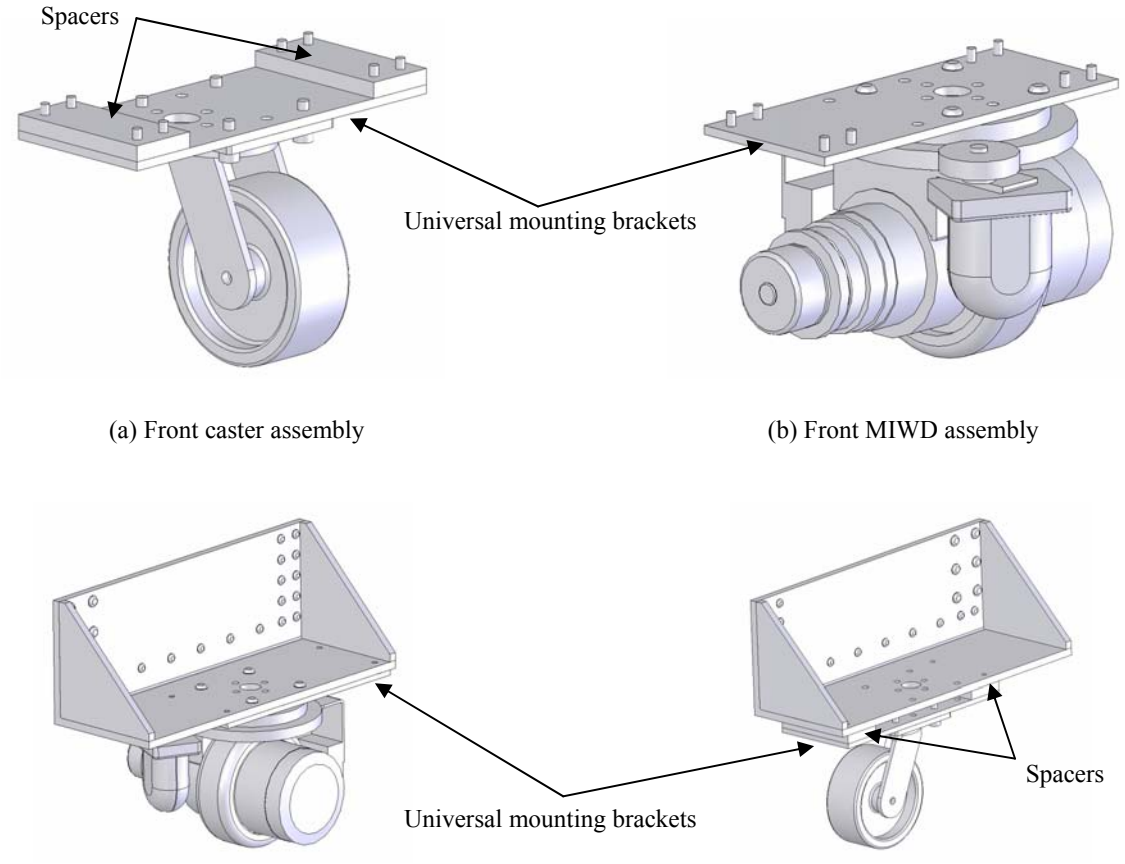


Figure 3.6 Caster and MIWD subassemblies

3.2 X-Z TABLES

Specifications state that the TFS must produce full-range-of-motion x-ray videos of the ankle, knee, or hip. The previous section discussed the floor drive system, which is used to move the entire TFS platform to maintain a set-point distance from the subject. Joint tracking involves moving the fluoroscope system relative to the platform to view the joint through the entirety of the testing procedure. Because the fluoroscope system will be moved relative to the TFS platform, the required motion constraints can be compared to following a person's joint as they walk on a treadmill. If viewing a two-dimensional fluoroscopic video of a person's joint as he/she walks, the movement occurs in two directions; side-to-side in the x-direction and up-and-down in the z-direction. For the purpose of this thesis, the term x-z table will represent a two-axis linearly servo-driven actuator table. Using an x-z table to move the x-ray source on one side of the joint and another x-z table to move the x-ray detector on the other side of the joint, full-range-of-motion data can be obtained. Figure 3.7 shows terminologies associated with the chosen x-z tables. Sizing and procurement of the tables are presented in the following section.

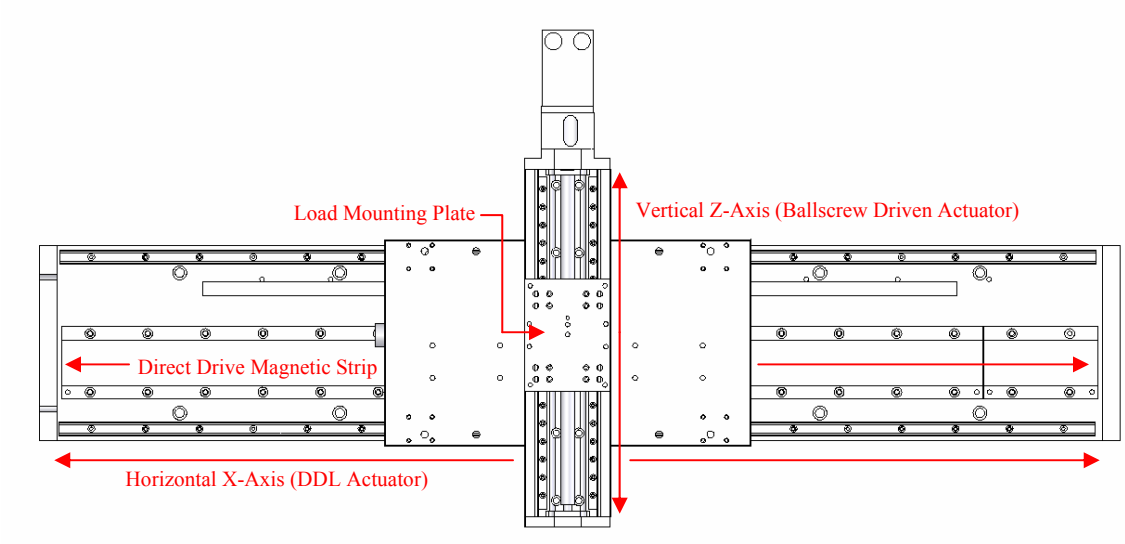


Figure 3.7 X-Z table terminologies

3.2.1 X-Z Table Procurement

Specifying the x-z tables requires an understanding of a variety of anthropomorphic data related to the maximum movement in the x- and z-directions and accelerations of the joints relative to the platform. Many other issues arise such as maximum weight of the system, power supply capabilities, and feedback strategy for control. The process for choosing a suitable x-z table system is described in the following sections.

Anthropomorphic Data. Research was performed to determine the maximum walking speed, step frequency, and step lengths for people 10-79 years old. TFS requirements specify that the system must satisfy the maximum constraints for a 95% prediction interval of the entire population. It is assumed that human subjects less than 10 years of age and greater than 79 years of age will not exceed the maximum requirements of the TFS. According to research performed by Alek Karsznia, Tommy Oberg, and Kurt Oberg [1], the 95% prediction interval data sets are presented in Table 3.3. The maximum of the maximum 95% prediction interval values for walking speed, step frequency, and step lengths are 1.754 m/s, 2.560 steps/s, and 0.786 meters respectively and are outlined in the Table 3.3. For visual column graphs of the data, refer to Appendix A, Figures A.1, A.2, and A.3.

Table 3.3 Max step parameters for 95% prediction intervals for various ages

"Normal" Walking Speed						
Age	**Walking Speed (m/s)**		**Step Frequency (steps/s)**		**Step Length (m)**	
	Women	Men	Women	Men	Women	Men
10 to 14	1.332	1.754	2.34	2.56	0.606	0.701
15 to 19	1.624	1.644	2.49	2.46	0.688	0.786
20 to 29	1.600	1.460	2.40	2.25	0.723	0.690
30 to 39	1.686	1.631	2.49	2.29	0.708	0.746
40 to 49	1.549	1.534	2.50	2.24	0.649	0.725
50 to 59	1.309	1.624	2.30	2.34	0.590	0.761
60 to 69	1.508	1.537	2.44	2.24	0.641	0.726
70 to 79	1.376	1.505	2.32	2.20	0.620	0.722

Sizing the X-Axis. Similar data to Table 3.3 was obtained for "fast walking" but the maximum values slightly exceed the maximum platform speed of 2.2 m/s. Therefore, to size the x-axis of the x-z table, the data presented in Table 3.3 was used.

Figure 3.8 shows displacements of the ankle, knee, and hip relative to the trunk during normal walking speeds for average male subjects [2]. Each joint completes a cycle in the same amount of time but the ankle travels longer distances and will experience higher accelerations. Therefore, data associated with the ankle should be used to size the x-z tables. Given the close proximity of the ankle to ground level, the maximum step length value from Table 3.3 can be used to estimate the horizontal distance traveled.

Acceleration is defined as distance divided by time squared [3]. If the maximum step length is distance, then the inverse of the step frequency is the time associated with the distance. Relative to the subject's trunk, an ankle traveling forward accelerates through the first half of the step length and decelerates through the last half of the step length. To obtain an average acceleration of the ankle through one step length, half of the inverse of the step frequency should be used as the time associated with the step length as shown in Equations 3.1 and 3.2.

$$acceleration = \frac{DISTANCE}{TIME^2} = \frac{step\,length}{\left(\frac{1}{step\ freq} \cdot \frac{1}{2}\right)^2} \tag{3.1}$$

$$acceleration = \frac{0.786\,m}{\left(\frac{1}{2.560\,steps/s} \cdot \frac{1}{2}\right)^2} = 20.565\,m/s^2 \tag{3.2}$$

Equation 3.2 shows that the estimated acceleration of the ankle is about 2G's in the x-direction. The associated maximum step length in the 95% prediction interval is also the maximum stroke length required in the x-direction, and is 0.786 meters.

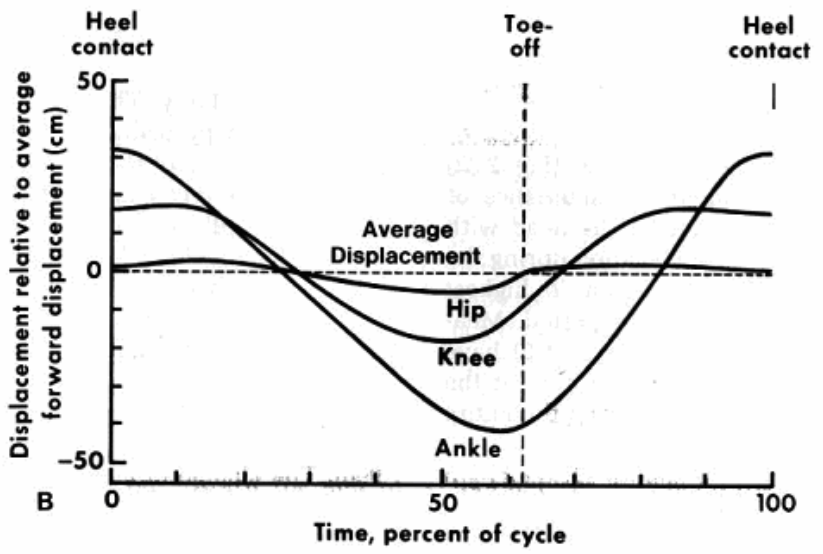


Figure 3.8 Forward displacements of joints relative to trunk displacement

It must be noted that the acceleration calculation is only an estimation. The ankle joint is subjected to higher accelerations for shorter periods of time, and vice versa, during walking. In Chapter 2 of this thesis, it was specified that the fluoroscope unit obtain a 150 – 230 mm image of the joints. When controlling the x-z tables with feedback from such a large image, the acceptable error within the fluoroscopic image should be sufficient to keep the ankle within the field of view. In other words, the ankle will most likely remain in the image during higher accelerations allowing the x-axis enough time to "catch up" to the centroid of the joint during periods of lower acceleration. Chapter 4 presents a summary of the control system strategy. The x-axis should be able to accommodate knees and hips because the length of travel and maximum accelerations of the knees and hips are less than that for ankles.

Sizing the Z-Axis. The z-axis acceleration and stroke length requirements must now be determined. Figure 3.9 shows the vertical displacement of the ankle, knee, and hip of male subjects during normal walking speeds at a step frequency of 1.85 steps per second [2]. Ankle displacement is the largest of the three joints at just under 0.20 meters and will be used to size the vertical z-axis of the x-z table.

The maximum displacement of the ankle occurs in about 25% of the step cycle and returns to zero vertical displacement in the last 25% of the cycle. Using a step frequency of 1.85 steps per second, a maximum vertical displacement of 0.20 meters, and Equation 3.3, the acceleration can be calculated.

$$acceleration = \frac{0.20\,m}{\left(\frac{1}{1.85\,steps/s}\cdot\frac{1}{4}\right)^2} = 10.95\,m/s^2 \qquad (3.3)$$

The estimated maximum vertical acceleration of the ankle is about 1G. Considering that a 150 – 230 mm inch image will be used for feedback control of the vertical axis eliminates the need for a more detailed acceleration analysis. The maximum displacement of the ankle is about 20 cm. The vertical axis should be able to sufficiently follow the ankle, knee, and hip through the entire walking cycle with a standard stroke length of 200 mm and acceleration capabilities of 1G.

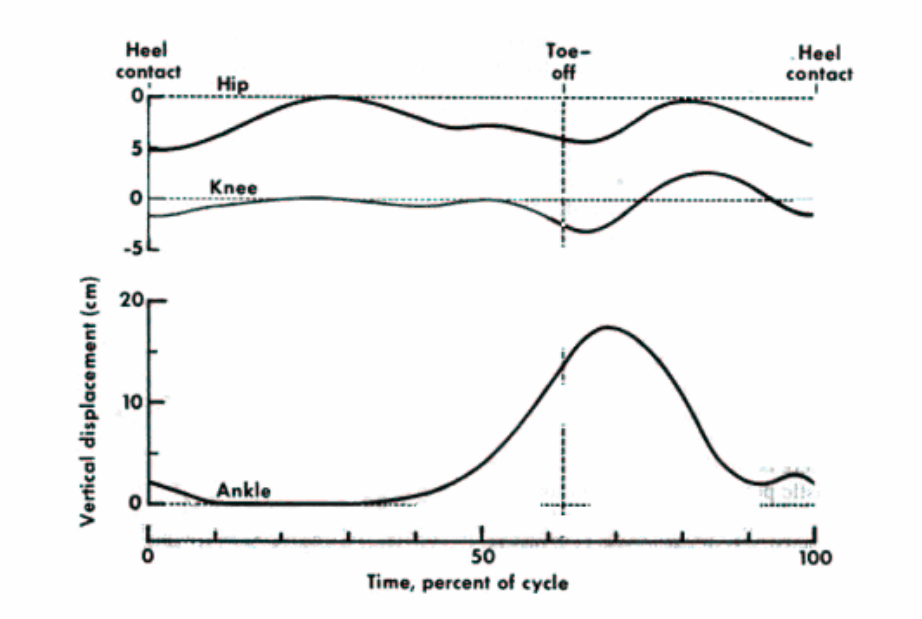


Figure 3.9 Vertical displacements of joints relative to initial static height of joints

Load Capabilities. The fluoroscope system of the TFS consists of two x-z tables, which servo-drive the x-ray source and x-ray detector. The weight of the moving load must be known in order to correctly size the x-z tables. Chapter 5 addresses several issues regarding the weight and capabilities of typical x-ray sources and detectors. Typical x-ray sources which meet TFS requirements weigh about 15 kg or more. Image intensifiers are typically used in fluoroscope applications and weigh about 20 kg or more. Assuming the x-z tables could be sized to actuate 20 kg at 2G's acceleration, there are many safety issues related to the momentum of a moving mass traveling at high accelerations. The frame of the TFS is designed to be as light as possible and to move on MIWDs and free-spinning casters. If 20 kg were actuated back and forth at 2G's acceleration, the entire platform would become unstable and unsafe. In addition to safety hazards, an x-z table sized to carry 20 kg would cost much more than the budget allows. During procurement of the x-z tables, the funding which was allocated to TFS research needed to be spent by the end of the quarter. At that time, a suitable fluoroscope strategy had not been finalized and assumptions needed to be made to procure an x-z table before the deadline. Table 3.4 presents a summary of the x-z table specifications.

Table 3.4 X-Z table specifications

Two x-z axis tables		
Load mounted on z-axis		5 - 9 kg
Center of gravity from z-carriage		≤ 150 mm
x-axis	acceleration	2 G's
	stroke length	800 mm
z-axis	acceleration	1 G
	stroke length	200 mm
Encoders and limit position feedback		
Include all required cables, amplifiers, mounting hardware, etc.		

Chapter 5 will discuss potential strategies for reducing the moving mass of the fluoroscope system. In summary, it was decided to assume a moving mass of 5 – 9 kg with a center of gravity located 150 mm or less from the mounting plate. In addition, the x-z tables are to be powered by 110 VAC instead of using the on-board batteries. In the interest of time and simplicity for the first-run TFS prototype, the x-z tables will be powered by a typical wall outlet using a tethered power cord. In future design modifications, the tables should be powered by on-board TFS batteries.

Three bid requests were sent out to different automation companies and the best designed system was chosen. Cornerstone Technical Group Inc. designed a system with a ball-screw driven z-axis actuator mounted to the carriage of a direct-drive-linear x-axis actuator. The load is mounted to the carriage of the z-axis actuator. Cornerstone's system provided a robust design with plenty of "overhead" in case the load requirements are increased in the future. Figure 3.10 shows one of the x-z tables with a mass simulation mounted to the z-axis. For testing of the control system, mass simulations and a black-and-white camera are used instead of a fluoroscope system.

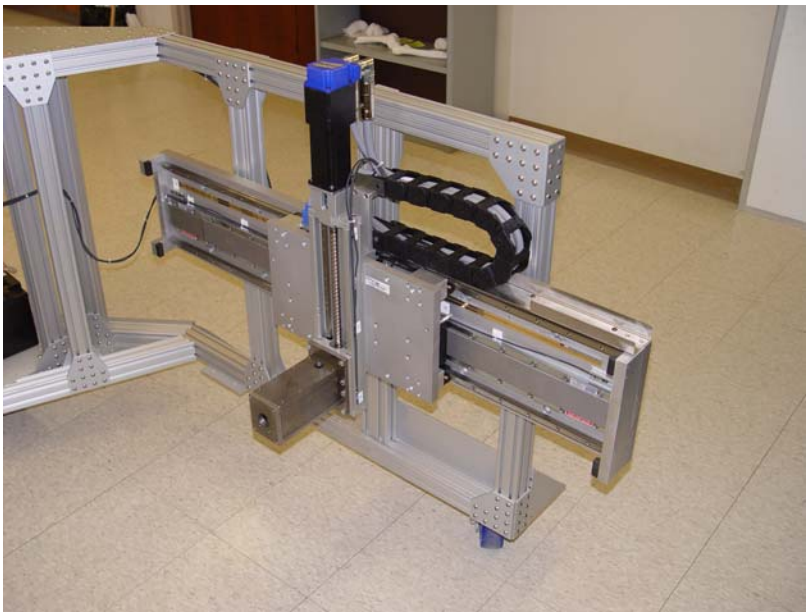


Figure 3.10 X-Z axis linear actuator tables with mass simulation

3.3 FINAL FRAME DESIGN

All components associated with the floor drive system and joint tracking system must be carried on-board the TFS platform with the exception of the user interface of the control system, which is a desktop computer connected wirelessly to an on-board computer. The on-board computer processes the feedback control systems, which allow the machine to track a subject. The MIWD units each have a driving amplifier and a steering amplifier, for a total of four amplifiers. The joint tracking system, or x-z table system, requires one amplifier for each axis, so two x-z tables require four amplifiers.

The TFS was originally intended to be completely battery powered. However, time constraints required that assumptions be made concerning the quantity of batteries. It was decided that eight, 12V, 42Ah batteries be used. The on-board computer, wireless device, laser, and x-z tables require 120 VAC power. The MIWDs are battery-powered. Any x-ray source which is chosen for the fluoroscope system will require a generator and will probably use a large amount of current. Preference was given to proving the control system and design rather than spending too much time on power supply details. In future designs, the power system should be modified so that everything is battery-powered.

The various components of the TFS require a certain amount of space and therefore constrain the shape of the frame. High power devices should be separate from low power devices to avoid signal confusion. Control cables should be routed separately from power supply cables when possible to avoid potential loss in feedback signals. The length, width, and height of the platform not only depend on the various components, but also depend on anthropomorphic data related to subject heights, widths, and stride lengths. Furthermore, the TFS must maintain as small a profile as possible, have the ability to integrate a walking path, and still be able to fit through a standard doorway. Design constraints are summarized in Table 3.5 [4, 5] and the assembled TFS platform is shown in Figure 3.11.

Table 3.5 Frame design constraints

Body Height	150 - 200	cm
Body Breadth	30 - 56	cm
Knee Height	43 - 61	cm
Hip Height	79 - 109	cm
Ankle Height	N/A	cm
Max Weight	115	kg
Doorway Dimensions	89W x 198H	cm
Walking Path Dimensions	61W x 36H	cm

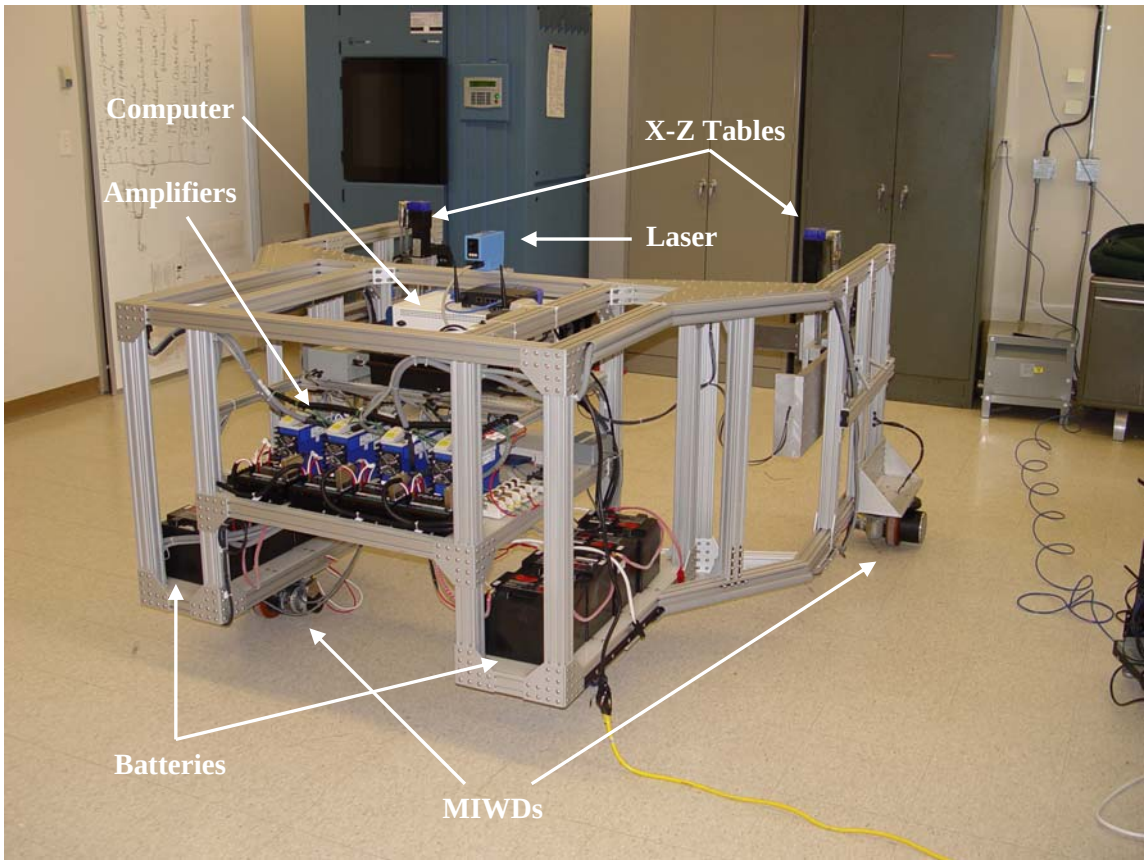


Figure 3.11 Rear view of final TFS assembly

Additional information concerning design constraints can be found in Appendix A, Tables A.1 and A.2. Figure A.4 in Appendix A shows the final SolidWorks 3D design of the TFS. Figures A.5, A.6, and A.7 in Appendix A show the body positions and x-z table positions for viewing the ankle, knee, and hip.

Carriage Design. The carriage of the TFS contains batteries, amplifiers for eight motion axes, an on-board computer, a wireless emitter, laser, and all associated electronics and hardware. As shown in Figure 3.11, the amplifiers are mounted on a lower level than the computer, laser electronics, and wireless emitter. Separation is necessary to avoid signal interference between high power and low power devices. The top shelf of the carriage is half of the size of the bottom shelf to ensure plenty of free air-flow to cool the amplifiers. The batteries are the heaviest components on the carriage and are therefore mounted as low to the ground as possible to maintain a low center of gravity. The current carriage design offers plenty of extra room for additional batteries, an x-ray generator, and associated electronics.

The bottom shelf support of the carriage is raised about 51 cm above ground level offering plenty of room for the height of a walking path. The clearance in width for a walking path is 71 cm, which allows for 5 cm of clearance on either side of the path. The bottom shelf support can be raised or lowered because the entire platform is constructed of slotted aluminum extrusion. The carriage dimensions are 102 cm tall by 127 cm wide by 86 cm deep. If the wings are detached from the carriage, the 86 cm depth of the carriage allows for transport through standard doorways. Additional casters can be mounted to the carriage and wings for support during transport.

Wing Design. The x-z tables must be manually positioned according to which joint is being viewed. The x-z tables are mounted on linear bearings which slide along the length of 80/20® tubing and lock in the desired position. The overall height of the TFS in combination with the 200 mm stroke length on the z-axis will accommodate most hip heights and should allow for all ankle and knee measurements. Table 3.5 does not

specify an ankle height because the TFS was designed such that a 150 mm diameter x-ray detector would have 5 cm of clearance from ground level. If an ankle measurement is less than two inches above ground level, a small walking path could be used to raise the joint to be within the field of view. The rear MIWD and caster are mounted to angle brackets so that the x-z tables may be positioned very close to the ground for ankle measurements.

The spacing between the wings was driven by the maximum body breadth of subjects as well as the space required for the fluoroscope system and additional clearance for safety reasons. The distance between z-axis mounting plates of the two x-z tables is about 145 cm. Assuming the x-ray source and detector each protrude about 18 cm from the mounting plate, and considering the maximum body breadth of 56 cm, the minimum remaining clearance on either side of the subject is 26.5 cm. The wings add larger dimensions to the overall platform than could fit through a door. Therefore, the wings have additional mounts for casters and are designed to unbolt from the carriage for transport between rooms.

Detailed and dimensioned drawings of all associated components of the TFS can be found in Appendix B. SolidWorks 3D modeler software was used for the entire mechanical design of the TFS and all figures in Appendix B were generated using SolidWorks. All SolidWorks drawing, part, and assembly files are on file with the Mechanical Aerospace and Biomedical Engineering department at The University of Tennessee.

CHAPTER 4. CONTROL SYSTEM

This chapter provides a brief summary of the control system architecture of the TFS floor drive and joint tracking systems. The controls for the x-z axis tables have not yet been implemented as of the writing of this thesis but a summary of the theory will be presented.

4.1 FLOOR DRIVE SYSTEM

Gabriel R. Preliasco's thesis explains the details of the TFS platform control system. Kinematic, dynamic, and stand-off distance control systems are analyzed in detail in *Motion Control for a Tracking Fluoroscope System* [6].

To begin, kinematic and a dynamic analyses of the TFS were performed. The dynamic analysis was not used because the tire and friction models resulted in problems when platform and human speed were close to zero. When the person would stop walking, the person's speed with respect to the speed and direction of the platform would change sign from positive to negative. The tire and friction models used in the dynamic analysis caused the platform to oscillate when the person stopped walking. This response was found to be unpleasant to the patient. The kinematic analysis does not assume a load on the driving motor, but rather an inertia that the motors must overcome. The kinematic model resulted in a much more desirable response when platform and human speeds were close to zero.

Human position is detected by a laser device. The input to the PID distance controller is the difference between the platform set-point position and the human set-point position. This input is the error of the platform position with respect to the human. The output of the distance controller is a voltage from the motion card to the MIWD units. Kinematic analysis assumes no slipping so that the wheel position is the same as the platform position. The MIWD units are evaluated separately and the two output position signals

are averaged and fed back to compare with the human position. The resulting error is sent to the PID controller. Figure 4.2 shows the stand-off distance control simulation of the TFS. For a more detailed analysis of the TFS control system, refer to *Motion Control for a Tracking Fluoroscope System* [6].

Using optimized proportional, integral, and derivative gains for the PID controller, the error can be plotted as shown in Figure 4.1. Human and platform position and motor current plots can be found in Appendix C, Figures C.1 and C.2 respectively. The maximum error is about 4 cm. As the person accelerates, the platform controller attempts to drive the error to zero. When the person walks at a constant velocity, the platform catches up and maintains close to zero error. As the person decelerates, the platform overshoots and negative voltage is applied to slow the platform down and drive the error to zero. When the person is close to zero velocity, the platform overshoots and negative voltage is applied to drive the error back to zero.

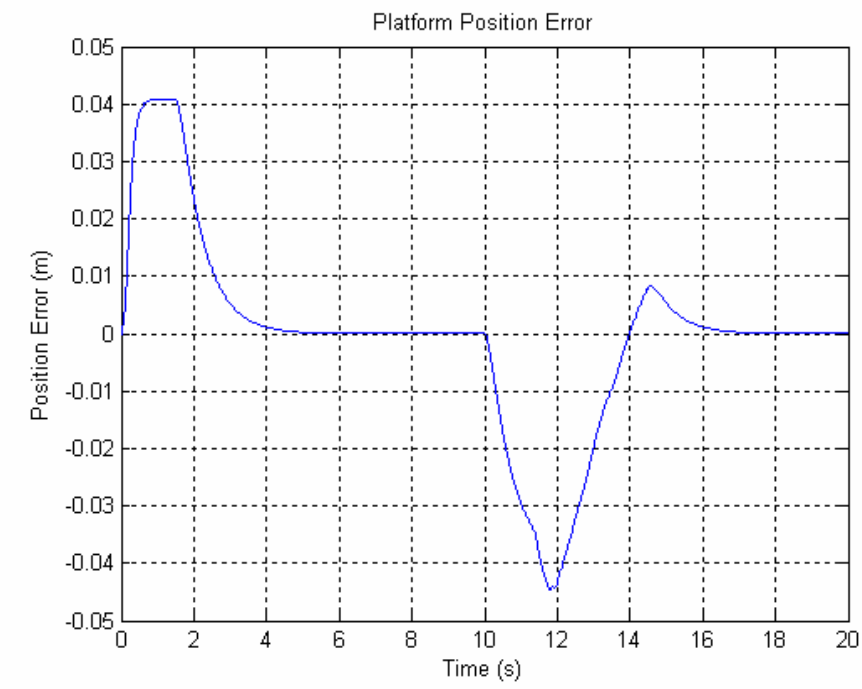


Figure 4.1 Platform position error response to PID control

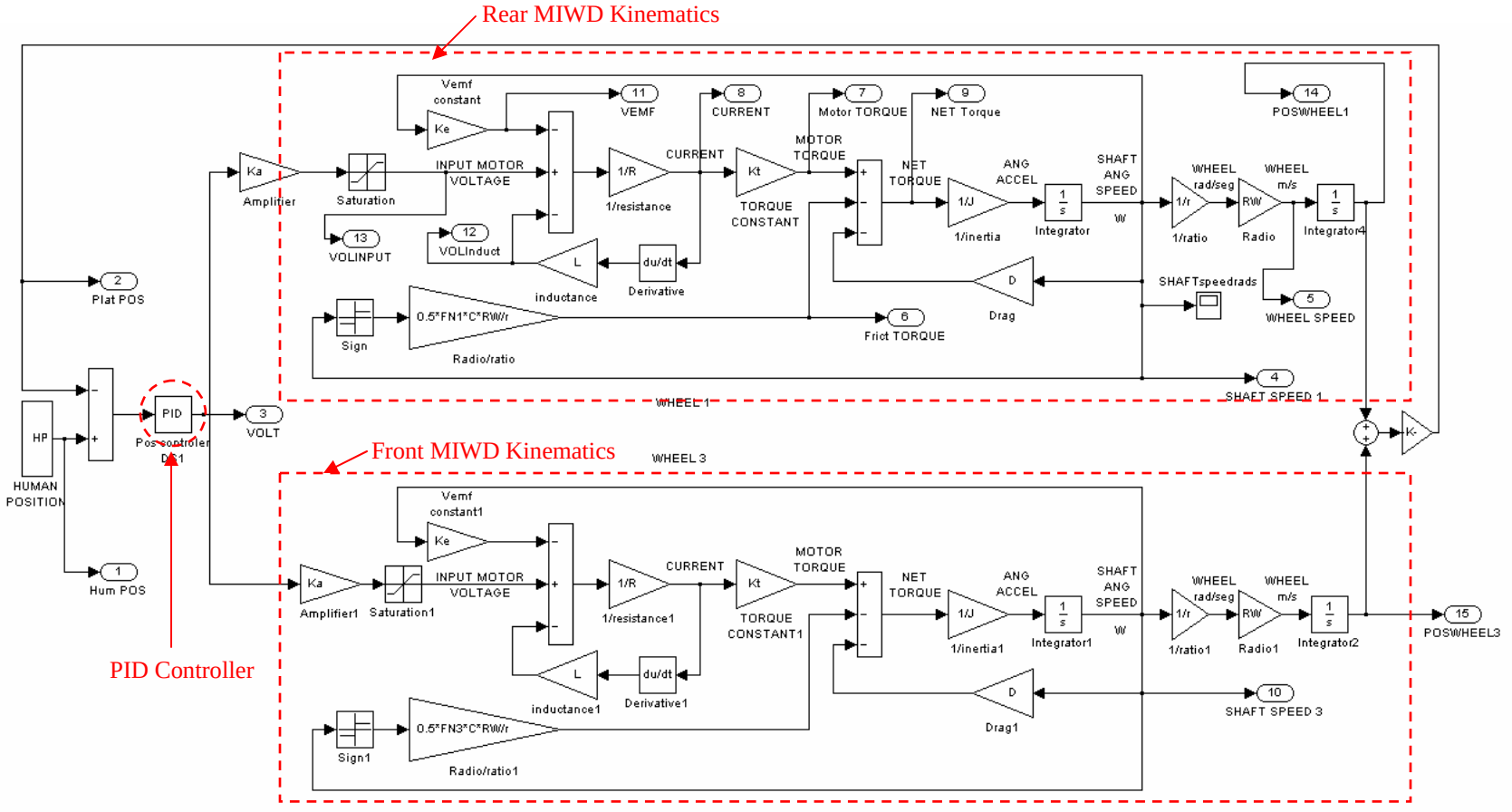


Figure 4.2 Kinematic stand-off distance control

4.2 JOINT TRACKING CONTROL

Joint tracking control uses feedback from the fluoroscopic image of the joint being tested. The x-ray source and detector create an x-ray image of the joint. An image processing algorithm calculates the position of the centroid of the joint with respect to the center of the image field-of-view. Two axes are used to servo-drive the fluoroscope in the x- and z-directions. Consequently, two error feedback signals are needed. The image processing algorithm calculates the distance from the center of the field-of-view, in the x- and z-directions to the centroid of the joint. This error is fed back to a PID controller and voltage commands are sent to the x- and z-axes to drive the errors to zero as quickly as possible.

4.3 CONTROL COMPONENTS

The various components associated with the floor drive system are explained in detail in *Motion Control for a Tracking Fluoroscope System* [6]. The host computer, which is carried on-board the TFS, is a National Instruments model PXI 8186. The host computer is connected to a remote desktop computer via a Linksys wireless router. Subject position with respect to the platform is obtained using a laser device, Sick model DME 3000-2. Eight servo amplifiers are used to supply necessary power to the eight axes of motion; two for the driving motors, two for the steering motors, two for the x-axis actuators, and two for the z-axis actuators. Eight 12V batteries are used, and connected in series of two batteries each, in order to provide 24V to the amplifiers. The drivers are controlled using an eight-axis motion card integrated into the host computer. Pictures of the previously mentioned components can be found in Appendix C, Figures C.3 – C.8.

CHAPTER 5. FLUOROSCOPE SYSTEM

Fluoroscope systems consist of an x-ray source and an x-ray detector. The x-ray source will be mounted on one x-z table while the x-ray detector will be mounted on the other x-z table. The weight of the actuated components is limited to 5 kg with a center of gravity 150 mm from the mounting base on the z-axis. Considering the load limit safety factor of the x-z tables and assuming the center of gravity is moved closer to the mounting base, the weight could be increased to around 9 kg. These weight limits are necessary to achieve the maximum accelerations required for tracking the ankle of a 95th percentile tall person walking at a speed of around 2 m/s.

When sizing an x-ray source, the necessary specifications include milliamps (mA), kilovolts (kV), exposure time, focal spot, physical size limitations, maximum weight, and beam coverage. The material of the tube is also important due to the high accelerations to which the moving mass will be subjected. To discuss the possibilities of designing a successful fluoroscope system, a short description of basic x-ray physics is necessary.

5.1 BASIC X-RAY PHYSICS

The following is a summary of *Adventures in Radiography* "Basic X-Ray Physics" [7].

5.1.1 Description of X-Ray Tubes

There are two common types of x-ray tubes; stationary anode and rotating anode. Figure 5.1 shows the schematic of a rotating anode tube. Electrons are accelerated from the cathode side to the anode side or target. The tungsten target is rotated by a motor to spread the heat produced by the change in kinetic energy of the accelerated electrons. For a stationary tube, the anode is a fixed piece of tungsten mounted onto a large copper slug. The copper slug transfers the heat from the tungsten to the surrounding medium, which is usually oil.

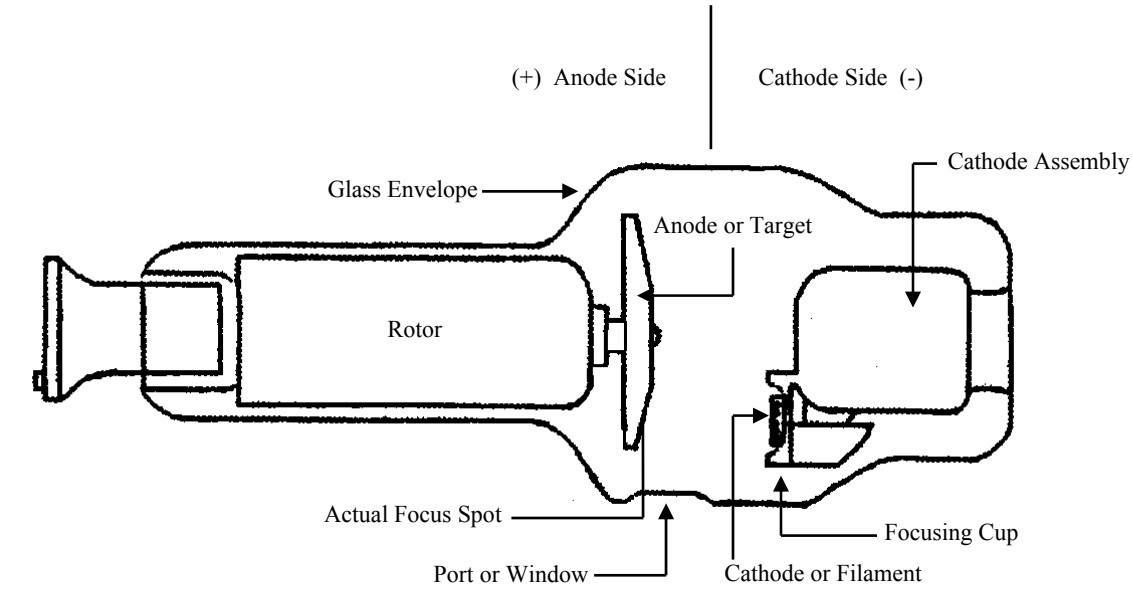


Figure 5.1 Schematic of a rotating anode x-ray tube

The cathode consists of a filament, which is a coil of tungsten wire, and a focusing cup, which surrounds the filament on three sides and directs the electrons toward the anode. The anode and cathode assemblies are enclosed in a glass envelope and a vacuum is drawn. In some cases, tubes can be designed with a ceramic envelope, which may be more durable and thus appropriate for the TFS. The envelope containing the cathode and anode assemblies is called an insert. The insert is mounted inside a metal enclosure lined with protective lead shielding everywhere except the port. The port allows the x-rays to escape from the tube in order to travel to the x-ray detector. Usually, the metal enclosure is filled with oil, which is used as an electrical insulator and a heat absorber. The oil helps to prevent arcing and discharging when high kilovolts are applied and it transfers the heat to the metal case, which transfers the heat to the surrounding air. An external heat exchanger could be used to circulate the oil to increase heat transfer capabilities while reducing the necessary moving mass of the source.

5.1.2 Producing X-Rays

Three things must happen to produce x-rays; there must be a source of electrons, the electrons must be accelerated, and the electrons must suddenly stop. The cathode side of the tube produces the electrons by applying mA to heat the tungsten filament. As the filament becomes hotter, more and more electrons drift away from their nucleus creating an electron cloud around the filament. To accelerate the electrons, kVs are applied across the tube. This causes the cathode to become very negative and the anode to become very positive. This difference in potential draws the electrons to the anode side of the tube. Higher kV creates higher electron acceleration.

The accelerated electrons hit the anode and stop suddenly, creating x-rays and heat. About 99% of the kinetic energy of the accelerated electrons is converted to heat. Only about 1% of the kinetic energy is converted to electromagnetic energy, or x-rays. The useful beam of x-rays is comprised of two types of radiation, characteristic radiation and Bremsstrahlung radiation. Figure 5.2 shows both types of radiation.

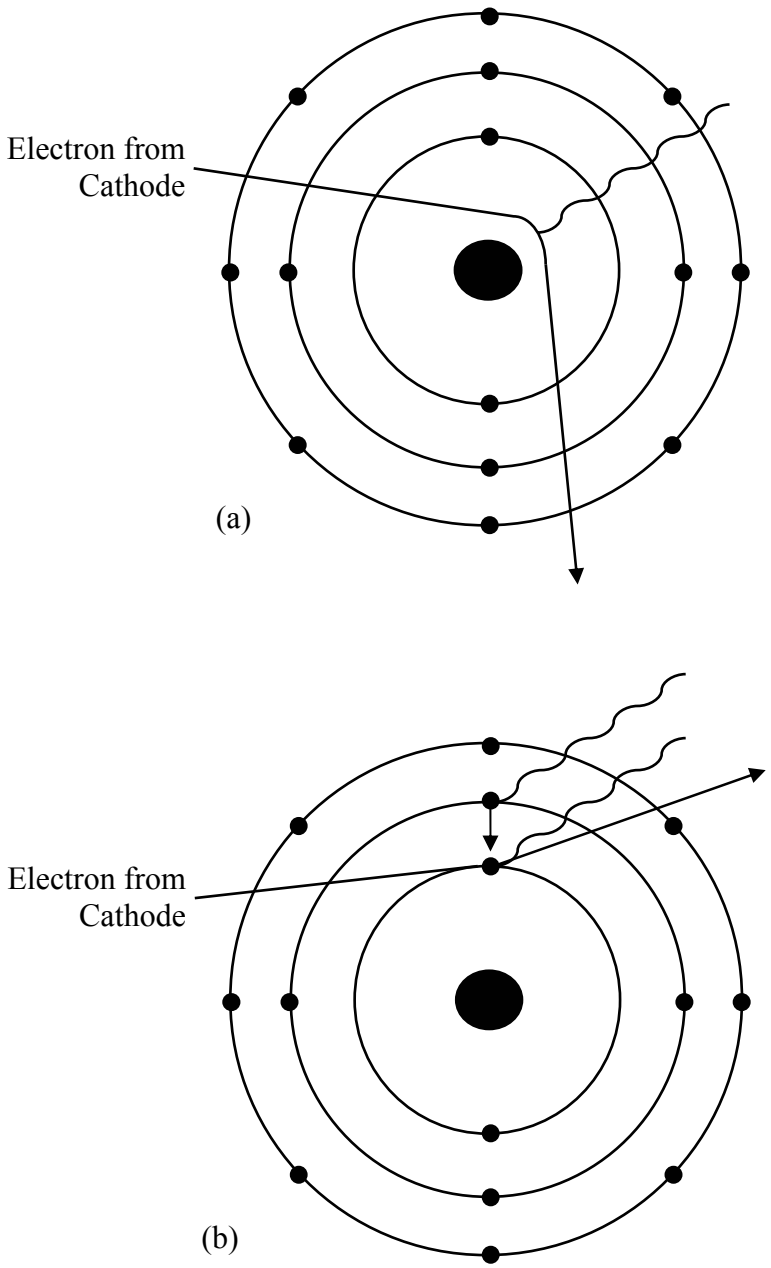


Figure 5.2 Characteristic (a) and Bremsstrahlung (b) radiation

Characteristic Radiation. In characteristic radiation, an electron, which is accelerated from the cathode to the anode, ejects an electron from the target atom's inner shell. The target atom is then unstable, so an electron from the next outer shell moves in to fill the vacancy caused by the ejected electron. The movement of electrons creates x-rays and accounts for about 10-15% of the useful beam.

Bremsstrahlung Radiation. In Bremsstrahlung radiation, an electron from the cathode side passes near the nucleus of the target atom and is deflected off its original path. In order for the electron to change directions, it must give up kinetic energy in the form of Bremsstrahlung radiation. This conversion of kinetic energy accounts for 85-90% of x-rays in the useful beam.

Focal Spot. The focal spot of an x-ray tube is determined by the size of the filament in the cathode assembly. Small filaments produce a small focal spot. The smaller the focal spot, the better the image detail. However, higher mA produces more heat on the filament to create more x-rays and therefore requires a larger filament to withstand the heat. The actual focal spot is the area on the anode where electrons from the cathode make contact. The effective focal spot is the same area as the actual focal spot but viewed from the perspective of the cathode. The effective focal spot must be specified when procuring an x-ray tube.

Heat Units. The number of heat units (*HU*) produced during an x-ray exposure can be determined by Equation 5.1.

$$HU = kV \cdot mA \cdot EXPOSURE\,TIME \tag{5.1}$$

Tube rating charts specify the maximum exposure time given a certain kV and mA. Manufacturer anode cooling charts can be used to determine the cooling time required if multiple consecutive exposures are made at a certain heat unit value.

5.1.3 X-Ray Detection

X-rays are emitted from an x-ray source and are absorbed at varying levels dependent on the target material density. If an x-ray beam is directed at a person's joint, the soft tissue around the joint does not absorb the x-rays as much as the hard material of the bone. The x-ray detector, typically an image intensifier, is placed on the opposite side of the joint on centerline with the x-ray source and absorbs the remaining x-rays. Larger concentrations of x-rays create a darker image on the film while lesser concentrations appear brighter. The contrast of dark and light produces a visible black and white image of the joint.

5.1.4 Basic X-Ray Physics Summary

Kilovolts control the quality of the x-ray beam and are responsible for accelerating electrons from the cathode to the anode. Faster electrons result in higher energy and the resulting x-rays can penetrate thicker materials. As kilovolts are increased, the contrast between black and white in the radiographic image decreases. Milliamps determine the number of electrons removed from the cathode into the electron cloud. Higher mA results in greater beam intensity and darker images. Exposure time is the length of time x-rays are produced. Longer exposure times result in darker radiographs than shorter exposure times. The focal spot determines the quality of the image and is dependent on the size of the filament, which is dependent on the required milliamps.

5.2 X-RAY SOURCE

As mentioned in previous sections, the moving mass of the x-ray source must be less than 9 kg. The weight of an x-ray source is dependent on the required kV, mA, focal spot, exposure time, and beam coverage. The higher the kV, mA, and exposure time, the more heat is produced which in turn requires more cooling. Cooling is typically achieved using oil contained within a heavy lead-lined enclosure. The following section discusses the specifications for a TFS x-ray source.

5.2.1 Specifications

The specifications for the x-ray source are assumptions based on previous research using stationary fluoroscope systems at the Center for Musculoskeletal Research at the University of Tennessee. Table 5.1 shows the desired specifications for an x-ray source to be integrated onto the TFS. Ankles and knees may be observed while maintaining a moving mass of 9 kg or less with current off-the-shelf x-ray sources. Source-Ray, Inc. model SR-100-3KF is a compact unit containing the x-ray source, generator, oil, and shielding, which weighs approximately 9 kg and costs $22,190. However, the hip joint probably requires more energy to obtain a suitable image.

These specifications are assumptions based on previous research. Phantom images of the joints should be taken to more accurately determine energy levels and exposure techniques. Energy level requirements are based on the density of the joint, desired resolution for real-time control, exposure time, and size of the imaging area. More cooling is required for higher energy levels resulting in more oil, which adds more weight. An external heat exchanger could be designed to circulate the oil through the tube housing. However, this may not be necessary depending on the actual energy requirements.

The mechanical integration of an x-ray source should minimize the chance of breaking the glass tube. Ceramic tubes do exist and may be a viable option for moving at high accelerations. As mentioned previously, only essential components should be servo-driven so that the moving mass is as light as possible.

Table 5.1 Desired x-ray source specifications

	Hips		Ankles/Knees	
Voltage	125	kV	100	kV
Current	5	mA	3	mA
Focal Spot	0.3 - 0.6	mm	0.3 - 0.6	mm
Weight	≤ 9	kg	≤ 9	kg

5.3 X-RAY DETECTOR

Most fluoroscope systems utilize image intensifiers to detect the x-ray beam and produce an image. This is not a realistic option for the TFS because image intensifiers typically weigh in the range of 20 to over 45 kg. The x-z tables are limited to carrying a load of 9 kg or less. Chapter 7 discusses alternative methods which would eliminate the need for x-z axis linear actuator tables. The following sections discuss systems which would be integrated on the x-z tables.

5.3.1 Specifications

Initial specifications for a TFS x-ray detector are shown in Table 5.2. As with the x-ray source, these specifications are assumptions based on previous research. Exact frame-rate and resolution required for acceptable real-time tracking will be determined in future experimental trials. Many inquiries have been made with vendors of x-ray detectors, and two main strategies have been explored thus far.

Security Defense Systems Corporation, a subsidiary of Kodex Inc., has performed analysis and testing of scintillation screens used in combination with high speed cameras. They have also proposed the use of flat panel digital x-ray detectors because such units are lighter-weight and display more uniform resolution when compared to image intensifiers. The following sections discuss the two methods proposed by Security Defense Systems.

Table 5.2 Desired x-ray detector specifications

Weight	≤ 9	kg
Frame-Rate	100 +	frames/s
Exposure Time	10	seconds
Resolution	12 +	lp/mm

5.3.2 High-Speed Camera with Scintillation Screen

Security Defense Systems suggested the possibility of using a stationary scintillation screen and servo-driving a light-weight, high-speed camera behind the screen to capture the images in real-time. This would greatly reduce the moving mass mounted to the x-z table. Scintillation screens are used in screen/film radiography and fluoroscopy to absorb x-ray beams so that an image can be retrieved from the screen. The screens are typically made of gadolinium oxysulfide and cesium-iodide (CsI) [8]. The scintillating material converts the x-ray photons, which are not already absorbed by the target, into visible light photons. The high speed camera would be used to capture the visible light photons from the screen. The screen and camera would have to be housed in a light-tight enclosure.

Security Defense Systems tested three different types of screens with Redlake high-speed camera model MotionXtra HG-LE, shown in Figure 5.3. The tests results produced images of very good quality at sufficient frame-rates. However, the dosage requirements were far too high to meet FDA requirements for human exposure limits.

5.3.3 Flat-Panel Detector

The most realistic option for TFS x-ray detection with available technology may be a flat-panel detector (FPD). Varian Medical Systems offers the PaxScan® 2520, a 250mm x 200mm digital FPD which weighs around 9 kg. However, the maximum frame-rate is only 30 fps. The frame rate is limited by the scintillation material and integrated electronics. Higher performance FPDs do not exist in the current market.

In order to track the joint in real-time, error feedback will probably need to be updated over 100 times per second at the maximum desired walking speed. If the walking speed is slower, a lower frame-rate may be sufficient to prove the TFS prototype. When technological improvements are made to FPDs, a higher frame-rate detector could replace Varian's PaxScan® 2520 model.

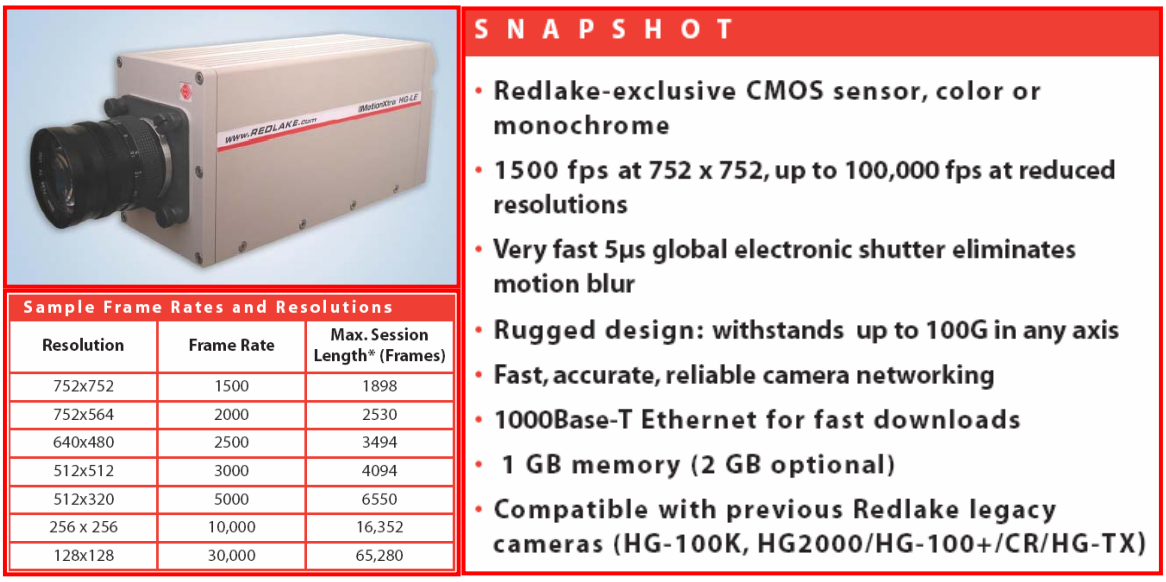


Figure 5.3 Redlake high-speed camera model MotionXtra HG-LE



Figure 5.4 Varian Medical Systems PaxScan® 2520 flat panel detector

In digital detection, the x-ray tube sends a beam of x-ray photons through the target. The remaining x-ray photons which are not absorbed by the target, strike a layer of the scintillation material. The scintillation material converts the x-ray photons into visible light photons. The light photons then strike an array of photodiodes which converts them into electrons. The electrons activate the pixels in a layer of amorphous silicon, which generates electronic data. The computer then converts the data into a high-quality image of the target [8]. This image would then be used to feedback the position of the joint with respect to the centerline of the frame. Varian Medical Systems has a technical publication brochure for the PaxScan® FPD which explains digital detection in detail. Appendix D contains the brochure material. Figure 5.4 shows the PaxScan® 2520 digital detector.

5.3.4 X-Ray Detector Summary

The first method of detection utilizes a scintillation screen and a servo-driven high speed camera. Test results showed sufficient resolution and frame rates, but the x-ray dose requirements were unacceptable. The second method of using a flat panel detector will work for slower walking speeds than those specified for the TFS design. Future FPD technology improvements will provide faster frame-rates and even lighter-weight assemblies. The TFS design will accommodate a faster FPD when such a product becomes available.

CHAPTER 6. SAFETY

As shown in Appendix A, Figures A.5, A.6, and A.7, the measurement cavity of the TFS surrounds the subject on three sides during operation and the subject walks within inches of the system. Three possibilities are of importance when improving the safety of TFS operation; (1) the fluoroscope line-of-sight being misguided, (2) the TFS overrunning the subject, or (3) the TFS running into external objects or people.

Many of the people who have undergone joint replacement procedures are elderly or impeded in their movement and are less likely to avoid a collision with the system. The three previously mentioned scenarios could occur because of sensor problems, drive motor electronic faults, or on-board computer malfunctions [9].

6.1 FLUOROSCOPE LINE-OF-SIGHT

Regulations on fluoroscope systems require that the subject not be exposed to unnecessary radiation. Calibrations are required to ensure that the cone of the emitted x-ray beam does not extend beyond the x-ray detector. The prevailing technique for meeting this expectation is to use a heavy, rigid c-bar structure to mechanically connect the x-ray source and image intensifier. Figure 6.1 shows the c-bar concept. This concept is not feasible for TFS design. The objective if the TFS is to allow the patient to feel as comfortable as possible while testing. If a c-bar were used to couple the x-ray detector and x-ray source, the structure would interfere with the walking motion of the subject. Different techniques must be used to prevent unnecessary radiation exposure.

The x-z linear actuators are used to servo-drive the x-ray source and x-ray detector on the TFS. The control systems for these tables provide the precision necessary to maintain the required line-of-sight. However, hardware and software faults could cause the drives to lose synchronization. Therefore, multiple layers of safety constraints should be implemented to back up initial safety constraints.

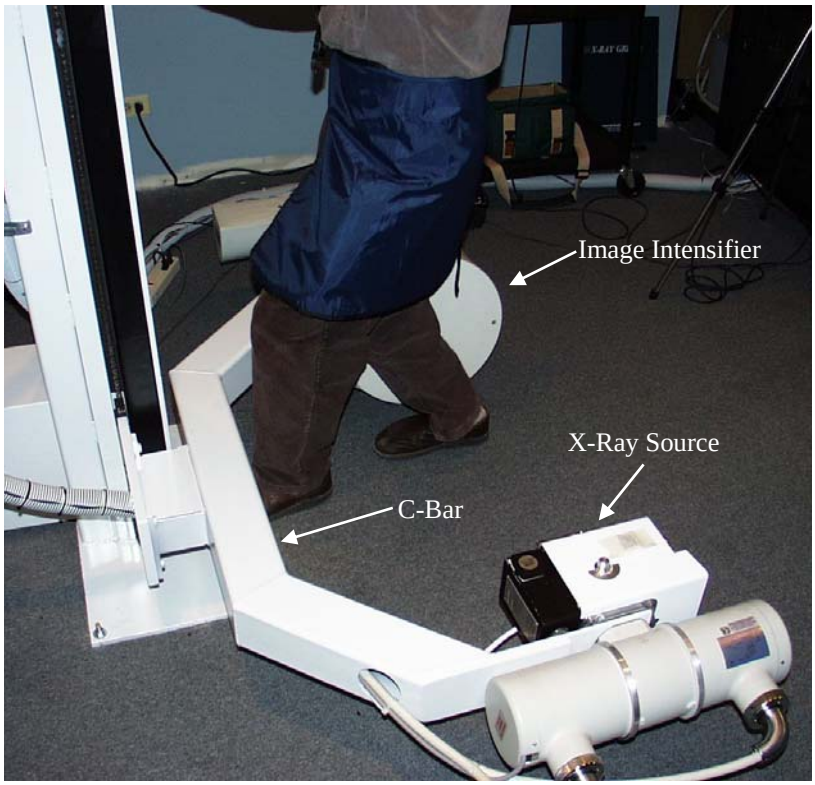


Figure 6.1 Stationary c-bar style fluoroscope unit

The mechanical design of the joint tracking system assures that the center of the fluoroscope line-of-sight is localized to the center of the ankle, knee, or hip region. It is possible that the alignment between the x-ray source and x-ray detector could drift and leak unnecessary radiation. This drift could be detected using a simple laser beam projection from one side to the other. Additionally, independent radiation sensors could be used to monitor the possibility of the x-ray beam traveling outside the x-ray detector field-of-view.

As with all applications involving radiation exposure, lead shielded clothing should be used to protect areas of the body which should not be exposed to radiation. Only the operator and subject should be allowed in the testing area and radiation exposure time should be kept to an absolute minimum. As an additional backup, the x-ray source should be aimed towards an outside wall of the building if possible.

6.2 MEASUREMENT CAVITY PROTECTION

The subject walks within the measurement cavity of the TFS and is only a short distance from the chassis and the joint tracking system x-z tables. The subject must be protected in every way possible from contact with the chassis and joint tracking system.

6.2.1 Chassis Protection

The key parameter in protecting the subject from impact with the TFS is measuring the standoff distance of the subject from various points on the frame within the measurement cavity. These measurement sensors and processing electronics should be independent of the on-board computer and should provide fast response. If the standoff distance sensors should fail, contact and proximity sensors, such as bumper switches and light curtains, could be used as a second line of defense. If the person were too close to the carriage, the light curtain would de-energize the TFS. If the light curtain or other proximity sensors should fail, and the chassis comes in contact with the person, bumper switches would de-energize the system.

Operational levels and conditions of the MIWD units should be monitored as an additional line of defense. Motor currents can be compared to speed values to determine if the chassis has encountered an obstruction. Drive wheel accelerations and speeds should be monitored as well to determine if the movement of the chassis is within appropriate bounds.

Many TFS applications do not involve utilizing the full speed capabilities of the MIWD units. Therefore, the power output to the motors should be limited except in special cases. Power output to the motors could be controlled by a manual, on-board, hard-wired switch. In addition, the user interface software should require confirmation if the power output to the motors needs to be increased.

6.2.2 Joint Tracking Protection

As mentioned in previous chapters, the fluoroscope system is servo-driven up to 2G's acceleration in the x-direction and up to 1G acceleration in the z-direction. The momentum resulting from accelerating a 5 – 9 kg load within inches of the subject could be extremely hazardous. If possible, a stationary physical boundary should be used to guard the subject from the moving components. If a stationary boundary impedes the x-ray emission and detection process, then proximity sensors, in combination with contact sensors, should be implemented onto and around the moving objects. If any part of the subject is too close to the fluoroscope system, the x-z tables should de-energize, apply the brakes, and maintain their current position. Sensor response times should be sufficient to stop all motion before contact. Figure 6.2 shows a possible layout of standoff distance sensors and bumper switches.

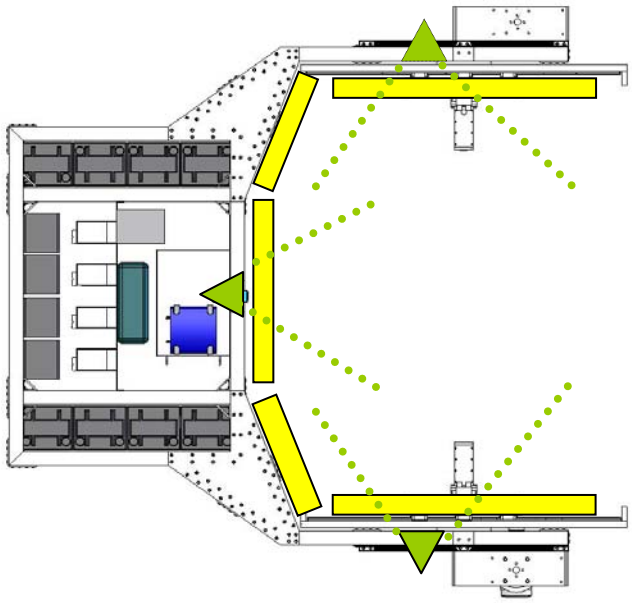


Figure 6.2 Possible standoff distance sensor layout and bumper switch layout

The x-z tables are manually positioned, vertically, on the wings of the TFS platform before testing depending on which joint is being viewed. Figures A.5, A.6 and A.7 in Appendix A show the three configurations for viewing ankles, knees, and hips respectively. The TFS frame design allows the x-z tables to be positioned very close to the ground for ankles. When the stroke length of the z-axis is considered, the fluoroscope system could easily come in contact with the floor. To avoid this potential safety hazard, there should be a mechanical limit on the linear bearing used to manually adjust the x-z table position. Software limits could also be implemented to maintain a certain distance from ground level to avoid damaging the fluoroscope system.

6.3 EXTERNAL PROTECTION

The TFS is designed to allow for an arbitrary walking path as determined by the patient. The patient can not be expected to pay attention to outside obstacles such as walls, appliances, or other people while performing a fluoroscope test. It is imperative that the subject's only concern be that of walking naturally. Therefore, there must exist multiple layers of protection to prevent the patient from "walking the machine" into or over an external object.

Sonar sensors emit a cone of sonar at an angle which is dependent on the type of sensor used. If an object appears within the cone at a predetermined distance from the sensor, feedback from the sensor can be used to de-energize the system. Sonar proximity sensors should be used to detect any object which is too close to the TFS chassis and shut everything down or at least halt the motion of the floor drive system. The TFS weighs approximately 454 kg and can travel up to 2.2 m/s. The dynamic friction coefficient of the MIWDs according to Transbotics' calculations is 0.5. The equation of motion of the machine is friction force equals mass times acceleration. The maximum distance it would take to stop the machine would occur when the MIWDs slip rather than roll. The acceleration of the machine equals the acceleration of gravity times the friction coefficient. Equations 6.1 and 6.2 show the equation of motion and acceleration

relationship. Equations 6.3 - 6.5 show time, velocity, and distance relationships used to calculate the maximum distance the TFS would travel if stopping began at full speed and the MIWDs experienced slipping [3].

$$F = ma \tag{6.1}$$

$$a = gf \tag{6.2}$$

$$v = v_o + at \tag{6.3}$$

$$t = \frac{-v_o}{a} \tag{6.4}$$

$$d = d_o + v_o t + \frac{1}{2} a t^2 \tag{6.5}$$

The acceleration of gravity (g) is 9.8 m/s^2, the friction coefficient (f) is 0.5 and thus, the acceleration (a) in the forward direction is calculated to be -4.9 m/s^2. The initial velocity (v_o) is the maximum speed of the TFS, which is 2.2 m/s and the final velocity (v) is 0 m/s. Equation 6.3 is used to derive Equation 6.4, which is used to calculate the stopping time required, 0.449 seconds. If the initial position of the TFS, when the brakes are applied, is used as the origin then d_o is 0 meters. Finally, Equation 6.5 can be used to calculate the maximum stopping distance of the TFS if initially traveling at full speed.

The maximum stopping distance is calculated to be just under 0.5 meters. Using a safety factor of two results in a maximum stopping distance of one-meter. Sonar proximity sensors should be used to detect anything within one-meter of the TFS chassis during testing. The system would de-energize and the brakes would be applied, allowing plenty of time for the machine to stop before impact.

The proximity sensor layout should be designed so that all sonar cones overlap and surround the TFS chassis at its full height and detect any objects within one-meter of the entire chassis perimeter. Sonar could also be used for measurement cavity protection around the moving components of the fluoroscope system. Figure 6.3 shows a possible layout of sonar proximity sensors and a light curtain used for internal protection. The control architecture of the floor drive system could be designed such that if the proximity sensors detect an object within the one-meter buffer-zone, the MIWDs would stop moving but power would still be available to the drives. This would allow the subject to reverse direction and move away from the object to continue the test without the inconvenience of having to power up and reorient the machine.

6.4 OPERATOR INTERFACE, HARDWARE PROTECTION, AND E-STOPS

Multiple layers of safety strategy have been described for radiation protection, measurement cavity and subject separation, and external chassis protection. There are additional layers of safety which can be implemented to prevent unforeseen accidents.

The operator interface on the stationary desktop computer should be designed such that only the necessary controls are available for manipulation. For instance, if the operator needs to manually position the machine within the testing room, he or she would be required to select a "manual" button, and then a screen would appear to confirm the action. If confirmed, a new manual speed and position adjustment console would appear. If the speed is manually adjusted, there is always a chance of human input error. To avoid inaccurate speed adjustments, the control system is designed to limit the maximum speed of the machine to 0.5 m/s except in special high speed cases. In these cases, the operator would be required to select a "special case" button, which would also require confirmation before allowing the input of higher speed commands. Every control panel console should have a large and easily visible "STOP ALL" button which the operator can push to deactivate the control system at any time.

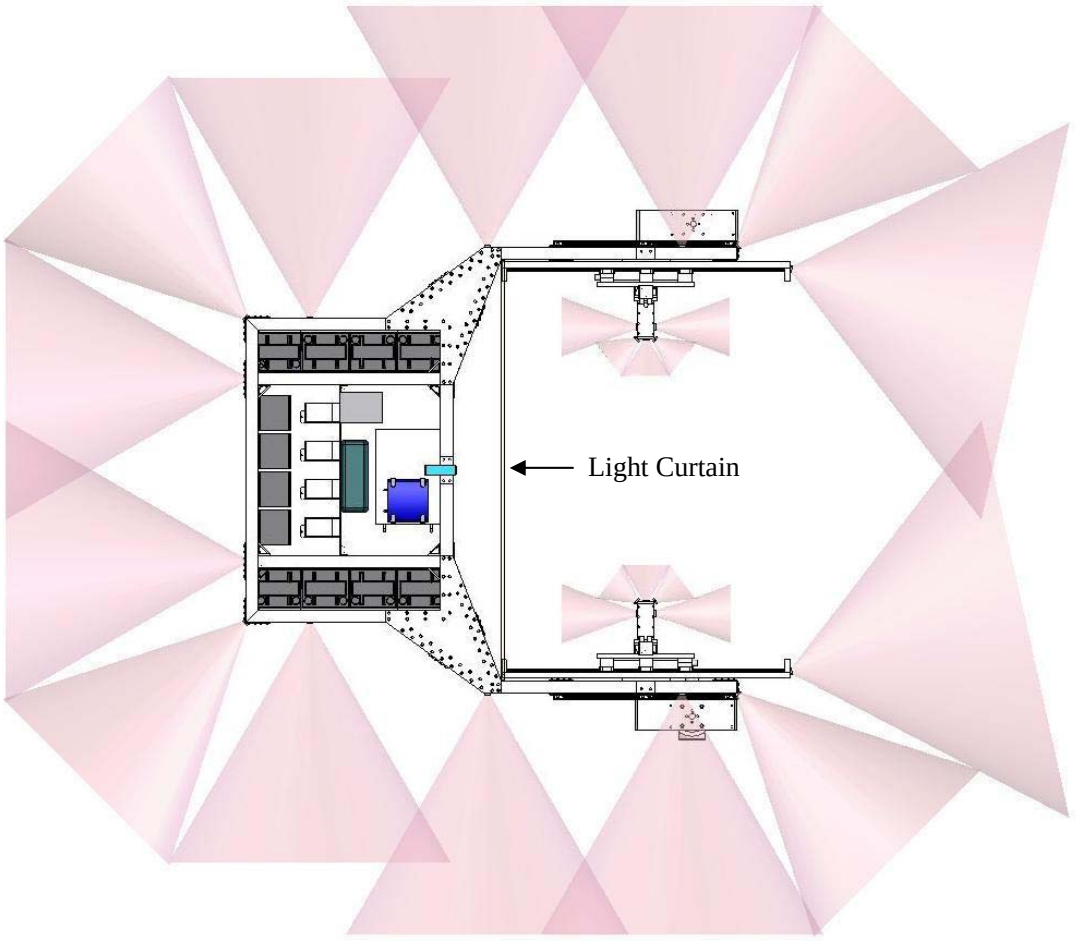


Figure 6.3 Possible sonar proximity sensor layout and light curtain

The carriage of the TFS chassis contains many electrical components and batteries which present the possibility of electrical shock. All components carried on the TFS should be secured to the frame to avoid shifting or contacting one another. The battery terminals should be covered to avoid shock hazards. The final design of the TFS should include a lightweight shell cover with doors to access components necessary for operation. Guarding techniques shall meet or exceed OSHA standards.

The final layer of safety should assume that unforeseen accidents are entirely possible. The only way to avoid such accidents is to disconnect all power from the TFS if something unexpected goes wrong. High-speed remote control switches should be provided to the operator and used to turn off power to all the drive motors in case of an emergency. Magnetic pull-cord e-stops could be attached to the subject so if she or he falls, the pull cord would deactivate all power supplies. There should also be a hard-wired e-stop button mounted on the chassis so that the subject and operator are able to push the button at any time.

6.5 SAFETY CONCLUSION

All of the previously mentioned safety improvements should be implemented with separate processing electronics and control systems. Regardless if anything happens to the on-board host computer, the safety devices should always be active. These active controls need to be implemented for high reliability and fast response times. The TFS should be operated with extreme caution and responsibility to protect the subject and operator from all predicted and unforeseen accidents.

CHAPTER 7. FUTURE WORK

The current version of the TFS is a prototype intended to prove the concept through extensive research, trials, and subsequent iterations. The TFS is ultimately intended to be used as a commercial product which would be manufactured and sold to hospitals and researchers. Many of the design considerations for a commercial product are different than those for a research prototype. This chapter presents a variety of the foreseeable design improvements and offers a glimpse at the possibilities for future applications of Tracking Fluoroscope Systems.

7.1 FRAME DESIGN

The current frame is constructed of 80/20® slotted aluminum extrusion as mentioned in Chapter 3 with an example shown in Figure 3.2. The reason for using 80/20® was to allow for design flexibility and easy modifications. The frame was designed and built before all additional components were received. Therefore, the size of the carriage could probably be reduced with some planning in the next design iteration. When the system has undergone sufficient testing and it is determined which components are absolutely necessary and which are not, the frame can be constructed of solid weldments of structural tubing. The wings would still have to be separate weldments than the carriage in order to fit through doorways. Structural 5cm x 5cm square aluminum tubing costs about $70 per 6.4 meters of length while 5cm x 5cm 80/20® extruded aluminum costs $136.73 per 6.4 meters. Regular aluminum tubing weighs about 1.64 kg/m while 80/20® weighs 2.18 kg/m [3, 10]. The current 80/20® frame is held together entirely by extruded tubing, brackets, and over 1000 bolts and nuts. If weldments were used, even more weight would be saved by not using as many nuts and bolts.

The wings are designed to detach from the carriage assembly. Additional casters and caster brackets can be mounted to the carriage and wings to support the wings and carriage assemblies independently. Currently, the power and control cables for the rear

MIWD unit are routed through the center of the 80/20® tubing. Also, the power and control cables for the x-z tables are mounted to the outside of the 80/20® frame continuously from wing to carriage. If the wings are removed, the cables will have to be disconnected from the drives. In a future design, cable disconnects should be implemented to allow for easy wing removal without having to re-route cables before and after moving through a doorway.

The geometry of the wings is dependent on the length of the x-z tables, the height of a tall person's hip, and the width of a larger person's body. In the hip configuration, the x-z tables are positioned at maximum height. In the ankle configuration, the x-z tables are positioned at minimum height. These constraints limit the angle of the structural support which attaches the wing to the frame. Figure 7.1 shows a detail of the wing support.

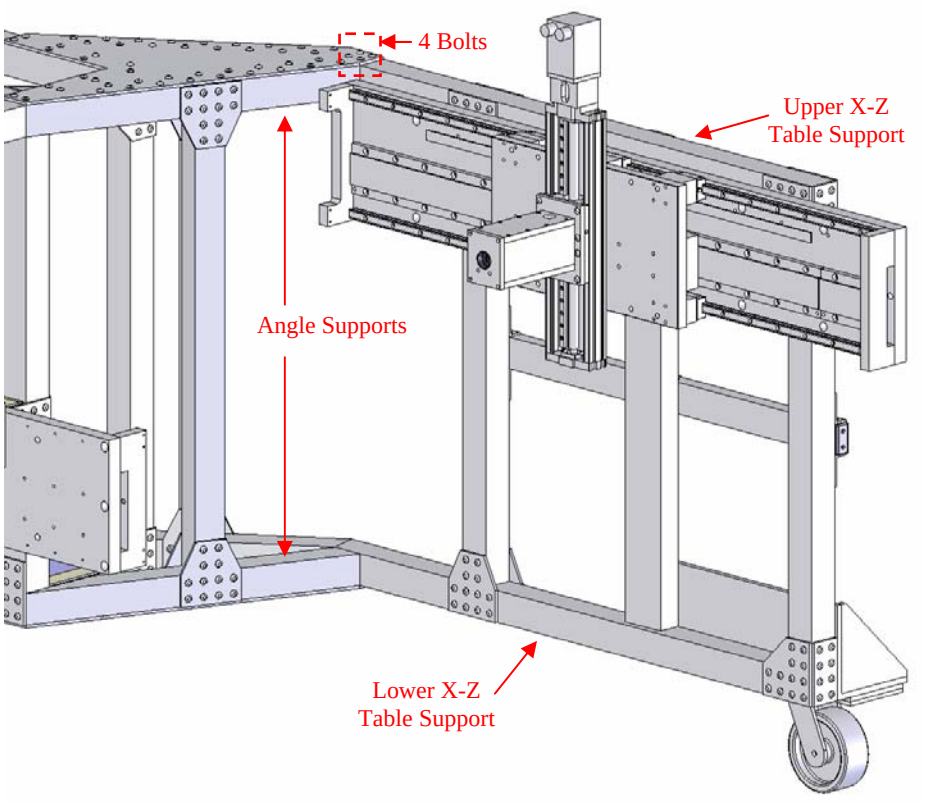


Figure 7.1 Hip configuration wing support detail

Only four bolts hold the upper x-z table support to the top angle support while four bolts hold the lower x-z table support to the bottom angle support. If the wing were a solid weldment, the connection joint would be much stronger. However, considering the geometric constraints of the frame and the use of 80/20®, there were not many other options. The vibration caused by servo-driving a load, in combination with the shear weight of the joint tracking system, may cause the eight connection bolts to slide within the extruded aluminum. To reinforce the wing support structure, temporary braces may be put in place depending on which joint is being tested. Figure 7.2 shows the knee configuration with additional support braces. To avoid interference with the x-axis table, bottom braces could be removed for ankle measurement and upper braces could be removed for hip measurement. Figures E.1 and E.2 in Appendix E show hip and ankle configurations.

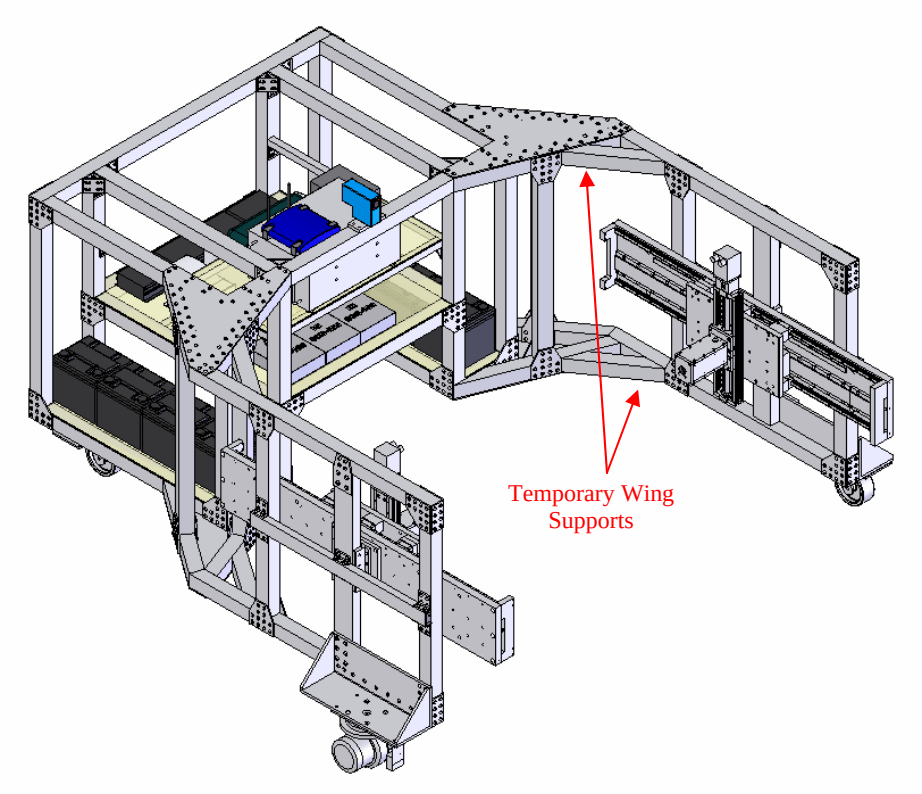


Figure 7.2 Temporary wing supports for knee configuration

Each x-z table is currently mounted to the wing using one 80/20® linear bearing, part number 6824, attached to the center of the x-axis table. Vibration is a major concern when producing a fluoroscopic image. The x-tables will need additional support on the sides of the table to prevent the tables from rotating about the center axis of the linear bearing. Linear bearing, 80/20® part number 6724, can be used to add support to the x-z tables as shown in Figure 7.3. The additional bearings were not purchased due to budgetary concerns. When all the frame components were purchased, the weight of the x-z axis tables was not known so the decision was made to try mounting the tables with one bearing and if additional support was needed, to purchase the extra bearings later. Side support linear bearings, 80/20® part number 6724, cost $65.50 each.

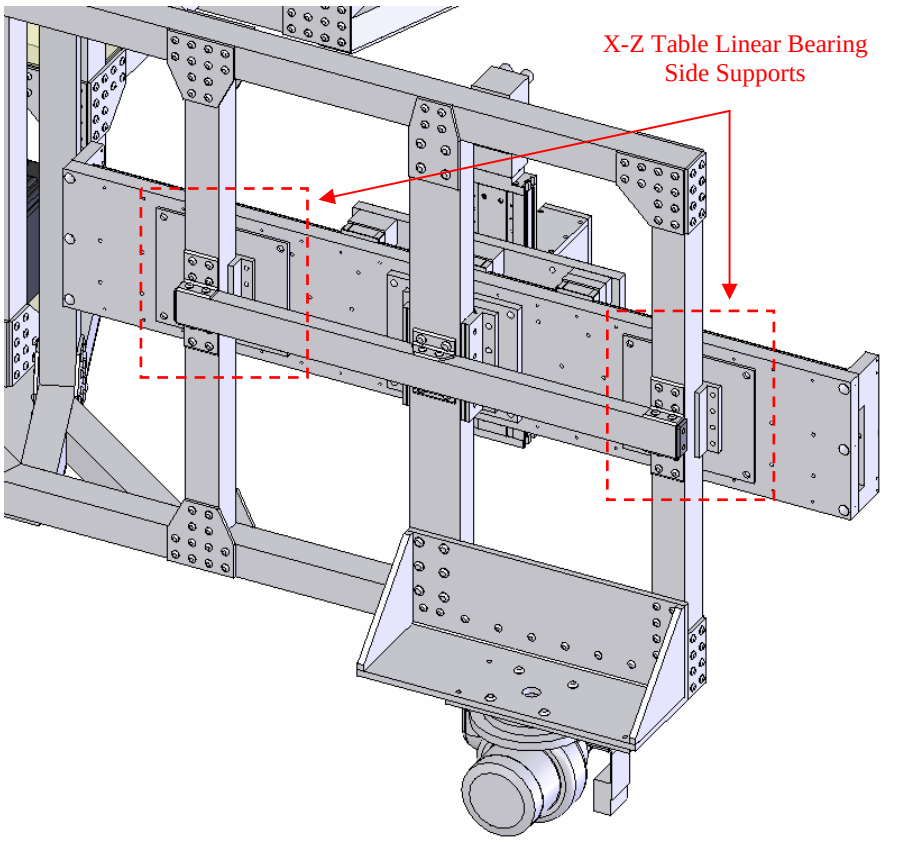


Figure 7.3 X-Z table linear bearing side support

7.2 ERGONOMICS

The current TFS design requires initial manual positioning of the x-z tables for each joint being measured. The x-z tables with the fluoroscope system mounted on the z-axes, will probably weigh, as a rough estimate, around 70 kg. Manual adjustment of the x-z tables requires two or three people to lower or lift to avoid the potential for injury. In future designs, a ball-screw driven actuator, either manual or automated, could be used to raise or lower the x-z tables to the initial desired height, which is dependent on each individual subject. Such a system was not included in the prototype for budgetary reasons. The concept of the TFS joint tracking system needs to be validated before investing additional funds. Section 7.4 of this chapter discusses the possibility of eliminating the x-z tables by using alternative x-ray source and detection strategies. If the x-z tables are not needed in the final design, then an automated height adjustment strategy may not be necessary.

The TFS is designed to be as comfortable to the patient as possible while providing an enjoyable and educational experience. When the system is tested and proven, a real-time LCD screen could be installed on the carriage of the TFS. This screen would allow the patient to view his or her joint through the entirety of the testing procedure. Additionally, as mentioned in Chapter 6, the entire chassis should be covered with an aesthetically pleasing cover, which would also provide additional safety from internal electronics.

7.3 POWER STRATEGY

Power is supplied to the TFS via on-board batteries and a tethered AC power cord. The host computer, wireless device, laser, and x-z table amplifiers all require AC power. The fluoroscope system power requirements are not yet known as of the writing of this thesis. In future designs, all on-board electronics should be powered by the on-board batteries if possible. An intermediate solution to this problem would be to use DC-to-AC power converters which could handle the Amp requirements for all the devices. Future component procurements should be handled with an ultimate power strategy in mind.

7.4 FLUOROSCOPE

Momentum created by accelerating 5 – 9 kg on each x-z table presents safety concerns as well as undesirable vibrations within the TFS chassis. Any feasible option which reduces the moving mass or eliminates the need for x-z tables is preferable to a servo-driven joint tracking system.

As flat-panel digital detectors become cheaper, lighter-weight, and have faster data transfer capabilities, another detection option could be to use a stationary array of detectors. The flat-panel array would cover the entire range of motion in the x- and z-directions and software could be used to track the image to feedback x- and z-axis errors to the x-ray source controller.

To minimize the movement of the x-ray source, a rotating tube could be designed. Instead of servo-driving the source through the entire range-of-motion, the source would follow the joint by rotating and redirecting the x-ray beam as the joint moves. This technique would require calibration and testing to ensure a sufficient dose of x-rays at all required angles. Energy requirements at extreme angles may not meet FDA dosage requirements so this method should be explored with caution.

Most of the weight of an x-ray source comes from the lead shielding and oil coolant. If a stationary lead cover were designed to enclose the entire x-z table, a movable window would have to be utilized as the tube is servo-driven. The x-ray beam would need to be directed out of the small movable window to avoid radiation leakage. Figure E.3 in Appendix E shows a preliminary conceptual design which incorporates a stationary shielding strategy. Another option, already mentioned previously, is to design a carriage-mounted heat exchanger which would circulate oil through the moving x-ray tube housing, thus reducing the moving mass. Only the necessary oil would be contained within the moving x-ray tube enclosure. The additional oil would be cooled in a stationary heat exchanger mounted on the TFS chassis.

7.5 DIRECTIONAL TRACKING

The feedback laser, which is currently used for stand-off distance control of the floor drive system, is only capable of tracking linear motion. The MIWD units on the TFS chassis provide omnidirectional capability. Eventually, a control system will be developed to track a subject in an arbitrary walking path. To achieve this objective, a new feedback sensor, or sensors, will need to be procured and installed in place of the current laser device. For example, a laser scanner or a smart camera could be used to sense directional changes in a person's walking path. The MIWD units would be driven and steered accordingly to maintain the desired subject position within the measurement cavity. Such a device has not yet been purchased due to budgetary limitations. It was decided to initially prove the system's capabilities with linear tracking and then explore directional tracking.

7.6 POTENTIAL TFS APPLICATIONS

Potential applications for Tracking Fluoroscope Systems are limited only by the imagination. Similar systems could be used to analyze athletic motions such as swinging a golf club, throwing a football, or running full-speed down a track. TFS could be used to aid surgeons during artificial implant procedures. For example, when a knee prosthetic is installed, the surgeon flexes the knee to check the alignment of the implants. TFS could be used to view the interactions of the implants within the leg which are not outwardly visible to the surgeon. Also, in the treatment of cancerous lung tumors, a large area of the lung is exposed to radiation due to the constant movement of the lung while the patient is breathing. Lung tissue is highly sensitive to radiation and can easily be damaged in this process. TFS could be used to maintain a visual "lock" on the tumor in order to apply radiation therapy to a more precise, and relatively smaller, area of the lung. Figures E.4 and E.5 in Appendix E show conceptual designs of an operating table TFS and a shoulder analysis TFS.

CHAPTER 8. CONCLUSION

The purpose of this thesis was to present the mechanical design approach to a Tracking Fluoroscope System, explore methods for integrating a feasible fluoroscope system, address safety concerns, and present future opportunities for improvement. Decisions made in the design process were based on a variety of constraints such as anthropomorphic data, maximum speeds of the floor drive system, the physical size of applicable components, and budgetary limits.

The current TFS design is capable of accommodating walking speeds of 2 m/s for the 95th percentile maximum stride length of a human's ankle, knee, or hip. The platform can rotate in any direction to allow for an arbitrary walking path which is determined by the subject. The frame is designed to be used in combination with a stationary walking platform in forward translation mode, to allow patients to walk up or down stairs and ramps. All associated components are contained within the TFS chassis. The frame is presently constructed of aluminum extrusion to allow for design modifications and adjustments during the trial stages of development.

The floor drive system utilizes feedback from a laser device, which determines the offset distance of the subject from the TFS chassis. The joint tracking system utilizes an image processing algorithm to determine the distance from the centerline of the joint to the centerline of the image frame. The x- and z-axis errors are used as feedback to maintain the joint within the image frame throughout the walking motion.

Chapter 5 presented the basic physics of x-rays and various options for integrating a fluoroscope system onto the chassis. Linear actuator tables will be used to servo-drive the x-ray source and detector in the x- and z-directions, independent of platform motion. Experiments need to be performed to accurately determine appropriate energy level requirements for an x-ray source and appropriate frame-rates and resolution requirements for an x-ray detector.

TFS operation requires that humans operate within close proximity to the robotic chassis. Many safety concerns were discussed and solutions were presented. The TFS should always be operated with the highest level of concern for safety.

Finally, future design improvements were presented including alternative fluoroscope strategies which may eliminate the need for x-z tables. Similar TFS designs could be used for a multitude of applications ranging from surgery assistance to rehabilitation to athletic motion analysis.

REFERENCES

[1] Oberg, T, Karsznia, A, and Oberg, K: *Basic gait parameters: Reference data for normal subjects, 10-79 years of age*, J of Rehab Res and Dev, 30, 2:210, 1993.

[2] Inman V.T., Ralston H.J., Todd F., *Human Walking*, Williams & Wilkins, Baltimore, MD, 1981.

[3] Oberg, E., Jones, F.D., Horton, H.L., Ryffel, H.H., *Machinery's Handbook*, 26th ed., Industrial Press, New York NY, 2000, pp.114, 152, 368.

[4] U.S. Department of Health, Education, and Welfare, *Weight, Height, and Selected Body Dimensions of Adults, United States, 1960-1962*, Rockville Maryland, June 1965.
<www.cdc.gov/nchs/data/series/sr_11/sr11_008.pdf>

[5] National Health and Nutrition Examination Survey, *Anthropomorphic Reference Data, United States, 1988-1994*, Tables 2, 3, 11, 12, 26, 27, Center for Disease Control.
<http://www.cdc.gov/nchs/about/major/nhanes/Anthropometric%20Measures.htm>

[6] Preliasco, G. R., *Motion Control for a Tracking Fluoroscope System*, Master of Science Thesis, Mechanical Aerospace Biomedical Engineering Department, University of Tennessee, Knoxville TN, 2005.

[7] Gregg, P. I., *Adventures In Radiography*, "Basic X-Ray Physics", Radiology Education Publications (A Division of Adventures, Inc.), Nashville TN, 2004.

[8] *PAXSCAN Flat Panel X-Ray Imaging*, Varian Medical Systems, Palo Alto CA, 11 Nov. 2004.
<www.varian.com/xray/pdf/Flat%20Panel%20Xray%20Imaging%2011-11-04.pdf>

[9] Hamel, W.R., *A Tracking Robot Concept for Human Musculoskeletal Diagnosis*, Mechanical Aerospace and Biomedical Engineering Department, University of Tennessee, Knoxville TN, 2005.

[10] 80/20 Inc., *80/20 The Industrial Erector Set*, Columbia City IN, 2004, pp. 44.

APPENDICES

APPENDIX A – ADDITIONAL MATERIAL FOR CHAPTER 3

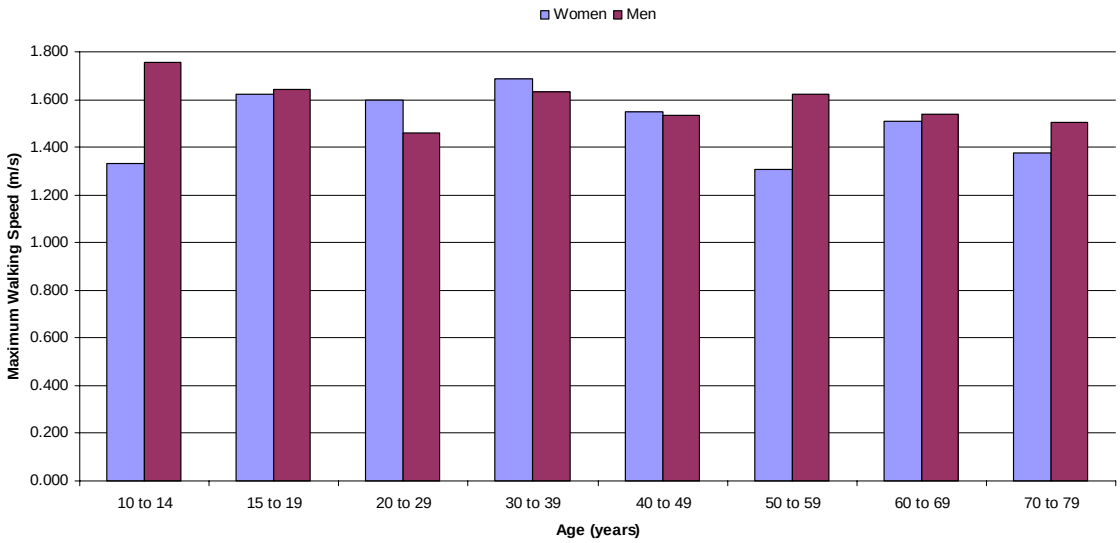


Figure A.1 Max walking speeds for 95% prediction interval of various age ranges

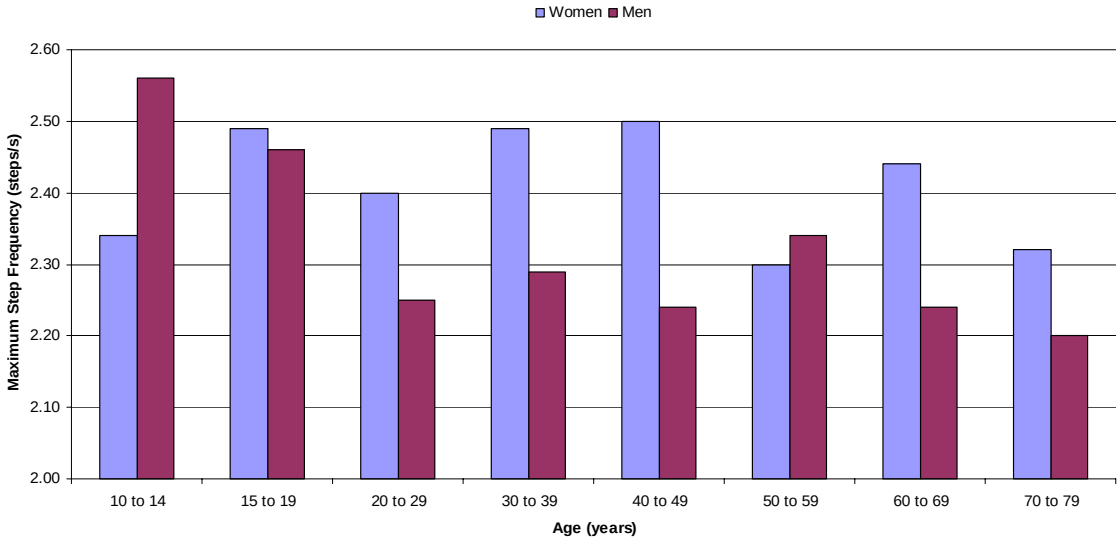


Figure A.2 Max step frequencies for 95% prediction interval of various age ranges

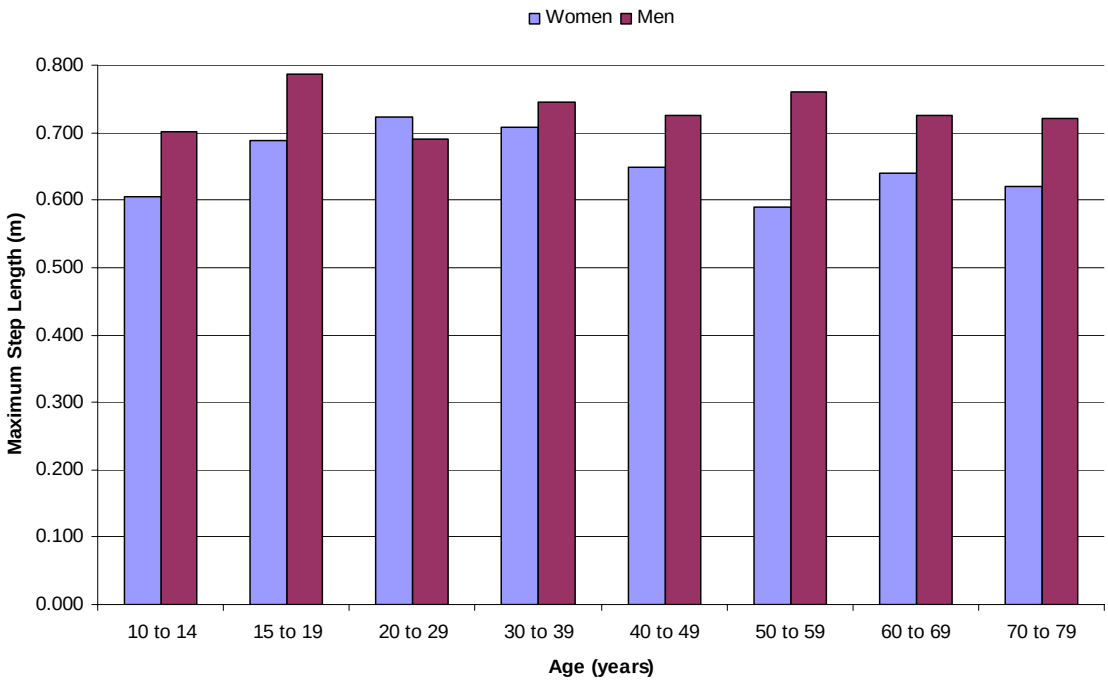


Figure A.3 Max step lengths for 95% prediction interval of various age ranges

Health statistics were obtained from a National Health Survey conducted from 1960-1962 [4]. This older data was compared to data obtained from 1988-1994 in a study conducted by the Center for Disease Control [5]. The extreme lower and upper limits of the data were respectively less than and greater than the limits for the most recent study. Therefore, the worst-case scenario data was used in sizing the x-z tables.

Table A.1 Health statistics of the National Health Survey in 1960-1962 for male

Men	Avg Height (cm)	Knee Height (cm)	Hip Height (cm)	Body Breadth (cm)	Weight (kg)
5 percentile	161.5	49.0	83.3	34.8	57.2
10 percentile	163.8	50.8	86.1	36.3	60.8
20 percentile	167.6	51.8	88.4	38.1	65.4
30 percentile	169.7	52.6	90.2	39.4	69.0
40 percentile	171.7	53.6	91.9	40.6	72.2
50 percentile	173.5	54.4	93.5	41.9	75.4
60 percentile	174.8	55.1	95.0	43.2	78.5
70 percentile	177.0	55.9	96.3	44.5	82.2
80 percentile	179.3	56.9	98.3	46.0	86.3
90 percentile	182.4	58.2	101.1	48.3	93.1
95 percentile	184.9	59.4	103.9	50.5	98.5
99percentile	189.5	61.2	108.5	54.4	109.4

Table A.2 Health statistics of the National Health Survey in 1960-1962 for female

Women	Avg Height (cm)	Knee Height (cm)	Hip Height (cm)	Body Breadth (cm)	Weight (kg)
5 percentile	149.9	45.5	78.7	31.2	47.2
10 percentile	151.9	46.2	80.0	32.8	50.4
20 percentile	155.2	47.2	82.8	34.3	53.6
30 percentile	157.0	48.5	84.6	35.8	56.8
40 percentile	158.5	49.0	86.4	37.1	59.5
50 percentile	159.8	49.8	87.9	38.4	62.2
60 percentile	161.8	50.3	89.4	39.6	65.4
70 percentile	163.6	51.1	90.9	41.4	69.0
80 percentile	165.4	52.1	92.7	43.4	74.5
90 percentile	168.7	53.3	95.5	46.5	82.6
95 percentile	170.4	54.6	97.8	49.0	90.3
99percentile	174.8	56.9	101.6	53.8	107.1

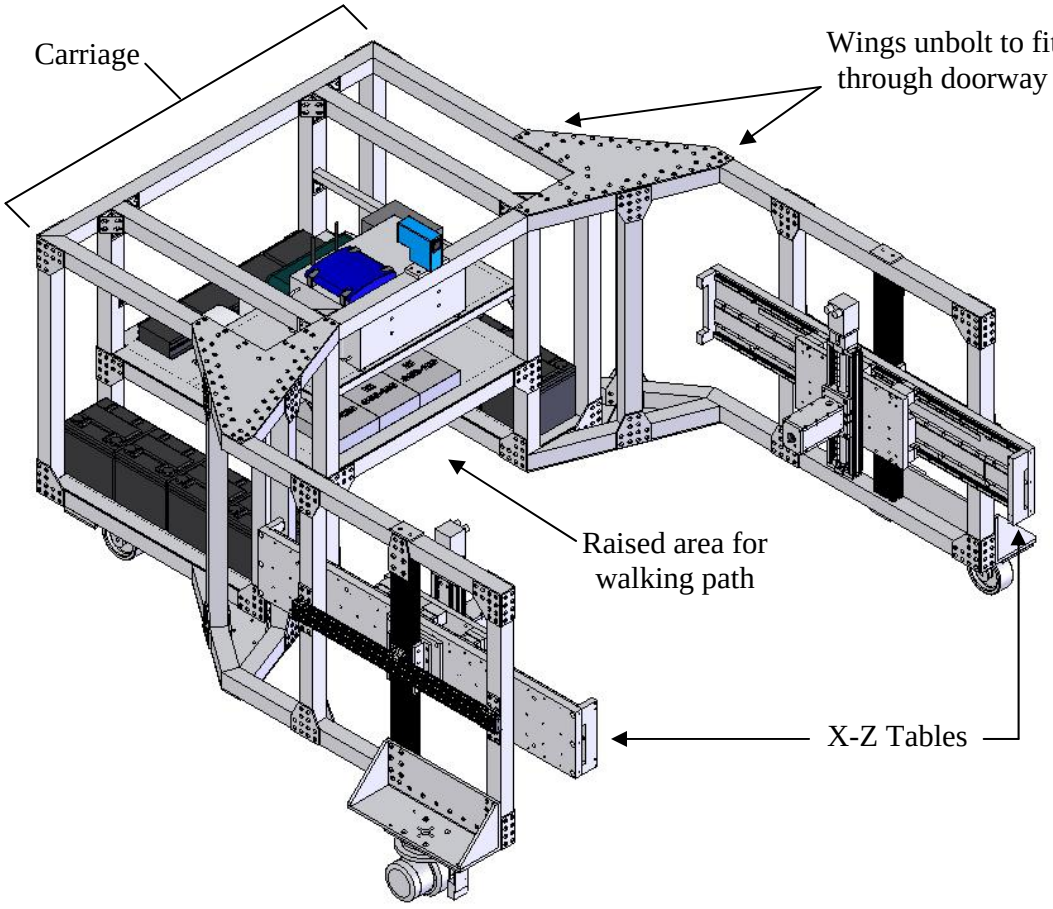


Figure A.4 Isometric view of final TFS assembly

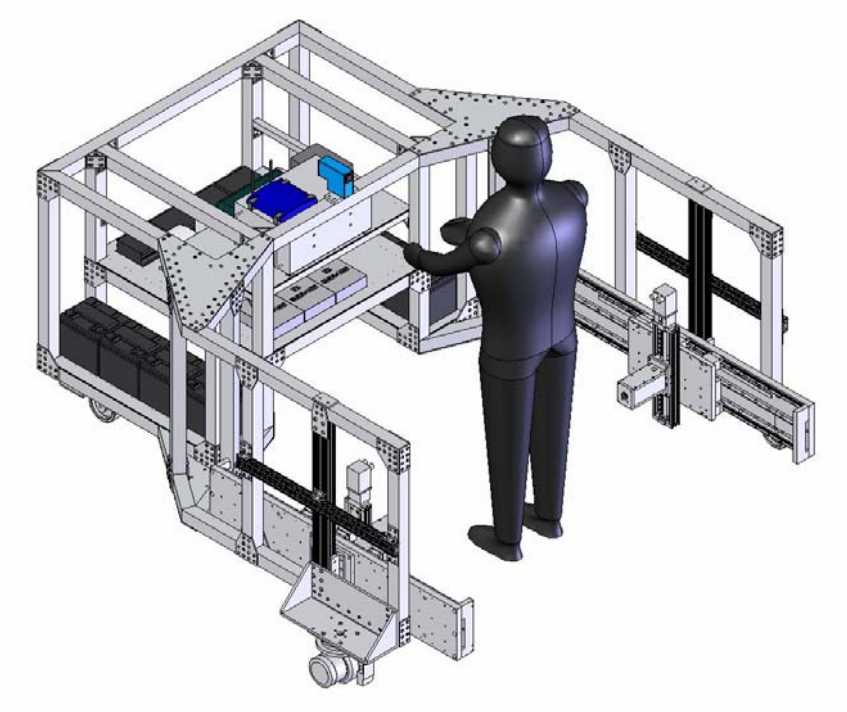


Figure A.5 Ankle configuration and body position

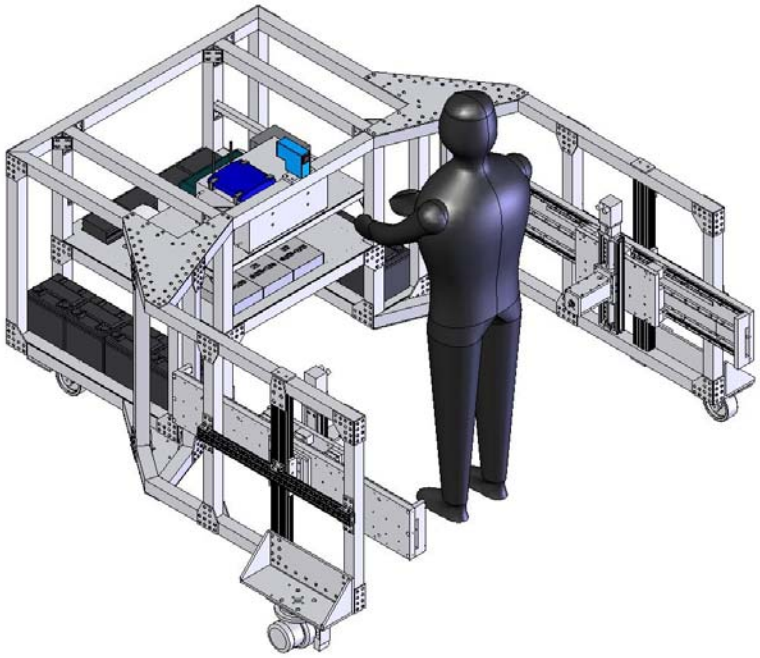


Figure A.6 Knee configuration and body position

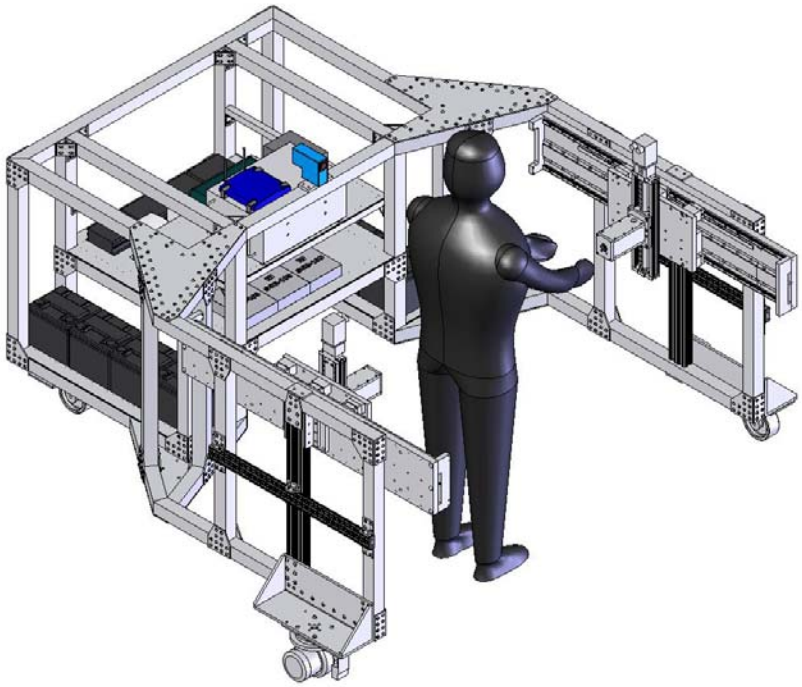
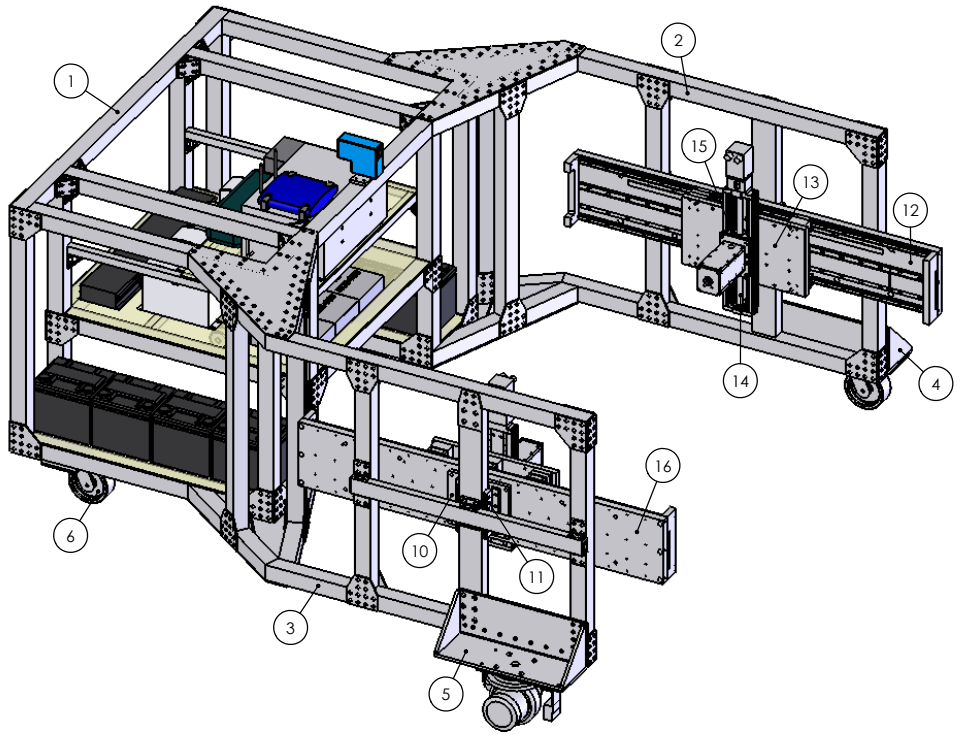
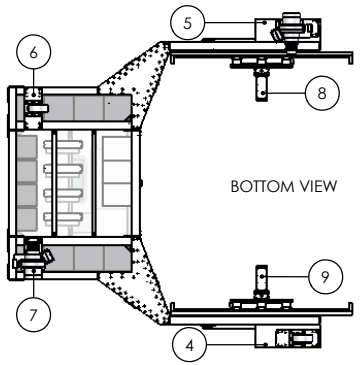


Figure A.7 Hip configuration and body position

APPENDIX B – TFS DETAILED DRAWINGS



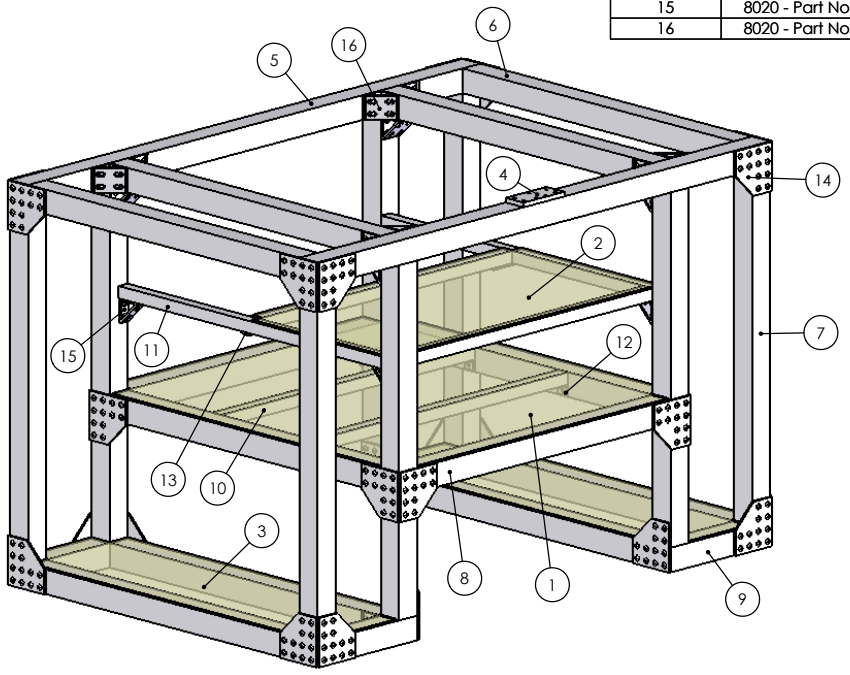
ITEM NO.	PART NUMBER	DESCRIPTION	1/QTY.
1	Carriage Assembly	Figure B.2	1
2	Wing Assembly	Figure B.3	1
3	Mirror Wing Assembly	Figure B.3	1
4	Rear Caster Assembly	Figure B.4	1
5	Rear MIWD Assembly	Figure B.5	1
6	Front Caster Assembly	Figure B.6	1
7	Front MIWD Assembly	Figure B.7	1
8	X-Ray Detector Simulation	Figure B.8	1
9	X-Ray Tube Simulation	Figure B.9	1
10	X Axis To 8020 Mounting Plate	Figure B.29	2
11	8020 - Part No. 6824	80/20	2
12	X_Table	Cornerstone	1
13	X_Carriage	Cornerstone	2
14	Z_Table	Cornerstone	2
15	Z_Carriage	Cornerstone	2
16	Mirror X_Table	Cornerstone	1

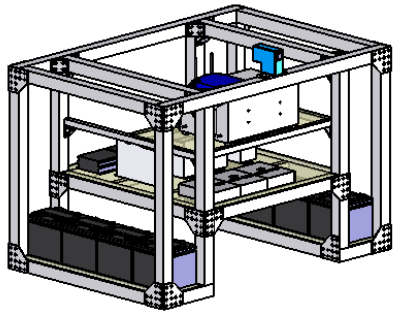


DRAWN:	R.B. CUNNINGHAM	CENTER FOR MUSCULOSKELETAL RESEARCH UNIVERSITY OF TENNESSEE	
CHECKED:	W.R. HAMEL		
DATE:	06-29-05	TITLE: Tracking Fluroscope Assembly	
MATL:	N/A		
NOTE:	N/A		
THE INFORMATION CONTAINED IN THIS DRAWING IS THE SOLE PROPERTY OF THE UNIVERSITY OF TENNESSEE. ANY REPRODUCTION IN PART OR AS A WHOLE WITHOUT THE WRITTEN PERMISSION OF THE UNIVERSITY OF TENNESSEE IS PROHIBITED.		DWG. NO. Figure B.1	QTY 1

Figure B.1 Tracking Fluroscope Assembly

ITEM NO.	PART NUMBER	DESCRIPTION	Frame/QTY.
1	Lower Shelf	Figure B.10	1
2	Upper Shelf	Figure B.11	1
3	Lower Side Shelf	Figure B.12	2
4	Laser Mount	Figure B.13	1
5	8020 - Part No. 2020 - 50 Inches	80/20 CUT TO LENGTH	2
6	8020 - Part No. 2020 - 30 Inches	80/20 CUT TO LENGTH	10
7	8020 - Part No. 2020 - 28.8 Inches	80/20 CUT TO LENGTH	8
8	8020 - Part No. 2020 - 28 Inches	80/20 CUT TO LENGTH	2
9	8020 - Part No. 2020 - 11 Inches	80/20 CUT TO LENGTH	4
10	8020 - Part No. 1010 - 28 Inches	80/20 CUT TO LENGTH	4
11	8020 - Part No. 1010 - 30 Inches	80/20 CUT TO LENGTH	2
12	8020 - Part No. 4108 - 2 Hole Inside Corner Bracket	80/20	4
13	8020 - Part No. 4118 - 3 Hole Joining Strip	80/20	2
14	8020 - Part No. 4128 - 12 Hole 90deg Joining Plate	80/20	30
15	8020 - Part No. 4136 - 4 Hole Inside Gusset Corner Bracket	80/20	4
16	8020 - Part No. 4138 - 8 Hole Inside Gusset Corner Bracket	80/20	14

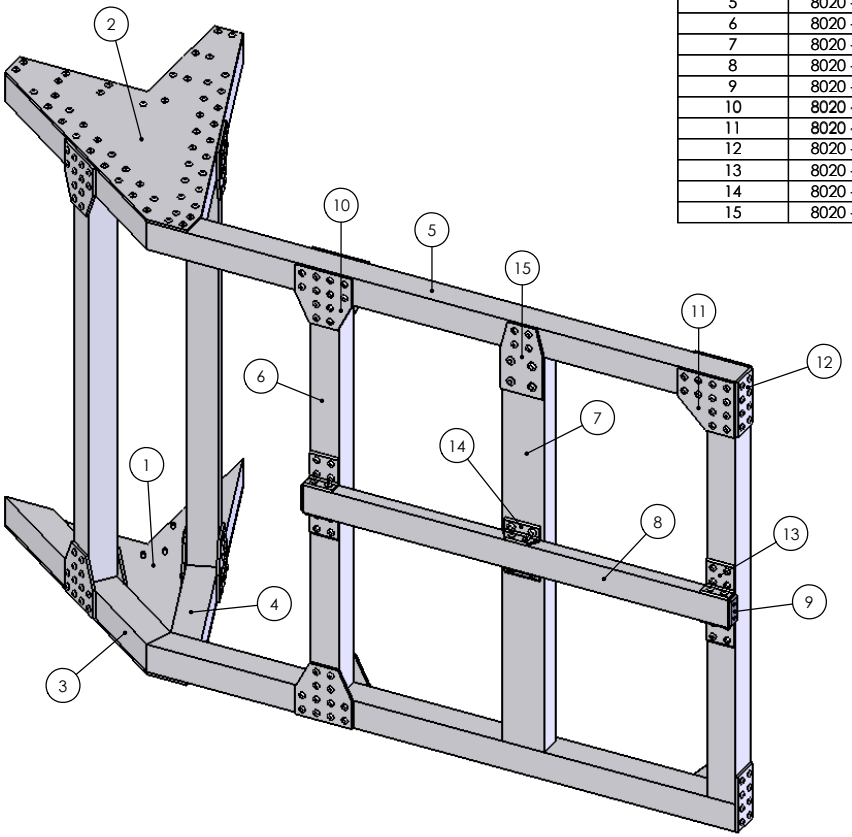




DRAWN:	R.B. CUNNINGHAM	CENTER FOR MUSCULOSKELETAL RESEARCH UNIVERSITY OF TENNESSEE	
CHECKED:	W.R. HAMEL		
DATE:	06-29-05	TITLE: Carriage Assembly	
MATL:	N/A		
NOTE:	N/A		
THE INFORMATION CONTAINED IN THIS DRAWING IS THE SOLE PROPERTY OF THE UNIVERSITY OF TENNESSEE. ANY REPRODUCTION IN PART OR AS A WHOLE WITHOUT THE WRITTEN PERMISSION OF THE UNIVERSITY OF TENNESSEE IS PROHIBITED.		DWG. NO. Figure B.2	QTY 1

Figure B.2 Carriage Assembly

ITEM NO.	PART NUMBER	DESCRIPTION	QTY.
1	Wing To Carriage Plate	Figure B.17	1
2	Wing To Carriage Plate Bottom	Figure B.17	1
3	8020 - Part No. 2020 - 20.019 Inches	Figure B.14	2
4	8020 - Part No. 2020 - 22.239 Inches	Figure B.15	2
5	8020 - Part No. 2020 - 41.588 Inches	Figure B.16	2
6	8020 - Part No. 2020 - 28.8 Inches	80/20 CUT TO LENGTH	4
7	8020 - Part No. 1530 - 28.8 Inches	80/20 CUT TO LENGTH	1
8	8020 - Part No. 1020 - 30 Inches	80/20 CUT TO LENGTH	1
9	8020 - Part No. 2025 - 1020 End Cap	80/20	2
10	8020 - Part No. 4125 - 12 Hole Tee Joining Plate	80/20	12
11	8020 - Part No. 4128 - 12 Hole 90deg Joining Plate	80/20	3
12	8020 - Part No. 4165 - 8 Hole Joining Plate	80/20	2
13	8020 - Part No. 4175 - 6 Hole Inside Corner Bracket	80/20	4
14	8020 - Part No. 4511 - 10 To 15 Double Wide Transition	80/20	2
15	8020 - Part No. 4518 - 10-15 Series 8 Hole Transition Strip	80/20	1



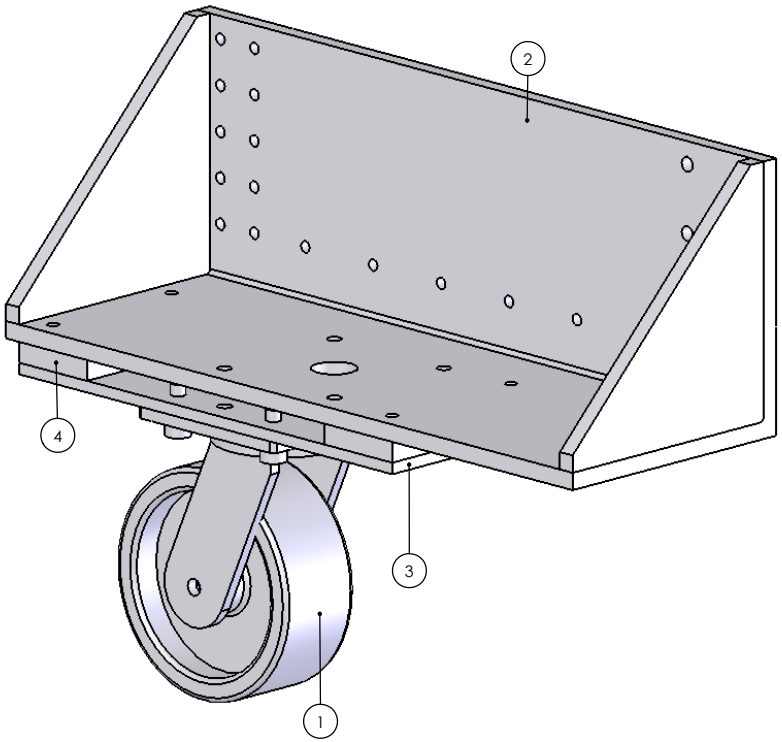
NOTE:

THE SECOND WING ASSEMBLY IS AN EXACT MIRROR IMAGE OF THE ASSEMBLY SHOWN HERE.

DRAWN: R.B. CUNNINGHAM	CENTER FOR MUSCULOSKELETAL RESEARCH UNIVERSITY OF TENNESSEE	
CHECKED: W.R. HAMEL		
DATE: 06-29-05	TITLE: Wing Assembly	
MATL: N/A		
NOTE: N/A		
THE INFORMATION CONTAINED IN THIS DRAWING IS THE SOLE PROPERTY OF THE UNIVERSITY OF TENNESSEE. ANY REPRODUCTION IN PART OR AS A WHOLE WITHOUT THE WRITTEN PERMISSION OF THE UNIVERSITY OF TENNESSEE IS PROHIBITED.	DWG. NO. Figure B.3	QTY 2

Figure B.3 Wing Assembly

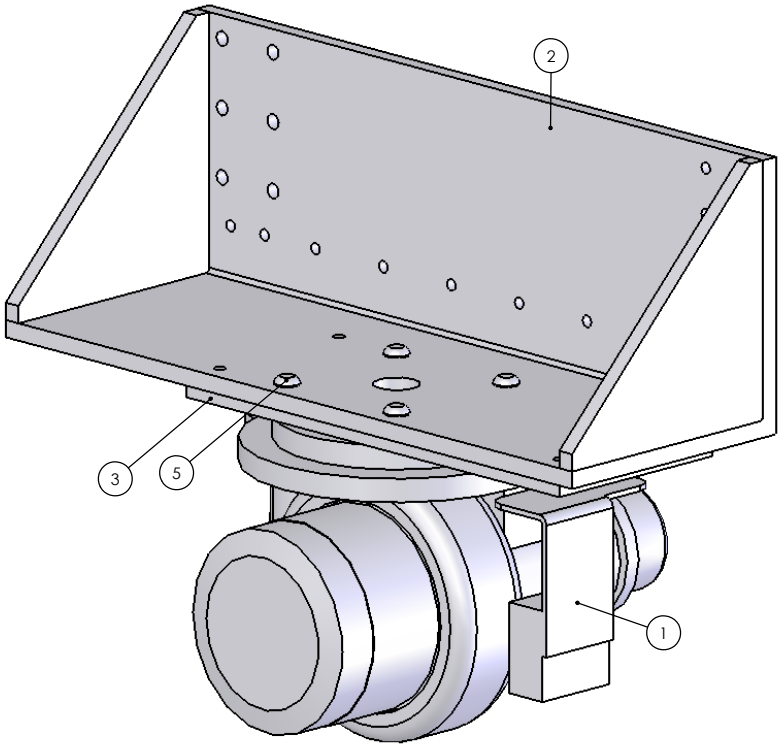
ITEM NO.	PART NUMBER	DESCRIPTION	QTY.
1	Hamilton S-EC-5SPB_2	Hamilton	1
2	MIWD & Caster Mounting Angle Assy	Figure B.18	1
3	MIWD & Caster Mounting Plate	Figure B.20	1
4	Caster Mount Spacer	Figure B.21	2
5	0.375-24-0.75 BHSCS		4
6	0.25-20-1.00 BHSCS		4



DRAWN:	R.B. CUNNINGHAM	CENTER FOR MUSCULOSKELETAL RESEARCH UNIVERSITY OF TENNESSEE	
CHECKED:	W.R. HAMEL		
DATE:	06-29-05	TITLE: Rear Caster Assembly	
MATL:	N/A		
NOTE:	N/A		
THE INFORMATION CONTAINED IN THIS DRAWING IS THE SOLE PROPERTY OF THE UNIVERSITY OF TENNESSEE. ANY REPRODUCTION IN PART OR AS A WHOLE WITHOUT THE WRITTEN PERMISSION OF THE UNIVERSITY OF TENNESSEE IS PROHIBITED.		DWG. NO. Figure B.4	QTY 1

Figure B.4 Rear Caster Assembly

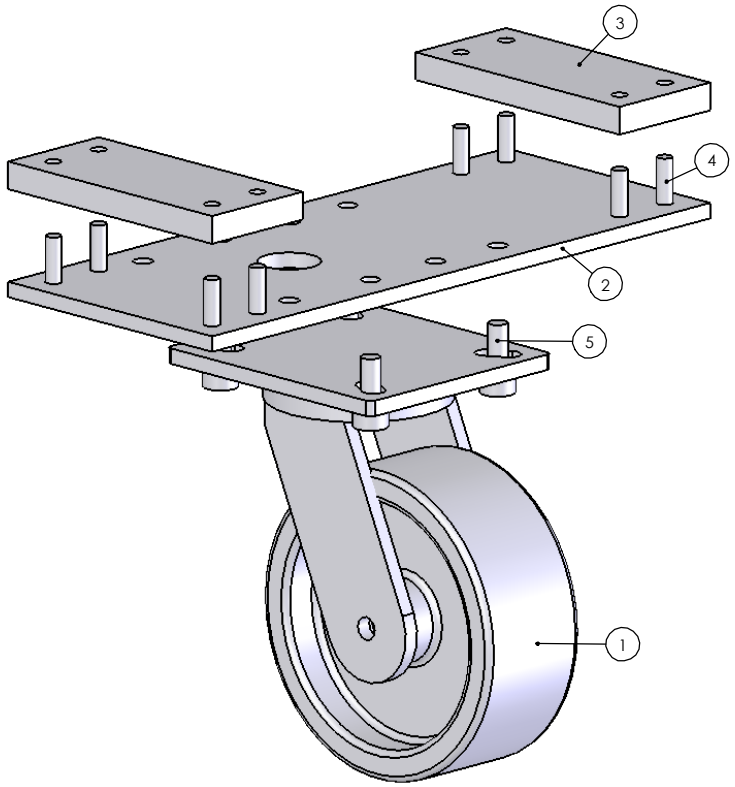
ITEM NO.	PART NUMBER	DESCRIPTION	QTY.
1	MIWD_15.60.14_85.35.20	Transbotics	1
2	Mirror MIWD & Caster Mounting Angle Assy	Figure B.19	1
3	MIWD & Caster Mounting Plate	Figure B.20	1
4	0.25-20-0.625 BHSCS		4
5	M8-16 BHSCS		4

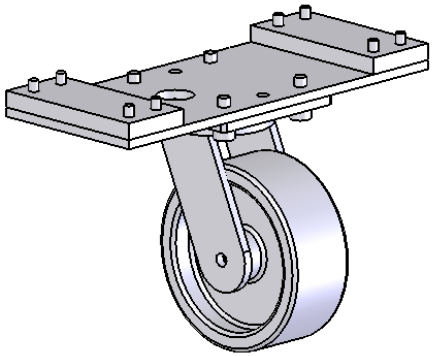


DRAWN:	R.B. CUNNINGHAM	CENTER FOR MUSCULOSKELETAL RESEARCH UNIVERSITY OF TENNESSEE	
CHECKED:	W.R. HAMEL		
DATE:	06-29-05	TITLE: Rear MIWD Assembly	
MATL:	N/A		
NOTE:	N/A		
THE INFORMATION CONTAINED IN THIS DRAWING IS THE SOLE PROPERTY OF THE UNIVERSITY OF TENNESSEE. ANY REPRODUCTION IN PART OR AS A WHOLE WITHOUT THE WRITTEN PERMISSION OF THE UNIVERSITY OF TENNESSEE IS PROHIBITED.		DWG. NO. Figure B.5	QTY 1

Figure B.5 Rear MIWD Assembly

ITEM NO.	PART NUMBER	DESCRIPTION	QTY.
1	Hamilton S-EC-5SPB	Hamilton	1
2	MIWD & Caster Mounting Plate	Figure B.20	1
3	Caster Mount Spacer	Figure B.21	2
4	0.25-20-1.00 BHSCS		8
5	0.375-24-0.75 BHSCS		4

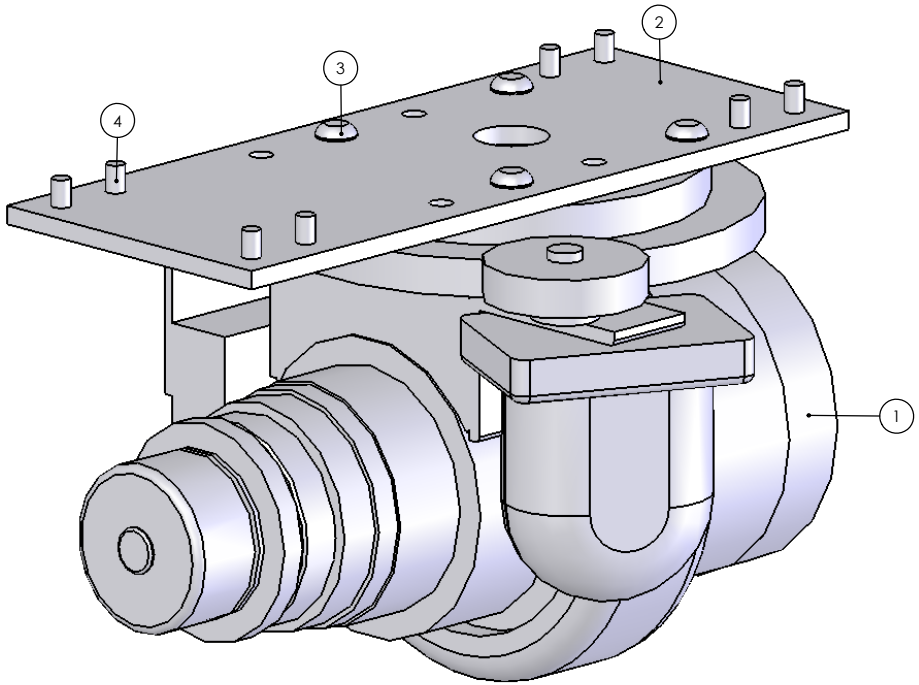




DRAWN:	R.B. CUNNINGHAM	CENTER FOR MUSCULOSKELETAL RESEARCH UNIVERSITY OF TENNESSEE	
CHECKED:	W.R. HAMEL		
DATE:	06-29-05	TITLE: Front Caster Assembly	
MATL:	N/A		
NOTE:	N/A		
THE INFORMATION CONTAINED IN THIS DRAWING IS THE SOLE PROPERTY OF THE UNIVERSITY OF TENNESSEE. ANY REPRODUCTION IN PART OR AS A WHOLE WITHOUT THE WRITTEN PERMISSION OF THE UNIVERSITY OF TENNESSEE IS PROHIBITED.		DWG. NO. Figure B.6	QTY 1

Figure B.6 Front Caster Assembly

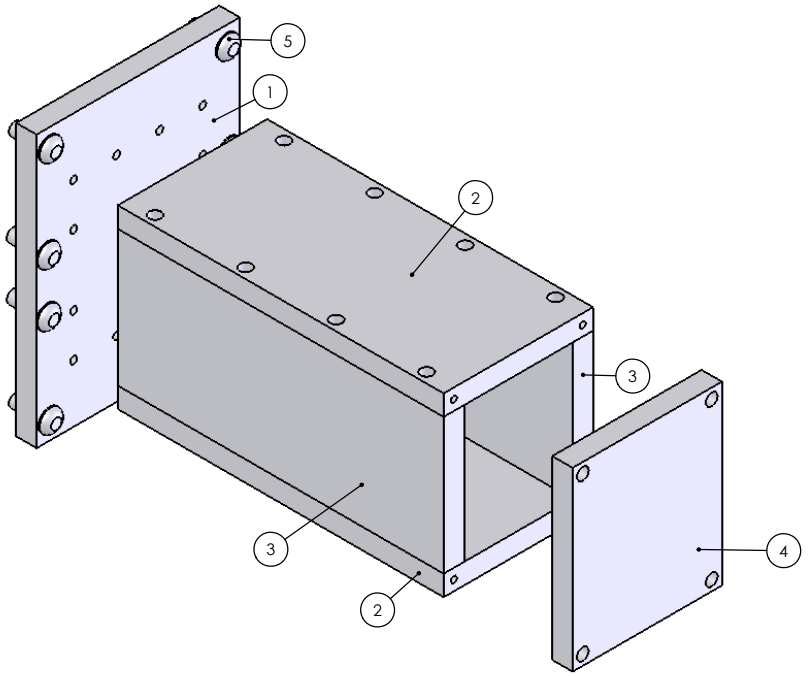
ITEM NO.	PART NUMBER	DESCRIPTION	QTY.
1	MIWD_15.60.14_85.35.20	Transbotics	1
2	MIWD & Caster Mounting Plate	Figure B.20	1
3	M8-16 BHSCS		4
4	0.25-20-0.625 BHSCS		8



DRAWN:	R.B. CUNNINGHAM	CENTER FOR MUSCULOSKELETAL RESEARCH UNIVERSITY OF TENNESSEE	
CHECKED:	W.R. HAMEL		
DATE:	06-29-05	TITLE: Front MIWD Assembly	
MATL:	N/A		
NOTE:	N/A		
THE INFORMATION CONTAINED IN THIS DRAWING IS THE SOLE PROPERTY OF THE UNIVERSITY OF TENNESSEE. ANY REPRODUCTION IN PART OR AS A WHOLE WITHOUT THE WRITTEN PERMISSION OF THE UNIVERSITY OF TENNESSEE IS PROHIBITED.		DWG. NO. Figure B.7	QTY 1

Figure B.7 Front MIWD Assembly

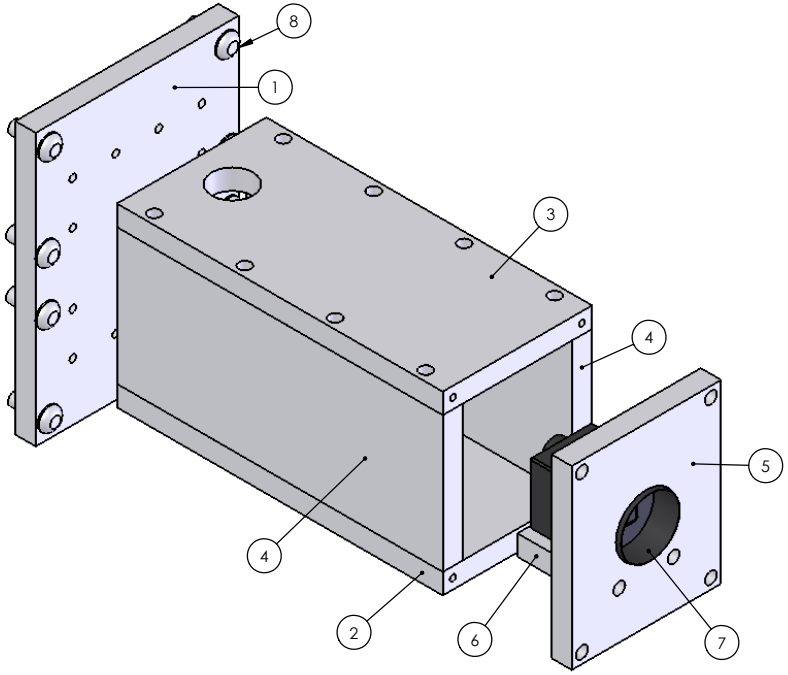
ITEM NO.	PART NUMBER	DESCRIPTION	QTY.
1	Mass Simulation Base	Figure B.22	1
2	Mass Simulation Body Bottom	Figure B.23	2
3	Mass Simulation Body Sides	Figure B.25	2
4	Mass Simulation End - No Camera	Figure B.27	1
5	M6-16 BHSCS		8

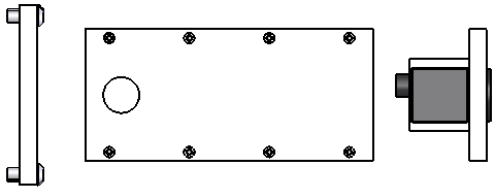


DRAWN:	R.B. CUNNINGHAM	CENTER FOR MUSCULOSKELETAL RESEARCH UNIVERSITY OF TENNESSEE	
CHECKED:	W.R. HAMEL		
DATE:	06-29-05	TITLE: X-Ray Detector Simulation	
MATL:	N/A		
NOTE:	N/A		
THE INFORMATION CONTAINED IN THIS DRAWING IS THE SOLE PROPERTY OF THE UNIVERSITY OF TENNESSEE. ANY REPRODUCTION IN PART OR AS A WHOLE WITHOUT THE WRITTEN PERMISSION OF THE UNIVERSITY OF TENNESSEE IS PROHIBITED.		DWG. NO. Figure B.8	QTY 1

Figure B.8 X-Ray Detector Simulation

ITEM NO.	PART NUMBER	DESCRIPTION	Exploded View/QTY.
1	Mass Simulation Base	Figure B.22	1
2	Mass Simulation Body Bottom	Figure B.23	1
3	Mass Simulation Body Top	Figure B.24	1
4	Mass Simulation Body Sides	Figure B.25	2
5	Mass Simulation End	Figure B.26	1
6	Mass Simulation Camera Base	Figure B.28	1
7	X-Ray Tube Camera		1
8	M6-16 BHSCS		8





TOP VIEW

DRAWN: R.B. CUNNINGHAM	CENTER FOR MUSCULOSKELETAL RESEARCH UNIVERSITY OF TENNESSEE	
CHECKED: W.R. HAMEL		
DATE: 06-29-05	TITLE: X-Ray Tube Simulation	
MATL: N/A		
NOTE: N/A		
THE INFORMATION CONTAINED IN THIS DRAWING IS THE SOLE PROPERTY OF THE UNIVERSITY OF TENNESSEE. ANY REPRODUCTION IN PART OR AS A WHOLE WITHOUT THE WRITTEN PERMISSION OF THE UNIVERSITY OF TENNESSEE IS PROHIBITED.	DWG. NO. Figure B.9	QTY 1

Figure B.9 X-Ray Tube Simulation

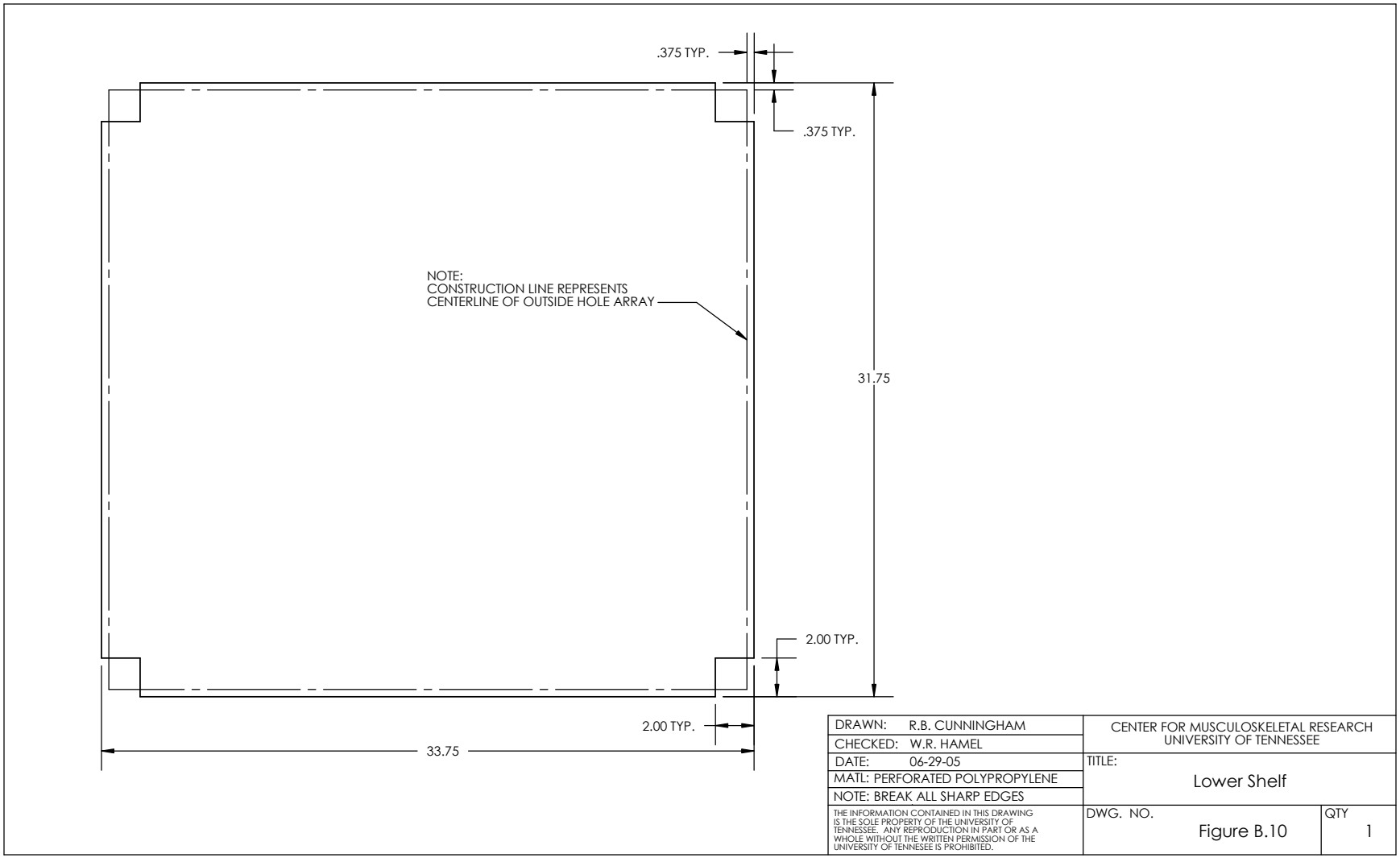


Figure B.10 Lower Shelf

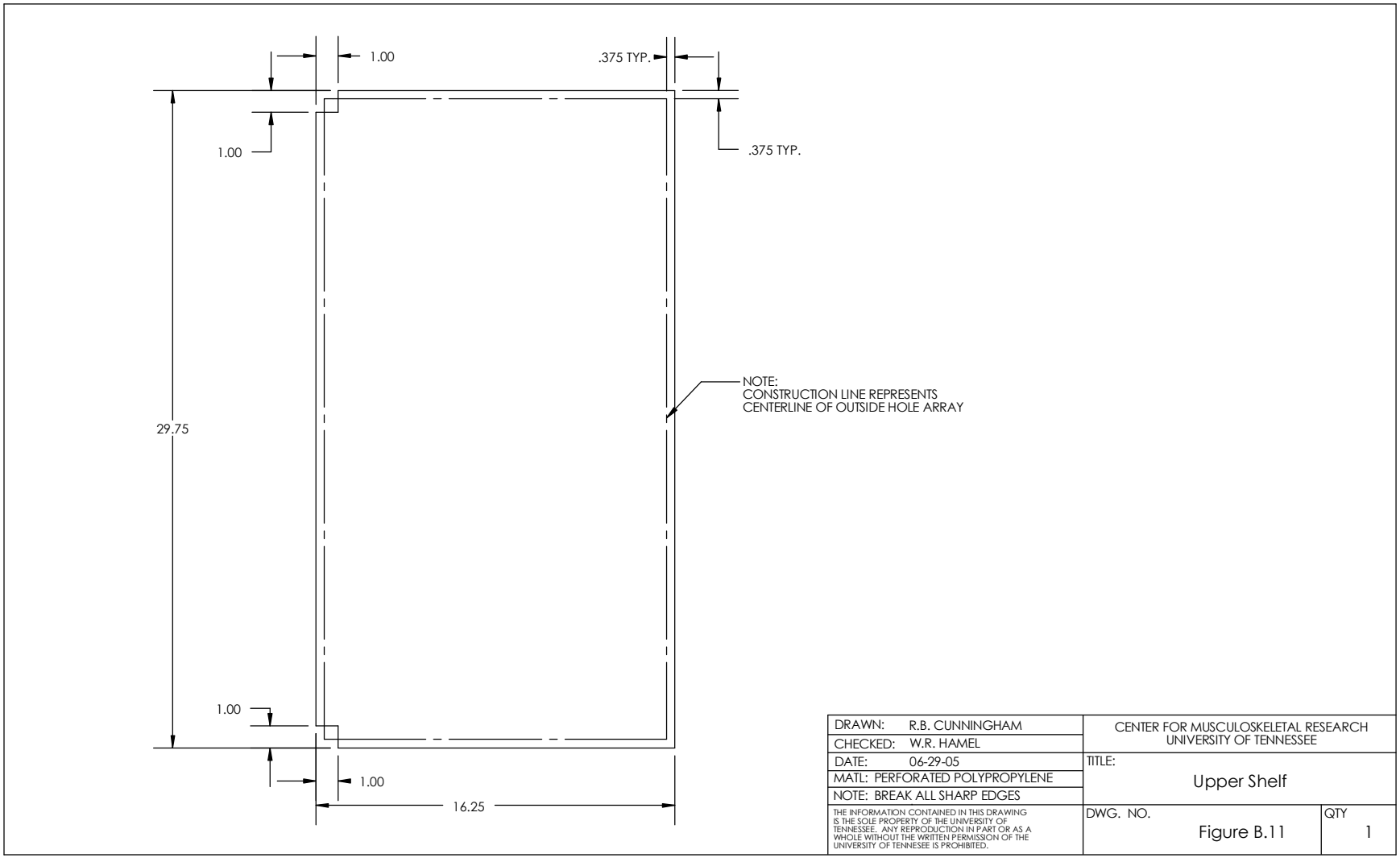
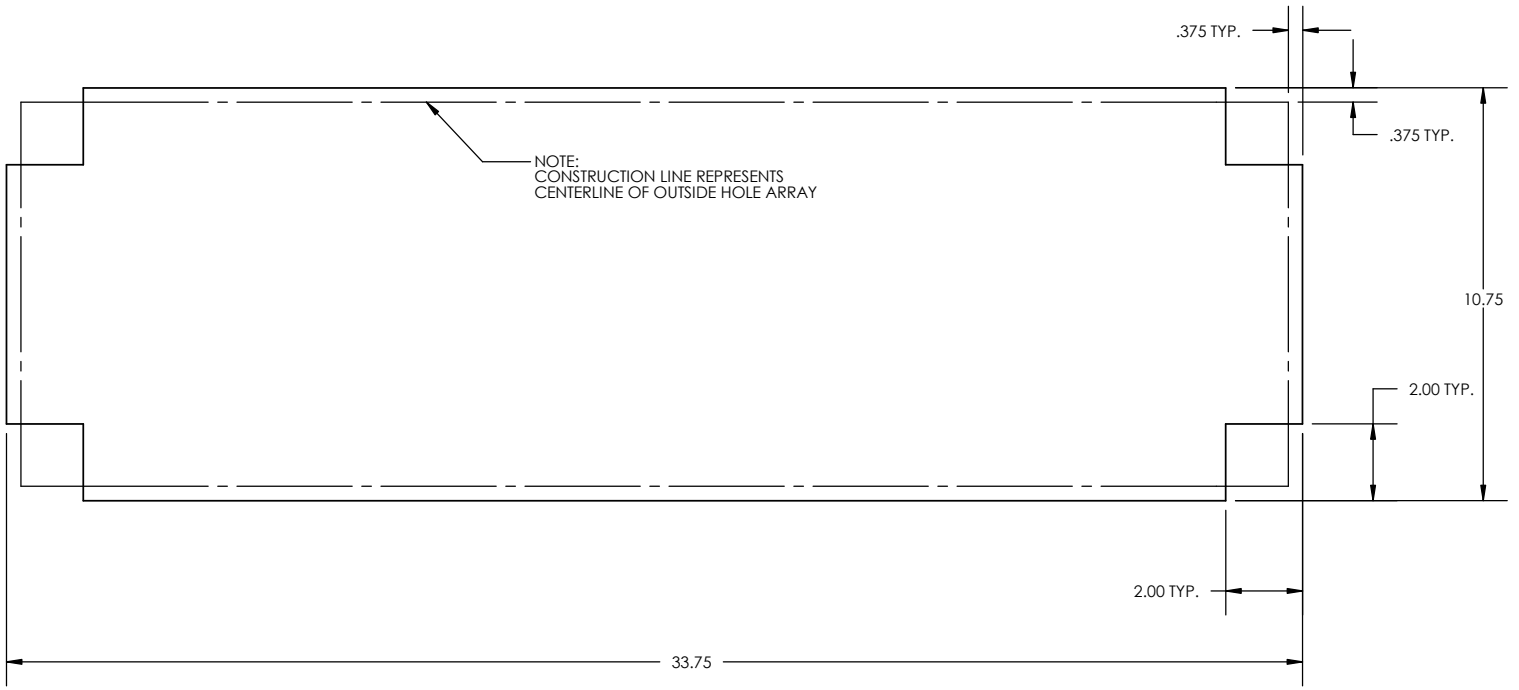


Figure B.11 Upper Shelf



DRAWN: R.B. CUNNINGHAM	CENTER FOR MUSCULOSKELETAL RESEARCH UNIVERSITY OF TENNESSEE
CHECKED: W.R. HAMEL	
DATE: 06-29-05	TITLE: Lower Side Shelf
MATL: PERFORATED POLYPROPYLENE	
NOTE: BREAK ALL SHARP EDGES	
THE INFORMATION CONTAINED IN THIS DRAWING IS THE SOLE PROPERTY OF THE UNIVERSITY OF TENNESSEE. ANY REPRODUCTION IN PART OR AS A WHOLE WITHOUT THE WRITTEN PERMISSION OF THE UNIVERSITY OF TENNESSEE IS PROHIBITED.	DWG. NO. Figure B.12 / QTY 2

Figure B.12 Lower Side Shelf

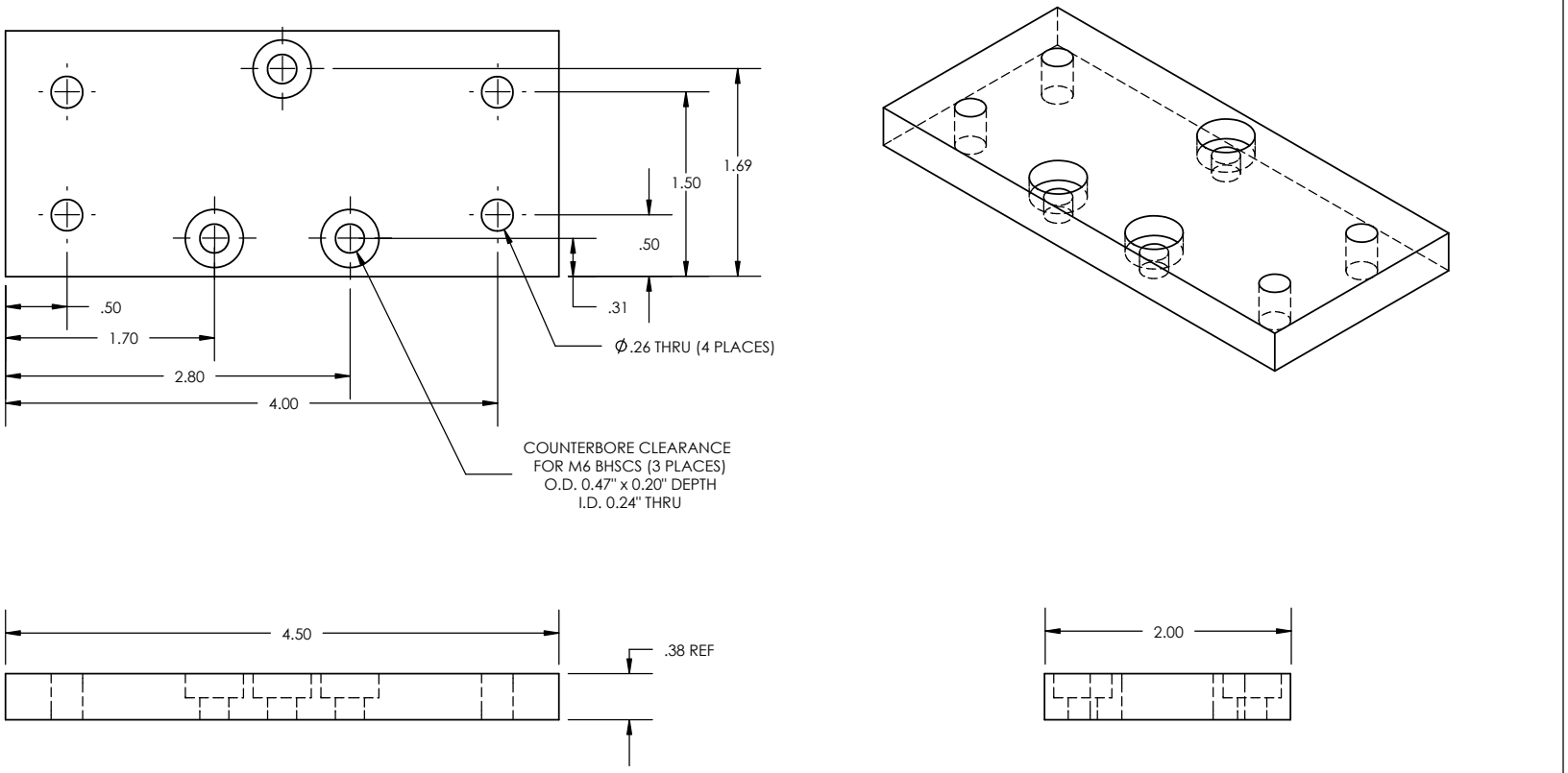


Figure B.13 Laser Mount

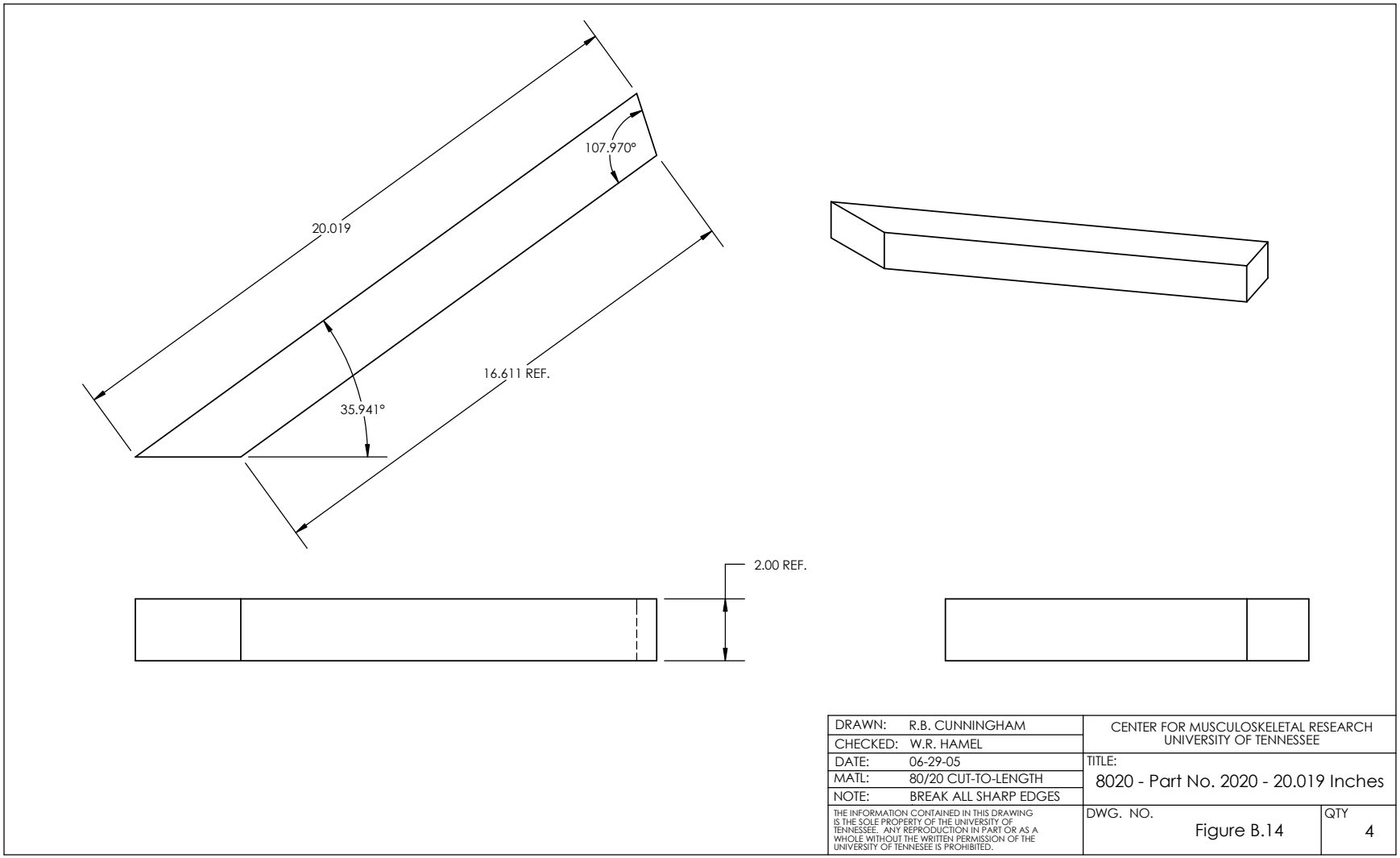


Figure B.14 8020 - Part No. 2020 - 20.019 Inches

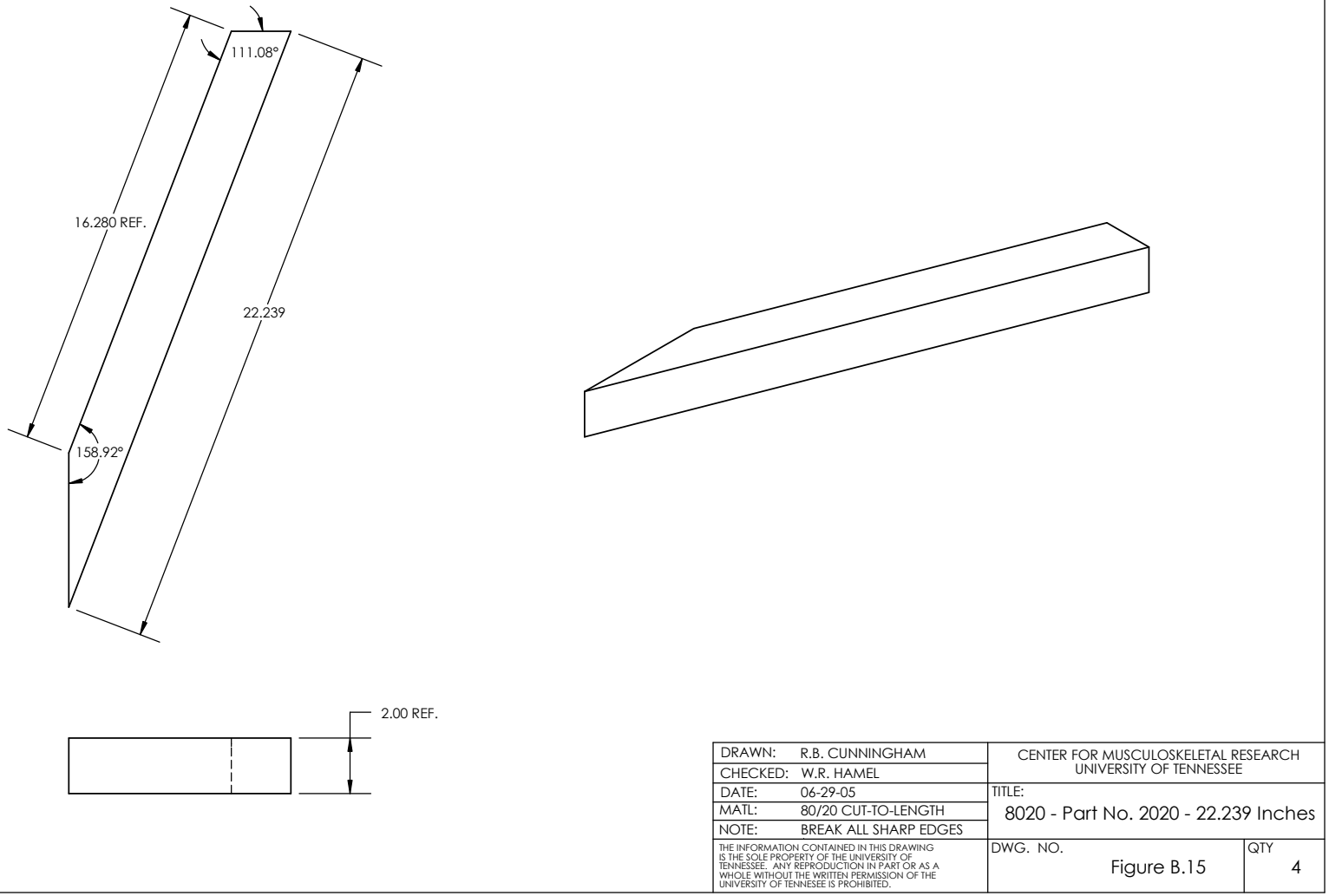
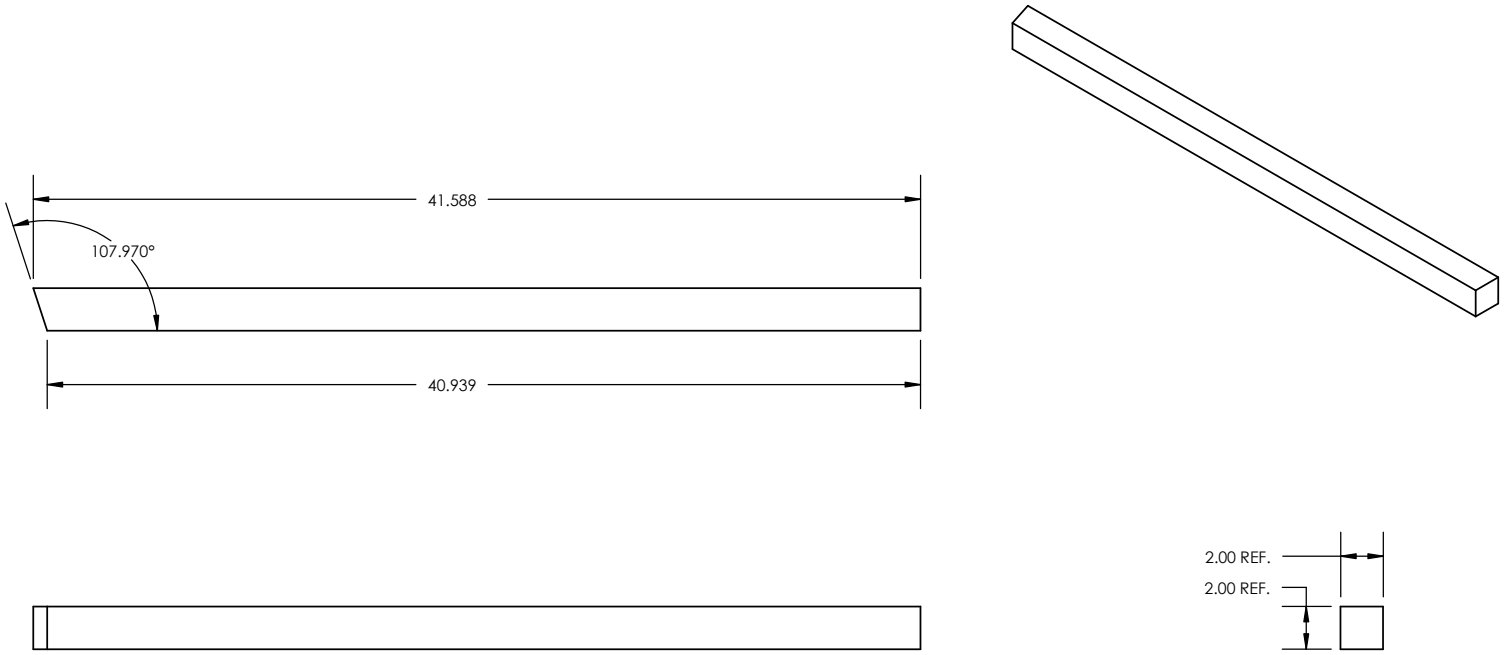


Figure B.15 8020 - Part No. 2020 - 22.239 Inches



DRAWN:	R.B. CUNNINGHAM	CENTER FOR MUSCULOSKELETAL RESEARCH UNIVERSITY OF TENNESSEE	
CHECKED:	W.R. HAMEL		
DATE:	06-29-05	TITLE: 8020 - Part No. 2020 - 41.588 Inches	
MATL:	80/20 CUT-TO-LENGTH		
NOTE:	BREAK ALL SHARP EDGES		
THE INFORMATION CONTAINED IN THIS DRAWING IS THE SOLE PROPERTY OF THE UNIVERSITY OF TENNESSEE. ANY REPRODUCTION IN PART OR AS A WHOLE WITHOUT THE WRITTEN PERMISSION OF THE UNIVERSITY OF TENNESSEE IS PROHIBITED.		DWG. NO. Figure B.16	QTY 4

Figure B.16 8020 - Part No. 2020 - 41.588 Inches

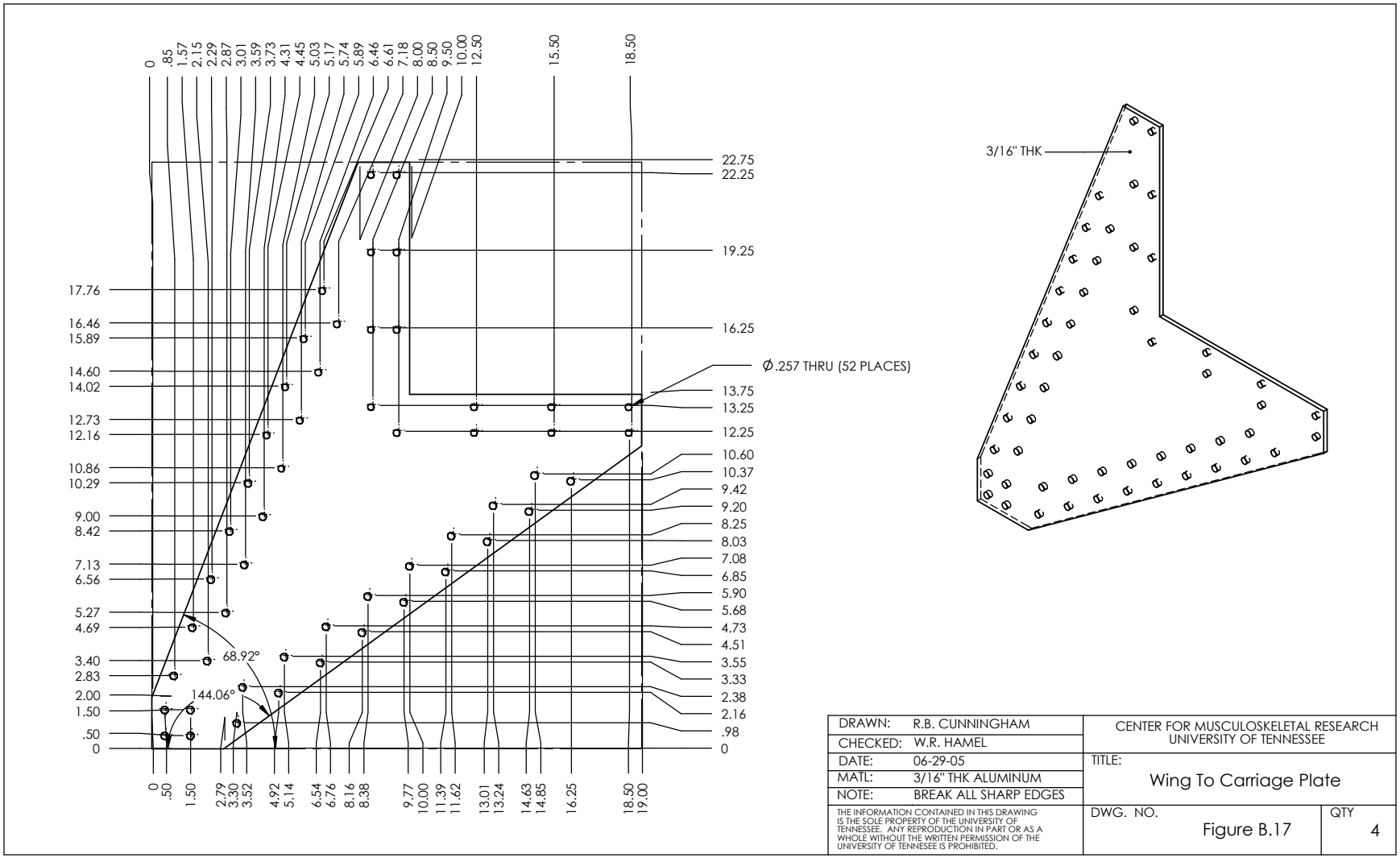


Figure B.17 Wing To Carriage Plate

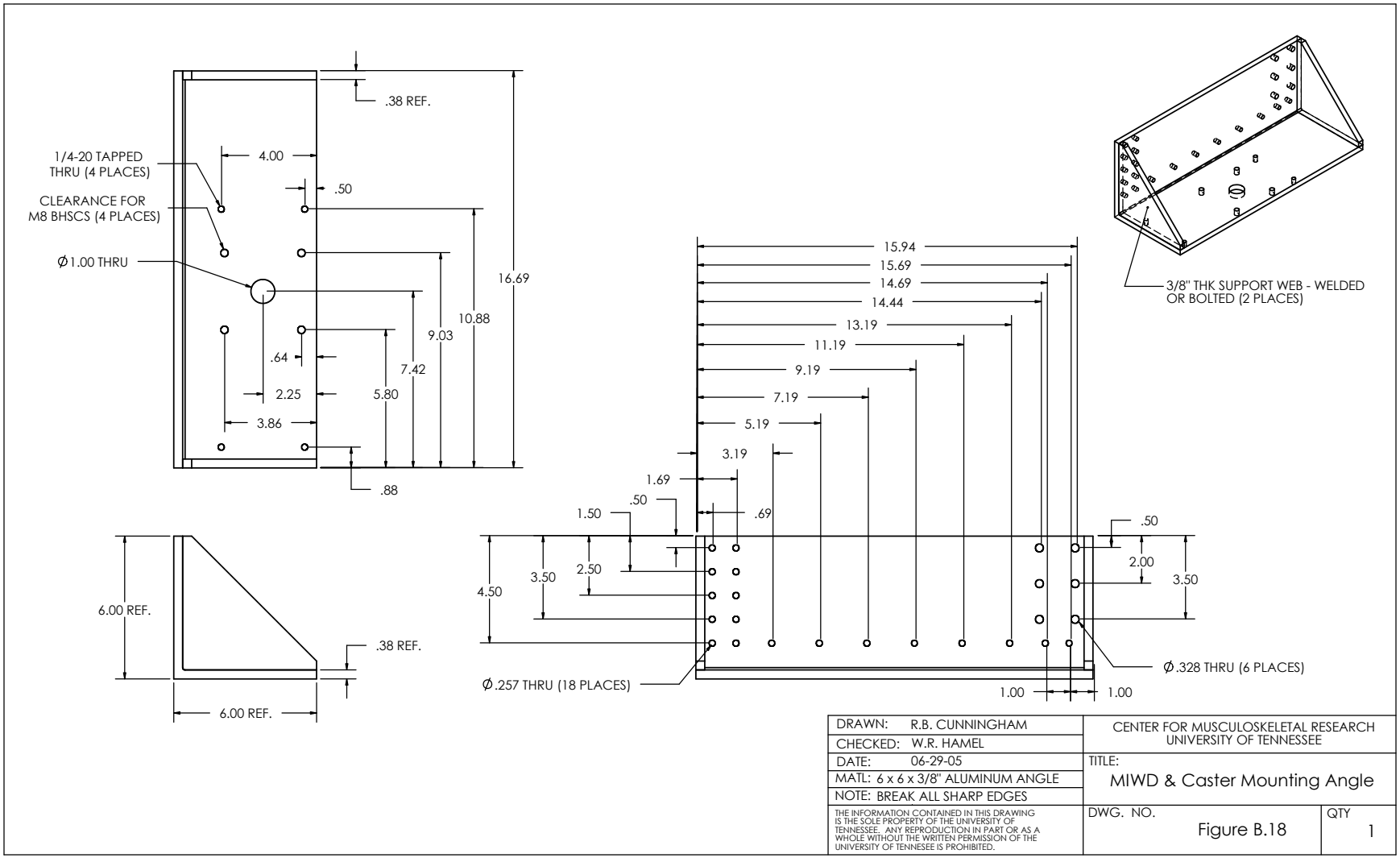
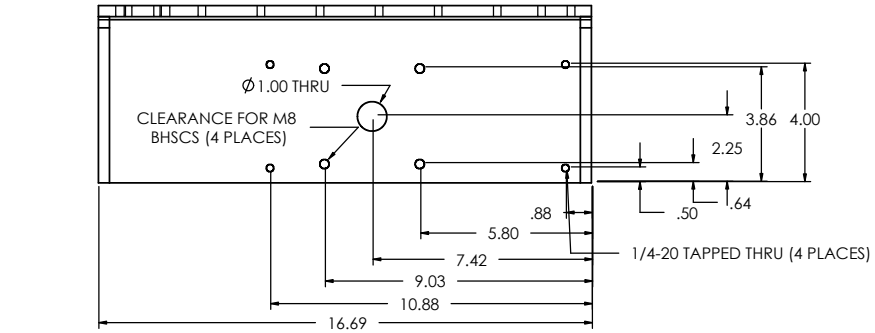
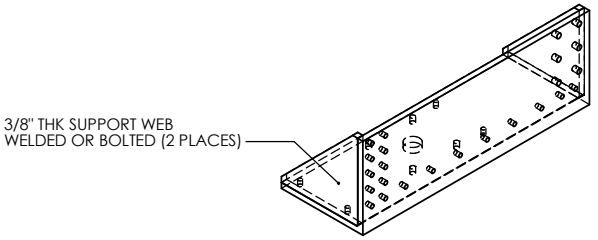
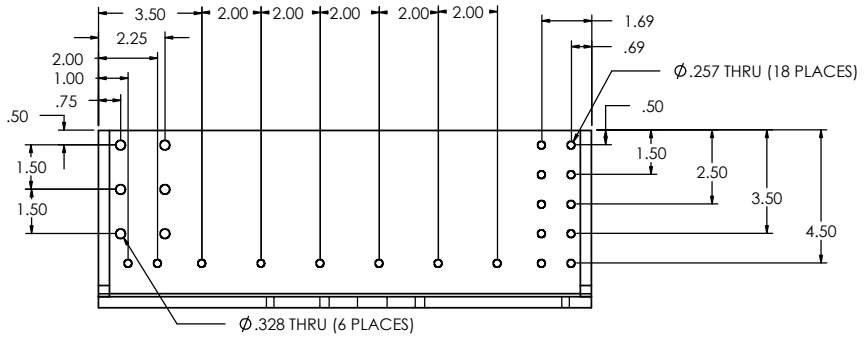
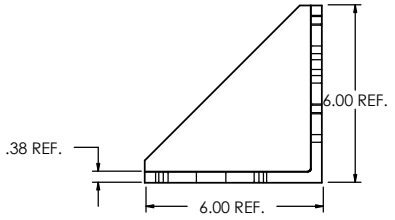


Figure B.18 MIWD & Caster Mounting Angle









DRAWN: R.B. CUNNINGHAM	CENTER FOR MUSCULOSKELETAL RESEARCH UNIVERSITY OF TENNESSEE
CHECKED: W.R. HAMEL	
DATE: 06-29-05	TITLE:
MATL: 6 x 6 x 3/8" ALUMINUM ANGLE	Mirror MIWD & Caster Mounting Angle
NOTE: BREAK ALL SHARP EDGES	
THE INFORMATION CONTAINED IN THIS DRAWING IS THE SOLE PROPERTY OF THE UNIVERSITY OF TENNESSEE. ANY REPRODUCTION IN PART OR AS A WHOLE WITHOUT THE WRITTEN PERMISSION OF THE UNIVERSITY OF TENNESSEE IS PROHIBITED.	DWG. NO. Figure B.19 / QTY 1

Figure B.19 Mirror MIWD & Caster Mounting Angle

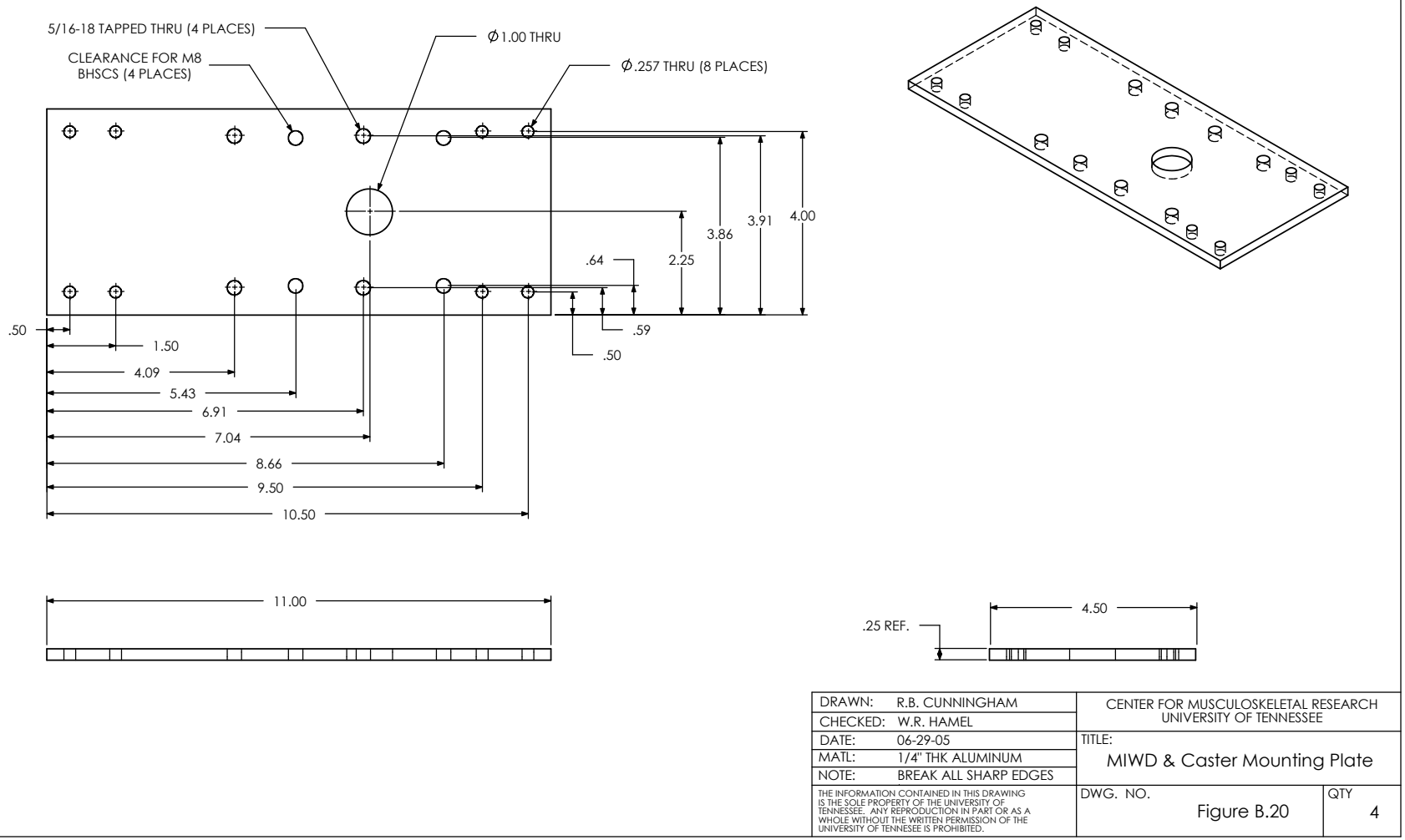


Figure B.20 MIWD & Caster Mounting Plate

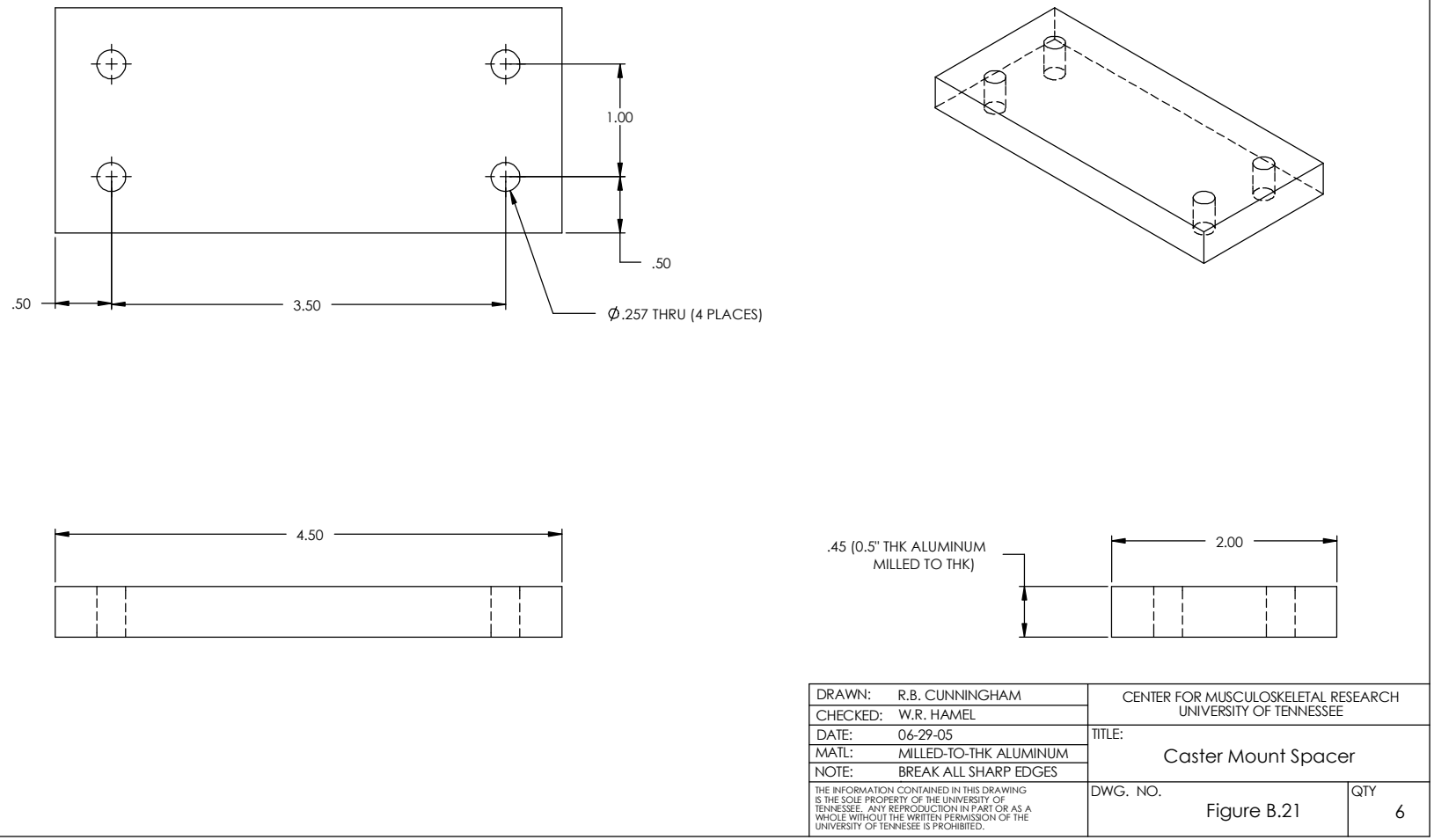


Figure B.21 Caster Mount Spacer

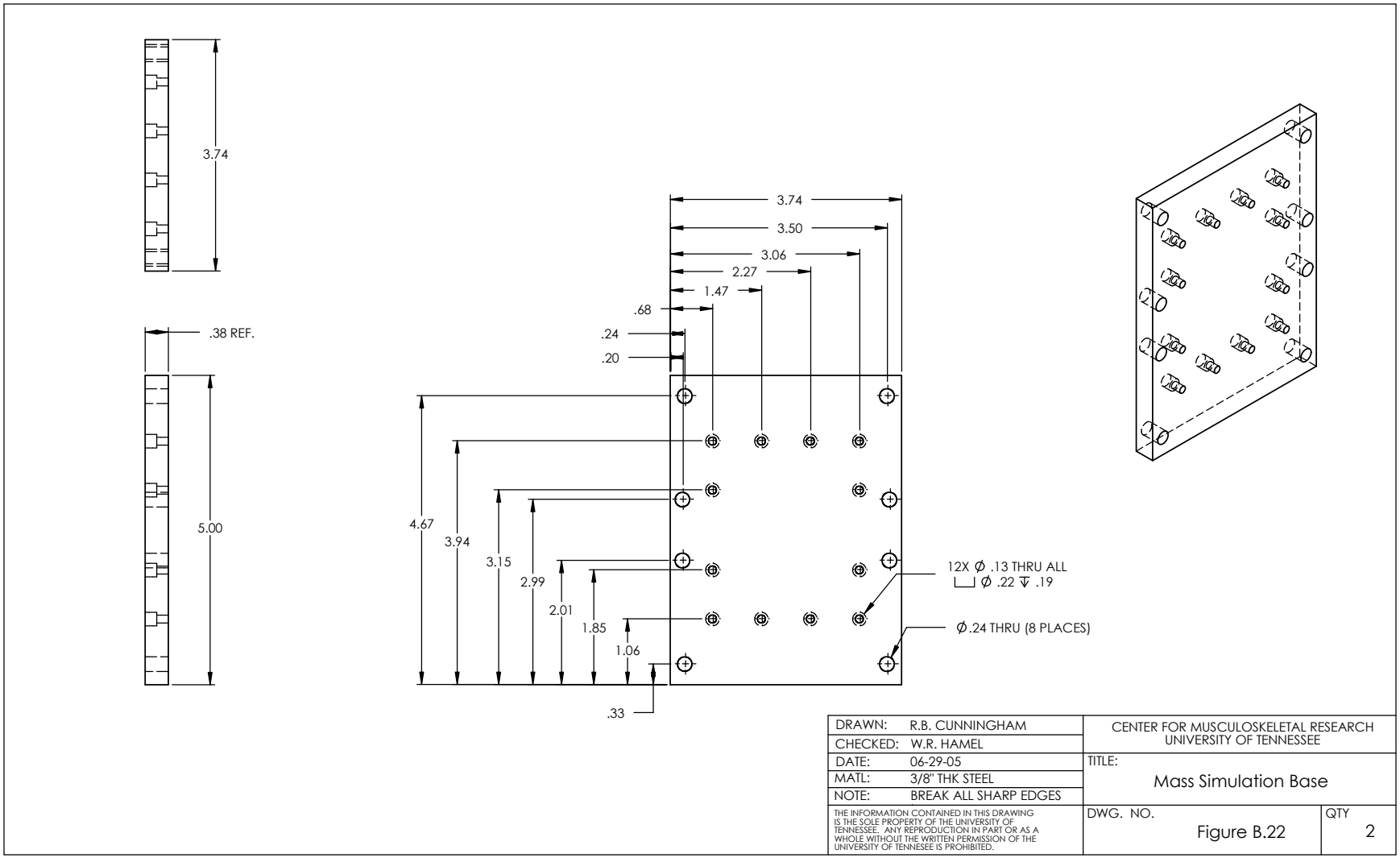


Figure B.22 Mass Simulation Base

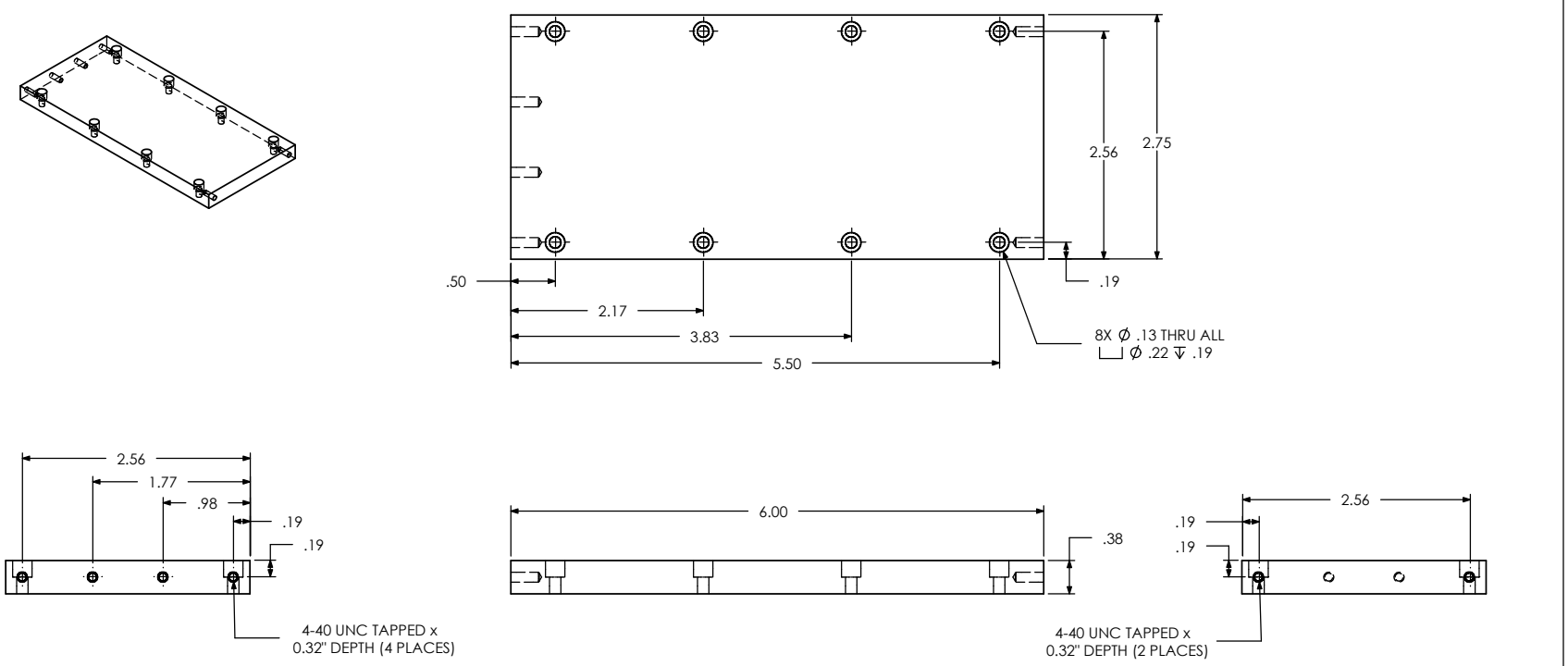


Figure B.23 Mass Simulation Body Bottom

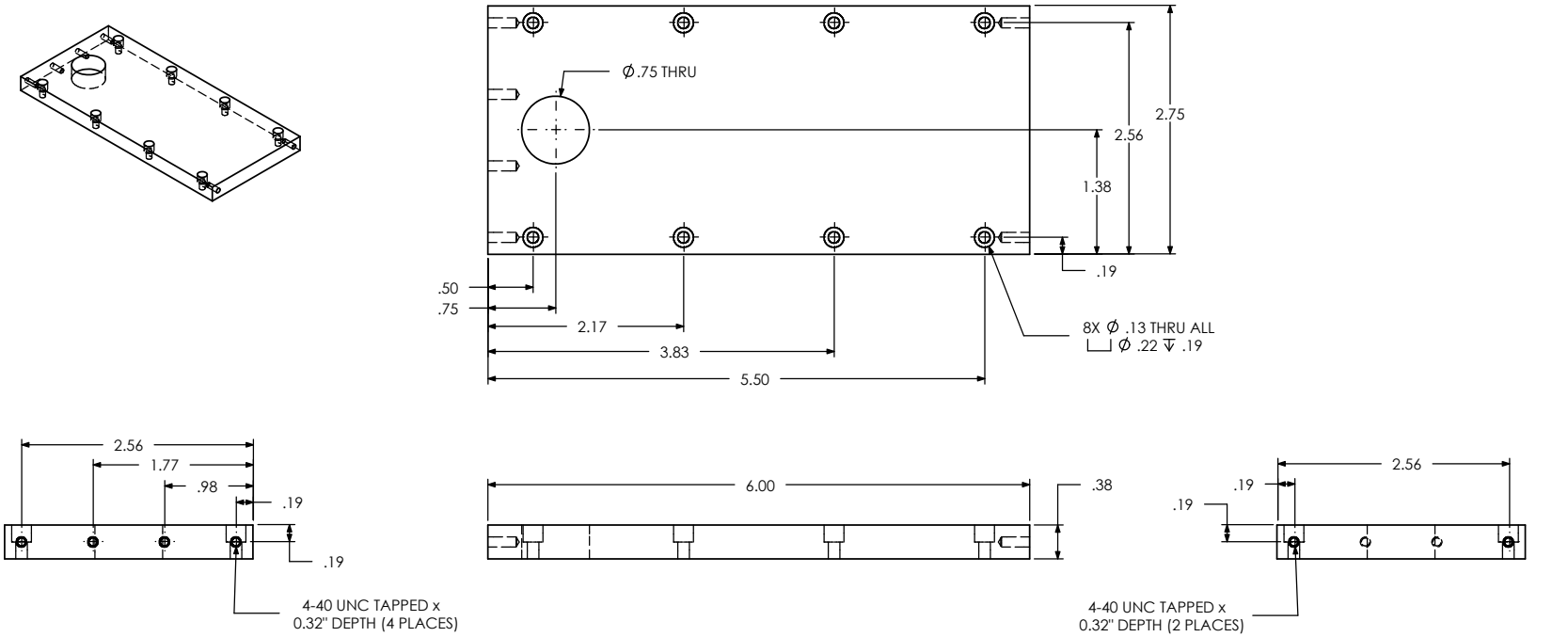
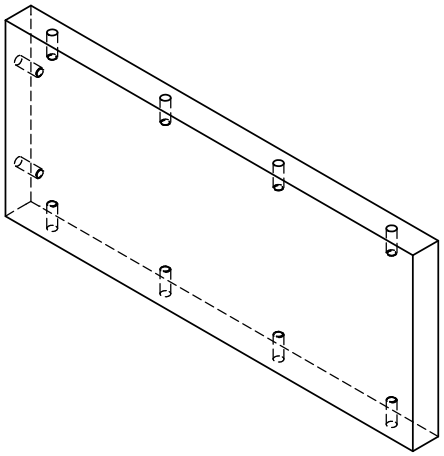
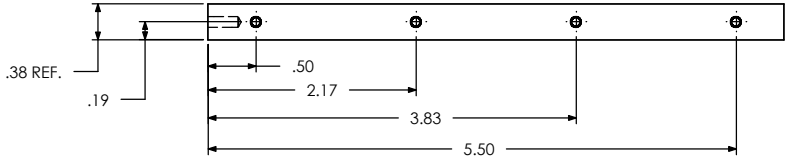
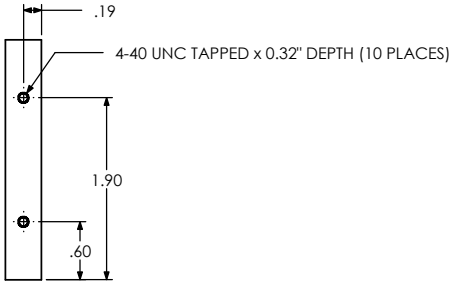
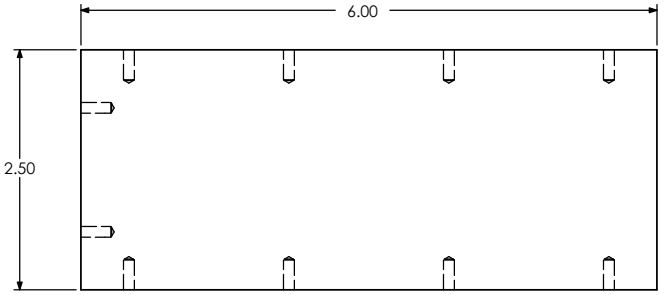


Figure B.24 Mass Simulation Body Top



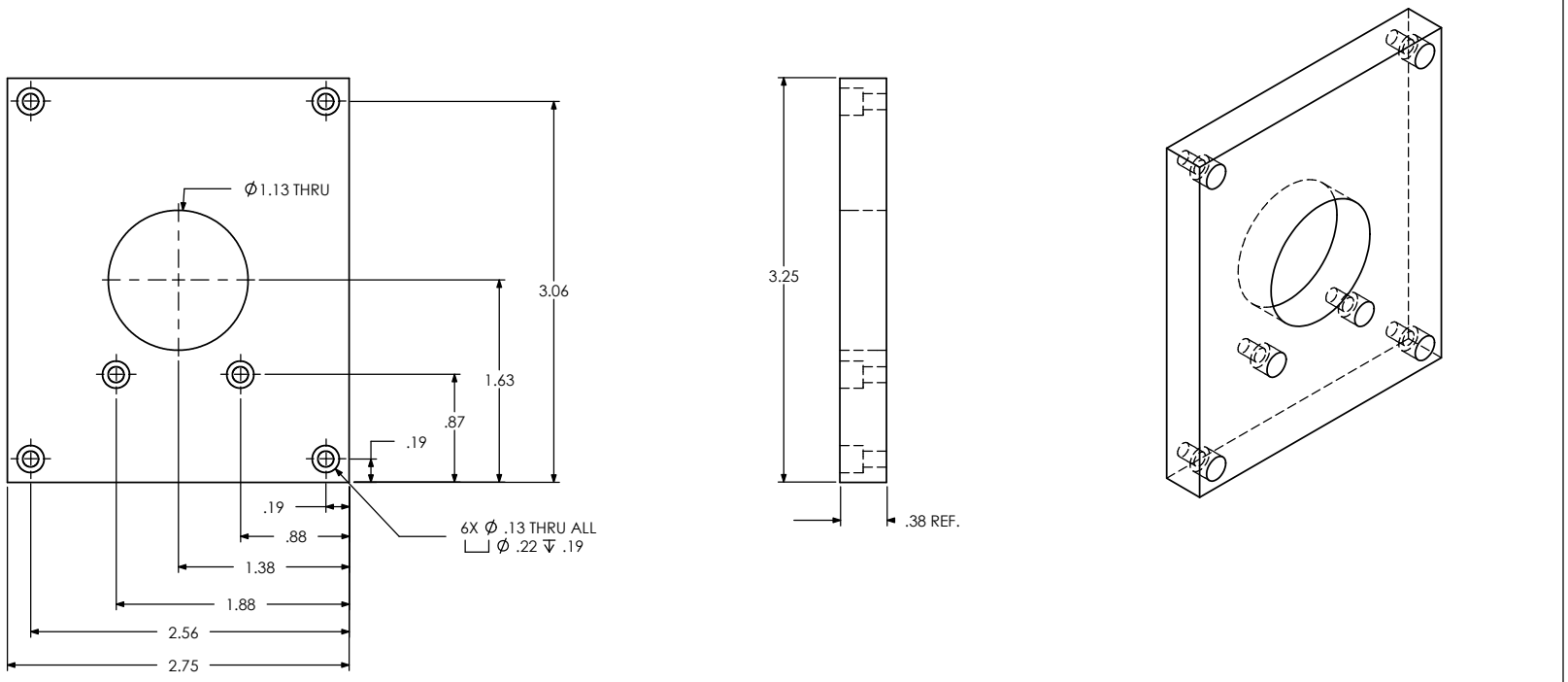






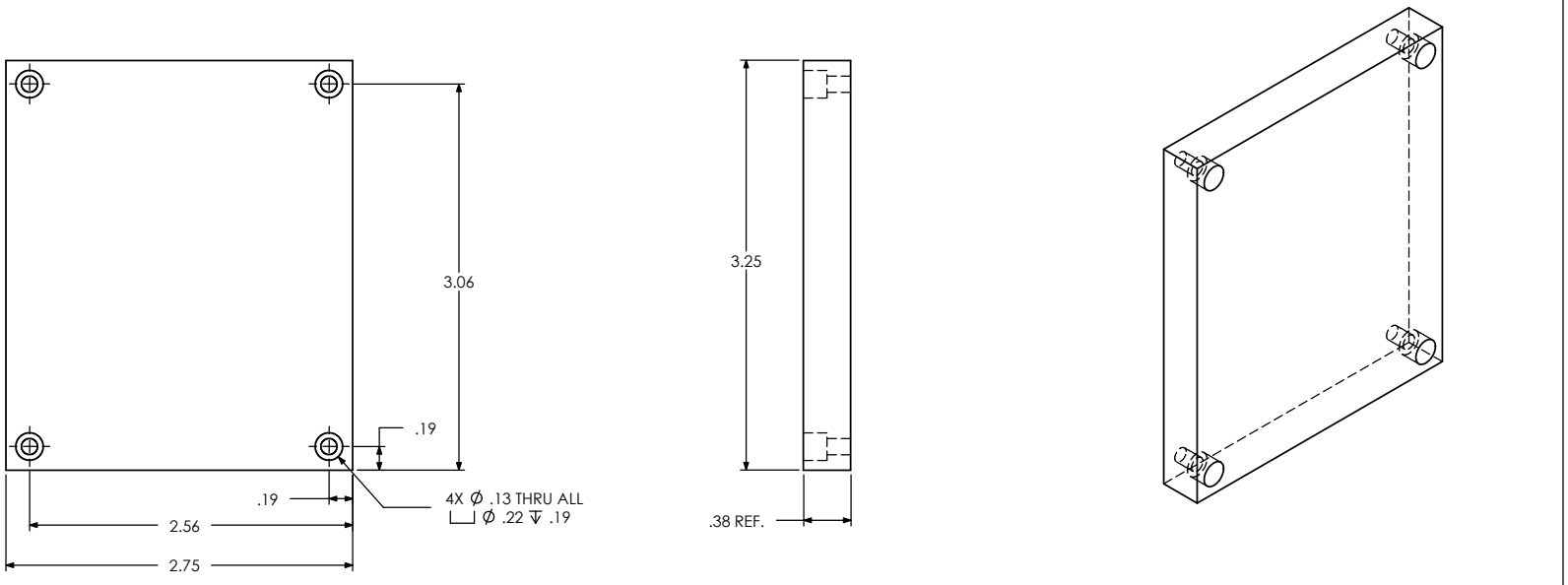
DRAWN:	R.B. CUNNINGHAM	CENTER FOR MUSCULOSKELETAL RESEARCH UNIVERSITY OF TENNESSEE	
CHECKED:	W.R. HAMEL		
DATE:	06-29-05	TITLE: Mass Simulation Body Sides	
MATL:	3/8" THK STEEL		
NOTE:	BREAK ALL SHARP EDGES		
THE INFORMATION CONTAINED IN THIS DRAWING IS THE SOLE PROPERTY OF THE UNIVERSITY OF TENNESSEE. ANY REPRODUCTION IN PART OR AS A WHOLE WITHOUT THE WRITTEN PERMISSION OF THE UNIVERSITY OF TENNESSEE IS PROHIBITED.		DWG. NO. Figure B.25	QTY 4

Figure B.25 Mass Simulation Body Sides



DRAWN:	R.B. CUNNINGHAM	CENTER FOR MUSCULOSKELETAL RESEARCH UNIVERSITY OF TENNESSEE	
CHECKED:	W.R. HAMEL		
DATE:	06-29-05	TITLE:	
MATL:	3/8" THK STEEL	Mass Simulation End	
NOTE:	BREAK ALL SHARP EDGES		
THE INFORMATION CONTAINED IN THIS DRAWING IS THE SOLE PROPERTY OF THE UNIVERSITY OF TENNESSEE. ANY REPRODUCTION IN PART OR AS A WHOLE WITHOUT THE WRITTEN PERMISSION OF THE UNIVERSITY OF TENNESSEE IS PROHIBITED.		DWG. NO. Figure B.26	QTY 1

Figure B.26 Mass Simulation End



DRAWN:	R.B. CUNNINGHAM	CENTER FOR MUSCULOSKELETAL RESEARCH UNIVERSITY OF TENNESSEE	
CHECKED:	W.R. HAMEL		
DATE:	06-29-05	TITLE: Mass Simulation End - No Camera	
MATL:	3/8" THK STEEL		
NOTE:	BREAK ALL SHARP EDGES		
THE INFORMATION CONTAINED IN THIS DRAWING IS THE SOLE PROPERTY OF THE UNIVERSITY OF TENNESSEE. ANY REPRODUCTION IN PART OR AS A WHOLE WITHOUT THE WRITTEN PERMISSION OF THE UNIVERSITY OF TENNESSEE IS PROHIBITED.		DWG. NO. Figure B.27	QTY 1

Figure B.27 Mass Simulation End - No Camera

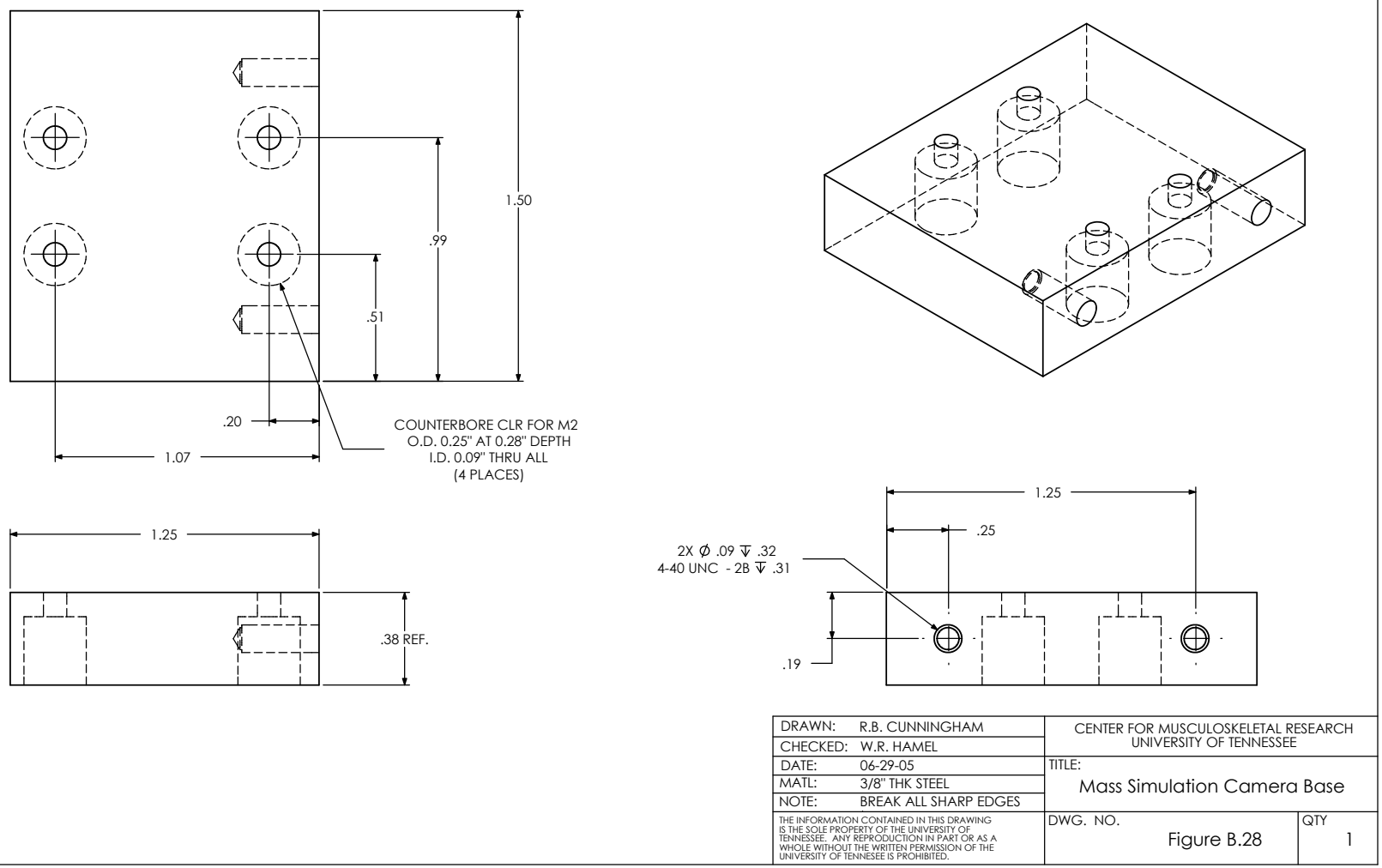
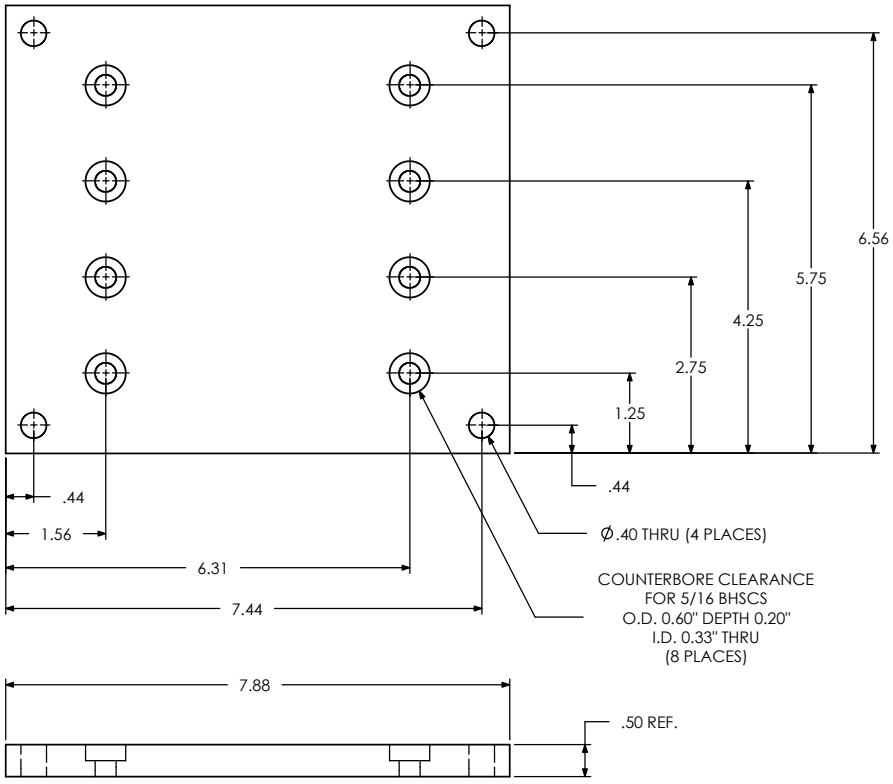
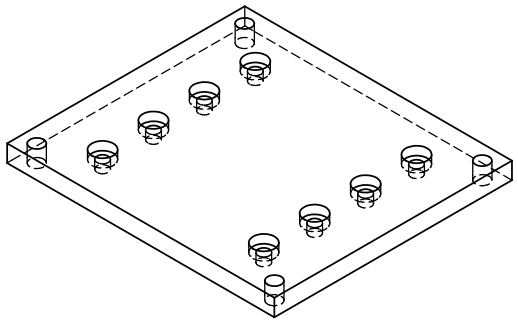
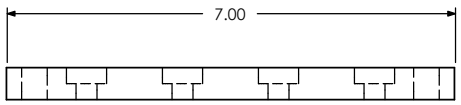


Figure B.28 Mass Simulation Camera Base







DRAWN:	R.B. CUNNINGHAM	CENTER FOR MUSCULOSKELETAL RESEARCH UNIVERSITY OF TENNESSEE	
CHECKED:	W.R. HAMEL		
DATE:	06-29-05	TITLE: X-Axis To 8020 Mounting Plate	
MATL:	1/2" THK ALUMINUM		
NOTE:	BREAK ALL SHARP EDGES		
THE INFORMATION CONTAINED IN THIS DRAWING IS THE SOLE PROPERTY OF THE UNIVERSITY OF TENNESSEE. ANY REPRODUCTION IN PART OR AS A WHOLE WITHOUT THE WRITTEN PERMISSION OF THE UNIVERSITY OF TENNESSEE IS PROHIBITED.		DWG. NO. Figure B.29	QTY 2

Figure B.29 X-Axis To 8020 Mounting Plate

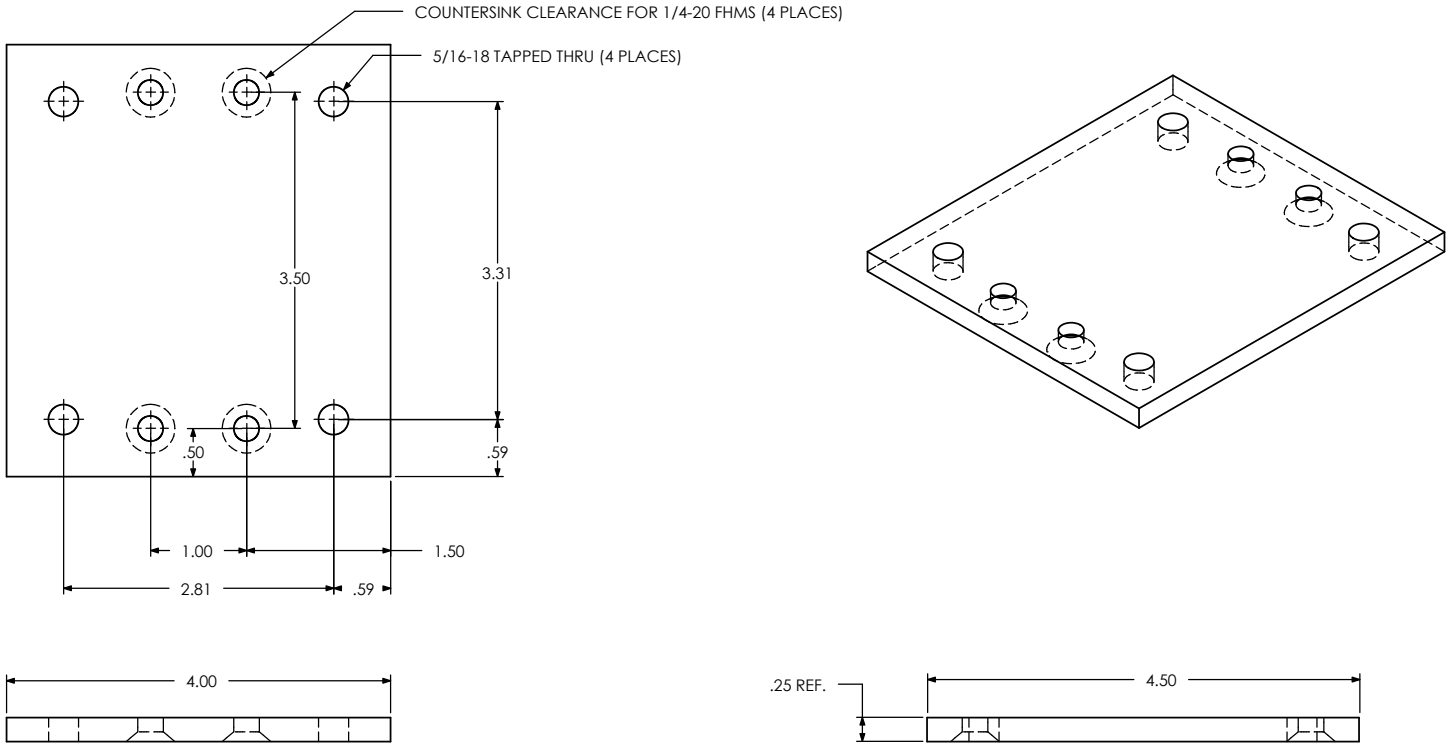


Figure B.30 Transport Caster Mounting Plate

APPENDIX C – ADDITIONAL MATERIAL FOR CHAPTER 4

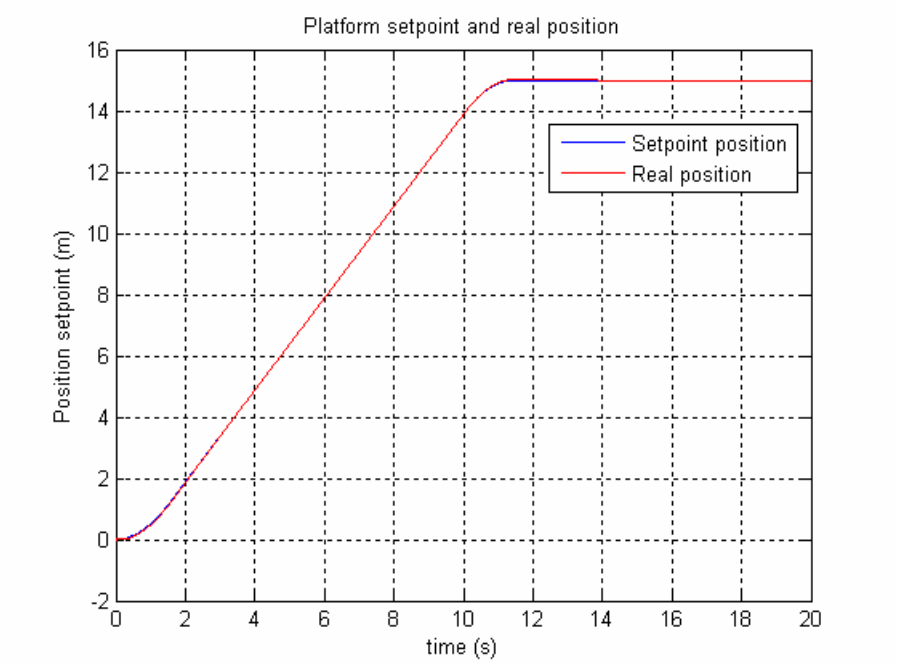


Figure C.1 Human position and platform position response to PID control

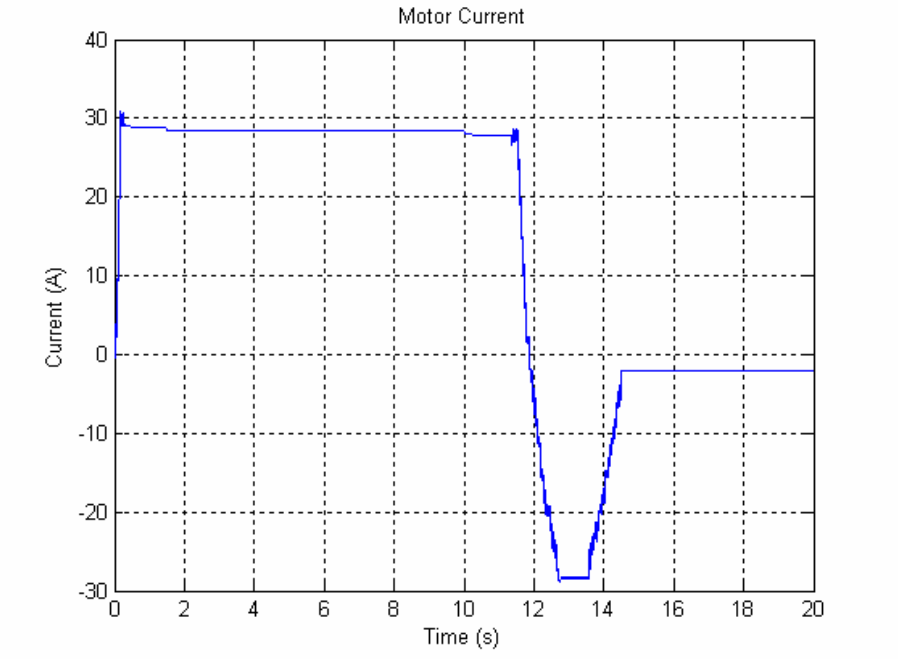


Figure C.2 Motor current response to PID control

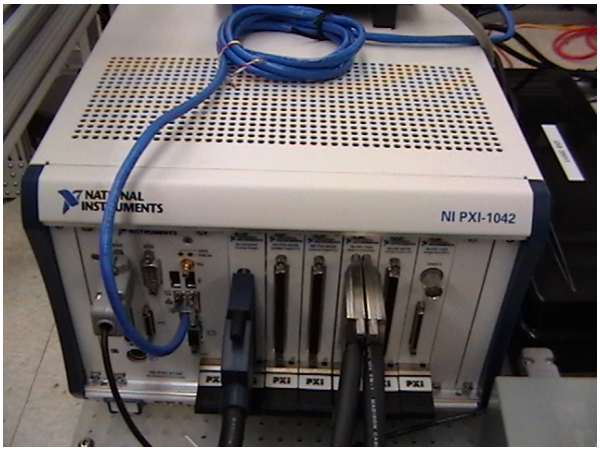


Figure C.3 Host computer NI PXI 8186



Figure C.4 Remote desktop computer

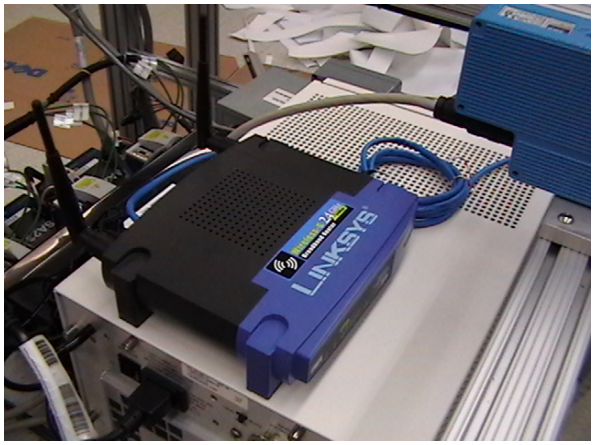


Figure C.5 Linksys wireless router



Figure C.6 Laser distance feedback device

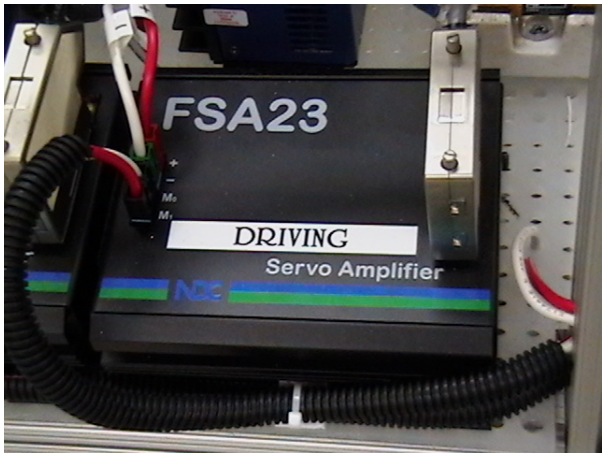


Figure C.7 Driving motor amplifier for MIWD unit



Figure C.8 Four of the eight batteries used to supply power to the amplifiers

APPENDIX D – PAXSCAN® 2520 DIGITAL DETECTION

PAXSCAN®

Flat Panel X-ray Imaging

Despite extensive and well-funded research stretching well back into the 70s, the effective design and manufacture of a reliable and affordable digital X-ray radiographic imaging system has proven elusive. Since the mid-80s, radiologists and hospital care-givers have patiently awaited a technology to eliminate film and chemicals in radiography, image plates in computed radiography, and bulky image-intensifiers in fluoroscopy with a smaller, lighter, more portable imager. Finally, late in the 90s, the first commercially available flat panel digital X-ray detector using amorphous silicon found its way out of Varian's Ginzton Technology Center in Silicon Valley and has begun to change X-ray imaging — forever!



VARIAN
medical systems

Why Flat Panel?

Flat Panel Detectors (FPDs) emerge as next generation digital X-ray technology.

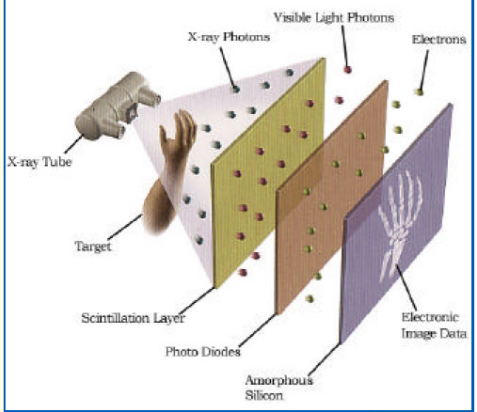
Digital technology has revolutionized our lives. We are collecting, storing, analyzing and using more and more information at a faster and faster pace. X-ray imaging is no exception. The forces behind the digital X-ray revolution are much the same as those driving home and office technologies. Digital devices are smaller and more robust. Once an image is digital, it becomes portable. The image can easily be made available in multiple locations simultaneously. It can be transmitted over long distances in real-time. Digital images make possible computer-assisted diagnosis. Digital images are far simpler to archive and much less costly than their analog counterpart, film. Digital images, video sequences and even volumetric data sets are easily linked to a patient's electronic record. And just as digital technologies have dramatically improved home audio and video fidelity, digital X-ray technology offers significant improvement in image quality and dose utilization.

Many medical modalities, such as CT, PET, SPECT, MRI and ultrasound are inherently digital. However, standard X-ray radiography and fluoroscopy are still primarily based on analog technologies, specifically, screen/film and the image intensifier. Flat panel detectors (FPDs) have emerged as the next generation digital X-ray technology. Flat panel X-ray imagers are based on solid-state integrated circuit (IC) technology, similar in many ways to the imaging chips used in visible wavelength digital photography and video. The primary difference between X-ray imaging and visible imaging is the size of the detector. CCD's and CMOS imagers found in cameras and video recorders are typically on the order of one to two cm in area. Since X-rays are not easily focused, the imager is necessarily on the scale of the object being imaged, which requires an enormous integrated circuit. Fortunately, a large-area IC technology exists in the form of amorphous-silicon thin-film-transistor (TFT) arrays. These TFT arrays are currently in many millions of laptop computers and their application is broadening as these displays increase in size and quality.

A number of detector technologies have been developed based on amorphous silicon TFT arrays, but the most successful and widely used detectors are called "indirect" detectors. These detectors are based on amorphous-silicon TFT/photodiode arrays coupled to X-ray scintillators. The fundamental X-ray conversion chain is shown in Figure 1. The most common scintillators used in flat panel imaging are the same ones used in standard

screen/film radiography and fluoroscopy, gadolinium oxysulfide and cesium-iodide (CsI). The success of the indirect FPD technology stems from the fact that both the amorphous silicon and scintillator technologies are well understood and have decades of research behind them.

Figure 1 - Flat panel detector signal chain.



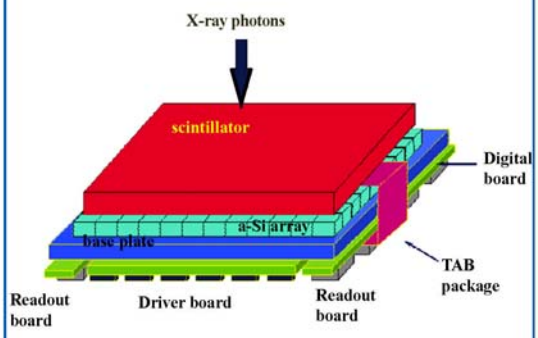
With indirect digital X-ray imaging, an X-ray tube sends a beam of X-ray photons through a target. X-ray photons not absorbed by the target strike a layer of scintillating material that converts them into visible light photons. These photons then strike an array of photodiodes which converts them into electrons that can activate the pixels in a layer of amorphous silicon. The activated pixels generate electronic data that a computer can convert into a high-quality image of the target, which is then displayed on a computer monitor.

With the indirect approach, the flat panel detector consists of a sheet of glass covered with a thin layer of silicon that is in an amorphous, or disordered state. At a microscopic scale, the silicon has been imprinted with millions of transistors arranged in a highly ordered array, like the grid on a sheet of graph paper. Each of these TFTs is attached to a light-absorbing photodiode making up an individual pixel (picture element). Photons striking the photodiode are converted into two carriers of electrical charge, called electron-hole pairs. An electron-hole pair consists of a negatively charged electron and a positively charged hole (a vacant energy space that acts as if it were a positively charged electron).

Since the number of charge carriers produced will vary with the intensity of incoming light photons, an electrical pattern is created that can be swiftly read and interpreted by a computer to produce a digital image.

Although silicon has outstanding electronic properties, it is not a particularly good absorber of X-ray photons. For this reason, X-rays first impinge upon scintillators made from either gadolinium oxysulfide or cesium-iodide. The scintillators absorb the X-rays and convert them into visible light photons that then pass onto the photodiode array.

Figure 2 - Flat panel detector internal architecture.



Because CsI is such an excellent absorber of X-rays, and coverts them to visible light photons at energies that amorphous silicon is best able to convert to charge carriers, the combination of these two materials has the highest-rated Detective Quantum Efficiency DQE) in use today. DQE is the yardstick by which the performance of imagers is measured. A high DQE means images can be acquired with either superior quality or the same quality at a lower dose.

Flat Panel Architecture

The construction of FPDs is similar in many ways to flat panel displays, and uses many of the same technologies. Figure 2 shows the construction of a typical FPD. At the core is an amorphous-silicon TFT/photodiode array. Closely coupled to the array is the X-ray scintillator. Generally, the X-ray conversion screen, rare earth screens such as gadolinium oxysulfide, can be a separate detachable sheet which is mechanically forced into close contact with the array. However, if a CsI screen is used, this is often directly deposited on the array, to give the best optical coupling efficiency. CsI is used in applications like low-dose fluoroscopy, where the photon flux is very low. Figure 3 shows a comparison between the absorption efficiency of CsI and gadolinium oxysulfide. In addition to its much higher absorption efficiency, CsI also produces roughly twice the light output of a gadolinium screen, which results in more than four times the signal at the photodiode for a

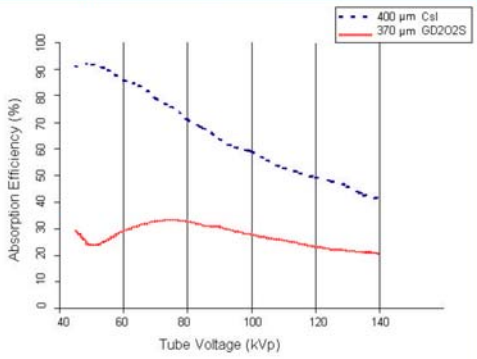
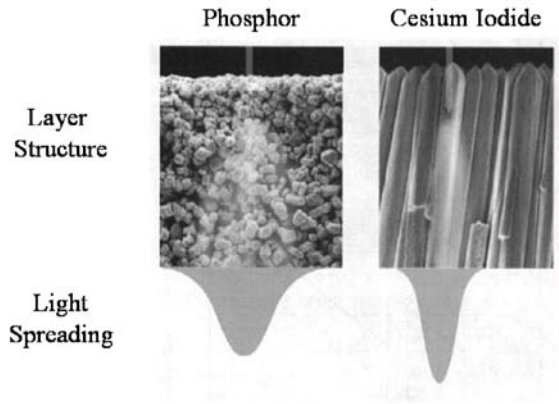


Figure 3 - Absorption efficiency of the primary scintillators used in FPDs. (Image courtesy of Thales Electron Devices.)

given dose. Furthermore, the thickness of the CsI can be greater than that of a rare earth screen because when CsI is deposited on the array it grows in a columnar structure. The columns tend to act as light pipes, reducing the amount of light spreading in the scintillator. So, for example, a 600µm CsI layer can have resolution similar to a 300µm thick rare earth screen. These screens such as gadolinium oxysulfide have the advantage of much lower cost and greater flexibility in that the screen can easily be changed to match the resolution requirements of the application.

The light generated by the scintillator is absorbed by the photodiodes in the array, creating electrons which are stored on the capacitance of the photodiode itself. The peak light absorption efficiency of the photodiodes is in the green spectrum, at 550nm wavelength. Both gadolinium oxysulfide and thallium doped cesium iodide, CsI(Tl), produce their peak light output at this frequency. The amorphous- silicon photodiodes are typically the "n-i-p" type. In other words, the layers in the photodiode consist of an electron-rich layer at the bottom, an intrinsic or undoped layer in the middle, and a hole-rich (positively charged) layer at the top. This type of amorphous-silicon photodiode has the advantages of low dark current and a capacitance that is independent of the accumulated signal. The thermally generated dark current intrinsic to the photodiodes is always working to charge the diode. If the photodiodes have large amounts of dark current, much of the diode's signal capacity will be filled up by charge with no signal information. Compared to crystalline silicon photodiodes like those used in CMOS imagers, the dark current in amorphous silicon photodiodes is orders of magnitude less. So it is not unusual for amorphous silicon flat panel arrays to be capable of more than ten second integration times at room temperature. The fact that the diode capacitance is independent of signal helps make the detection system linear.

Figure 4 - The relative light spreading of columnar CsI versus an amorphous phosphor screen. (Photograph courtesy of Hamamatsu Photonics.)



As is discussed later, the linearity of the detection system is critical to being able to efficiently correct for all the sources of non-uniformity in the array and the electronics.

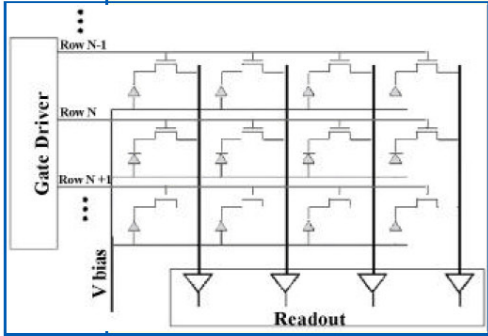
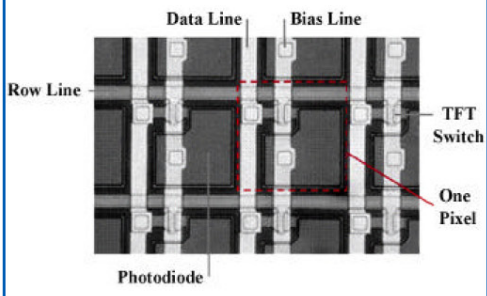


Figure 5 - TFT/Photodiode array schematic and view of a single 127µm pixel.

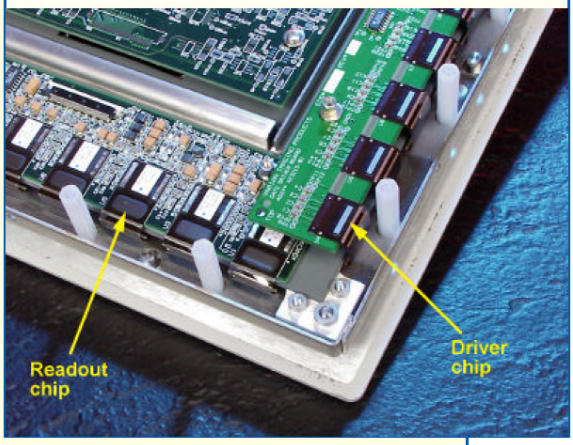


The TFT/photodiode matrix is normally scanned progressively, one line at a time from top to bottom. The TFTs are essentially switches. When a large positive voltage is applied to one of the gate lines, the switches (TFTs) in the selected row are closed, causing them to conduct electricity. With the TFTs energized, each pixel in the selected row discharges the stored signal electrons onto the dataline. At the end of each dataline is a charge integrating amplifier which converts the charge packet to a voltage. At this point the electronics vary by manufacturer, but generally there is a programmable gain stage and an Analog-to-Digital Converter (ADC), which converts the voltage to a digital number. One important aspect of the scanning is that the FPD is continuously collecting the entire incident signal; none is lost even during the discharge of the pixel. The FPD is an integrating detector and the integration time for each pixel is equal to the frame time.

The electronics can be mounted to the side of the array, out of the beam, as is done in higher energy (MeV) applications to protect against radiation damage. But for diagnostic and interventional procedures, to maintain the best view of the patient, the electronics can also be mounted behind the array and protected by a thin layer of lead. While amorphous silicon has properties sufficient for the detection electronics, it is not suited to the subsequent signal processing. For this reason, every column and row of the array is brought to the edge of the glass, where it is connected to a standard crystalline silicon chip by means of a TAB (tape automated bonding) package. The TAB package bridges the disparity between the connection

density on the glass and what a typical circuit board can handle. The glass side of the TAB package may have 128 channels at a 100µm pitch, while the board side connections of the package are on a pitch of 400µm with roughly forty or fewer connections. The chips that need to be directly connected to the array, the readout chip and the driver chip, are mounted in these TAB packages. Figure 6 shows a picture of the row driver and readout chips used in Varian Medical Systems' PaxScan® 4030A, 40x30cm (12"x16") angiography panel.

Figure 6 - Board-side view of TAB packaged row driver and custom ASIC readout chips.

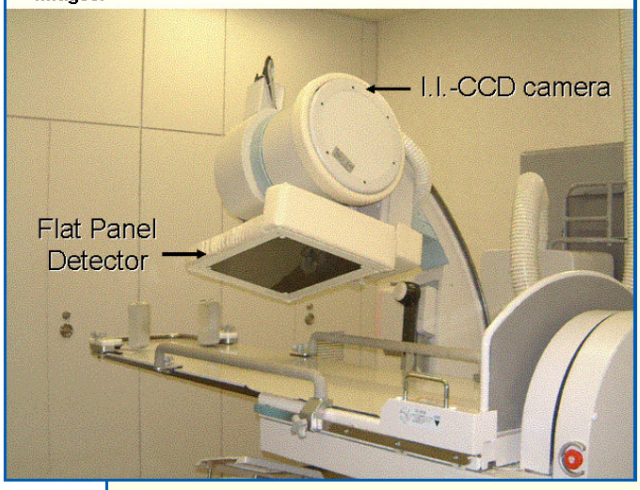


Flat Panel Operational Advantages

The most obvious advantages of flat panel imagers are size and weight. The Image Intensifiers Tubes (IIT) are large and bulky. An FPD with a 12"x16" active area (20" diagonal) takes up less than 25% of the volume of a 12" IIT and less than 15% of that of a 16" IIT. In addition, the FPD takes the place of not only the IIT, but also the attached image recording devices, including the CCD camera, 35mm Cine camera, and the spot film device. The result is vastly improved access to the patient in interventional procedures. In addition to the reduction in size, the weight of the flat panel imager is 60% less than that of the IIT-based imaging chain. Traditionally, the IIT side of the mechanical structure is the heaviest. With flat panels, the heavy side shifts to the X-ray tube, which offers the possibility of a reduction in the bulk and cost of the mechanical superstructure. Mounting a 16" IIT on a mobile C-arm is impractical because of its size and weight, but achieving an even larger active area with a flat panel imager on a mobile C-arm is now straightforward.

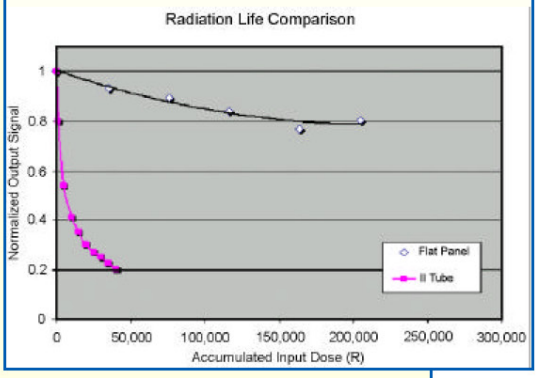
The fact that the recording devices attached to an IIT are not required with FPDs is a result of the multi-mode capability inherent in flat panel technology. From an electrical point of view, the array architecture and readout are very similar to those used for dynamic random access memory (DRAM). Accessing sections or regions-of-interest (ROIs) in the array is only a matter of addressing the proper columns and rows. As with DRAM, the signal is stored as a charge packet, which makes summing the data from more than one pixel a simple matter of combining the charge packets. Reading out a 2x2 neighborhood of pixels as one super-pixel is easily done by combining the signals from neighboring pixels at the front-end charge integrating amplifiers. Pixel binning offers two important opportunities for trade-offs. The first trade-off is sensitivity, since the super pixel will see more X-ray photons and so have higher signal-to-noise ratio (SNR). Very often the maximum digital data conversion rate of the panel is limited to a fixed value. Binning also can reduce the overall matrix size, thus allowing higher frame rates. For example, a 1024x1024 imager capable of 30fps can also be read out as 512x512 super pixels at 60fps or higher. The flat panel imager shown in Figure 7 typically has three modes: full field, full resolution at 7.5fps used for DSA and radiography; full field, half resolution at 30fps used for fluoroscopy and cine; and ¼ field of view, full resolution at 30fps which is used for fluoroscopic zoom mode. Since these modes are defined only by the method of

Figure 7 - This is experimental R&F equipment used by Hitachi in a clinical evaluation of flat panel technology. Here a 12"x16" (active area) FPD is mounted on the side of a 12" Image Intensifier Tube (IIT). With this system, either the FPD or IIT could be rotated into place, facilitating straightforward comparison images.



addressing the array, the panel can switch between modes in less than one second. Flat panels also are more economical than an IIT of comparable size considering that we know IIT image quality deteriorates as a simple consequence of everday X-ray use, and thus IIT's have a relatively short service life. Varian life tests have demonstrated that the service life of a typical flat panel is significantly longer than that of an IIT, assuming the same usage. In the most favorable cases, the flat panel will match the life expectancy of the equipment.

Figure 8 - Signal output comparison vs. X-ray dose between a PaxScan 4030A and an IIT of comparable size.



Flat Panel Image Quality

Beyond the improved form factor and flexibility of flat panels, there are also enhancements to the image quality. In IIT-based imaging there are many stages in the signal conversion chain, each of which is subject to losses and distortion. For example the electron optics inside the IIT is influenced by the earth's magnetic field. And the optics of the output phosphor is subject to veiling glare, which is a kind of a long-range crosstalk. The result is geometric distortion and brightness non-uniformity across the diameter of the image. In comparison, flat panels have a very direct, short signal conversion path, with essentially no optics.

Figure 9 - Comparison between a 12" IIT system and GE's 20cm Revolution flat panel detector. Clearly the image intensifier has both distortion and brightness non-uniformity which is absent from the flat panel detector. (Image courtesy of GE Medical Systems.)

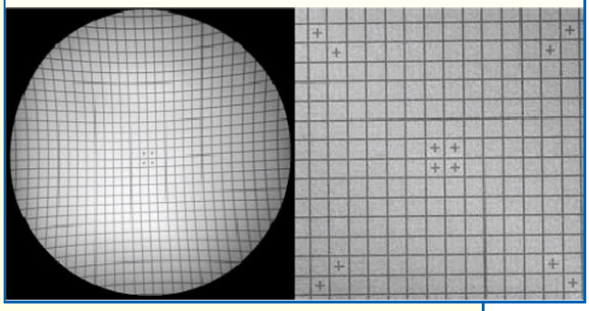
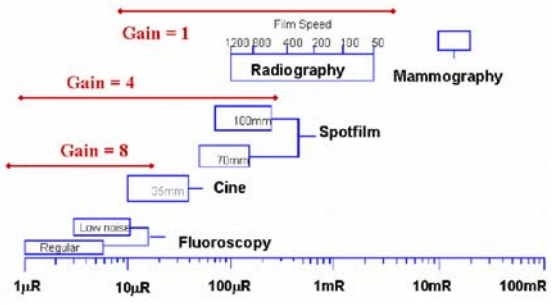


Figure 10 - Entrance dose per frame by application.



The result is a very flat, uniform "film-like" image from edge-to-edge. Similar to the distortion and brightness non-uniformity, the IIT/CCD image chain also suffers from contrast loss at the edges of the image, which is why the IIT performance is always specified at the center.

The ability of flat panel detectors to encompass multiple X-ray modalities is also a function of their very large dynamic range. Figure 10 shows the detector entrance dose per frame by application. An FPD designed for R&F applications can cover the entire range, from low-dose fluoroscopy to radiography. Generally, the Analog-to-Digital Converters (ADCs) inside the FPD have a fixed input range. In order to adapt the signal to that range, there is an analog gain stage prior to digitizing. Higher gain is used for smaller signals, but at the expense of the maximum dose per frame. Because of the very different resolution, energy and dose requirements, mammography requires a specialized flat panel detector. The large exposure latitude in flat panel imaging means that retakes, due to over and under exposure, are virtually eliminated. The large dynamic range also enables computed tomography applications, where the entrance dose per projection can vary from the low dose fluoroscopy level to the equivalent of radiography shots.

Figure 11 - Signal vs. entrance dose for a 194µm, 40x30 cm FPD.

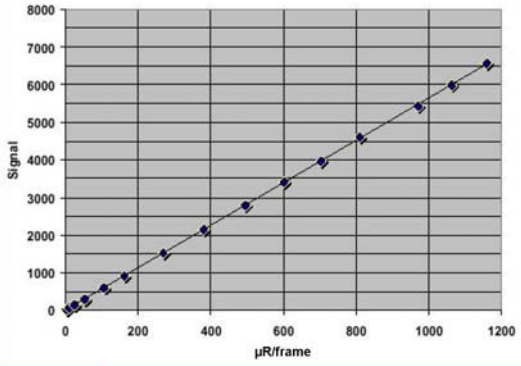


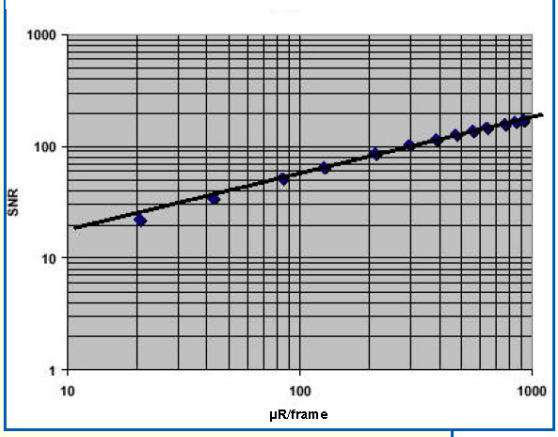
Figure 11 shows the signal response of an angiography flat panel in the full resolution mode,

over the dose range of 1μR to 1.2mR. Particularly for the amorphous silicon TFT/photodiode technology, the response to entrance dose of the FPD is extremely linear. The response of the imager deviates from the straight line curve by less than 0.01%. This degree of linearity is necessary to facilitate the real-timeoffset and gain correction that is normally performed for each pixel. Because each pixel in the array has its own gain value and zero signal level, the image would be very non-uniform without normalization. If the imager response is non-linear, the arithmetic for normalizing the pixel response in real-time becomes intractable.

Of equal importance is the Signal-to-Noise (SNR) behavior versus dose. The FPD contributes electronic noise to the image. However, if the electronic noise is low enough, the statistical noise in the X-ray beam is dominant. The noise in the beam follows Poisson statistics. In other words, the noise is equal to the square root of the number of incident X-ray photons.

As shown in Figure 12, the SNR of an FPD has a square root dependence on dose, i.e. is X-ray quantum limited over a very large range. This is an indication that the detector contributes effectively no noise to the image over this dose range.

Figure 12 - SNR vs. entrance dose for a 194μm, 40x30cm FPD.



A more accurate way to look at the sensitivity of an imaging system is to evaluate the Detective Quantum Efficiency (DQE) as a function of spatial frequency. Particularly for digital X-ray technologies, this single measure is a common reference point that accounts for noise, signal-loss mechanisms, sensitivity and resolution. Essentially the DQE is equal to the square of the ratio of the imager's output SNR to its input SNR.

$$DQE\left(\bar{q},u\right)=\frac{SNR_{out}{}^{2}}{SNR_{in}{}^{2}}$$

DQE is typically calculated using the formula:

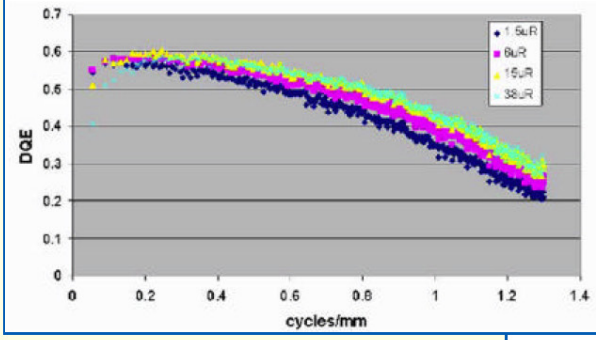
$$DQE\left(\bar{q},u\right)=\frac{\bar{d}^{2}*MTF^{2}\left(u\right)}{\bar{q}*NPS\left(\bar{q},u\right)}$$

where, for a given input dose, **d** is the average output signal produced, MTF is the modulation transfer function (a measure of resolution), **q** is the number of incident X-ray quanta and NPS is the noise power spectrum produced by the imager. Because the X-ray beam statistics are Poisson distributed, the input SNR 2 is in fact equal to the total number of X-ray photons, **q**. The rest of the equation defines the output SNR 2 as a function of signal, resolution and noise.

The DQE as a function of entrance dose (fluoro and cine range) for an angiographic flat panel imager is shown in Figure 13. This is typical of the indirect TFT/photodiode technology with a CsI scintillator. Because of the low-loss, high-absorption detection path, the DQE for indirect CsI-based flat panels is the highest available and is more than double that of computed radiography, film screen and CCD based technologies. Higher DQE translates directly into better imager quality for a given dose.

So with high DQE detection systems, it is possible to get the same image quality as a low DQE system like screen film at a fraction of the dose.

Figure 13 - DQE vs. spatial frequency over the fluoroscopic and cine dose range, for a 40x30cm angiographic flat panel.



Digital X-ray Radiography

The numerous advantages of flat panel detectors over X-ray film, computed radiography image plates, and image-intensifier tubes is clear. This is evident to the thousands of leading radiologists and cardiologists performing routine X-ray examinations, test engineers inspecting for cracks in aircraft structures, and security forces screening for and disarming explosives. Digital X-ray imaging available instantly just like that of modern digital cameras and camrecorders is the future. Please contact your local Varian sales office for the latest on our PaxScan family of flat panel X-ray detectors.

X-Ray Products

Headquartered in Salt Lake City our flat panel team is committed to meeting the diverse and growing needs of Digital Radiography in many markets: Medical, industrial/NDT, security, and scientific. World renown for our X-ray tubes, flat panel X-ray detectors are an important addition to our growing X-Ray business.



MISSION STATEMENT

To be the unquestioned worldwide leader in X-ray products by achieving superior product quality and customer satisfaction.

Ginzton Technology Center

The Ginzton Technology Center acts as Varian Medical Systems' research and development facility for breakthrough technologies and operates a brachytherapy business for the delivery of internal radiation to treat cancer. In addition to brachytherapy, current efforts are focused on emerging flat panel technologies. This business also conducts externally funded research related to medical technology, which leads to long-term partnerships and new business opportunities.

U.S. SALES OFFICES

X-Ray Products
1678 S. Pioneer Road
Salt Lake City, UT 84104
Tel: (801) 972-5000
Fax: (801) 973-5050

Customer Service
Tel: (800) 432-4422
Fax: (801) 973-5050

X-Ray Marketing & Product Support
Tel: (801) 973-5073
Fax: (801) 973-5023

X-Ray Products - Interay
3235 Fortune Drive
North Charleston, SC 29418
Tel: (843) 767-3005
Fax: (843) 760-0079
e-mail: interay.sales@varian.com

Customer Service
Tel: (800) 468-3729
Fax: (843) 760-0079

Technical Support
Tel: (843) 767-3005
Fax: (843) 760-0079

INTERNATIONAL SALES OFFICES

X-Ray Products
Kokermolen 2
3994 DH Houten, Netherlands
Tel: +(31) 30 635 11 05
Fax: +(31) 30 635 04 46
e-mail: xray.eu@varian.com

X-Ray Products
Varian Medical Systems GmbH
Karl-Arnold-Straße 12
D-47877 Willich, Germany
Tel: +(49) 2154-92 49 80
Fax: +(49) 2154-92 49 94
e-mail: sales-xray@varian.com

X-Ray Products
4F MY ARK Nihonbashi Bldg.
10-16 Tomizawa-cho
Nihonbashi,Chuo-ku
Tokyo 103-0006, Japan
Tel: +(81) 03 5652 4711
+(81) 03 5652 4712
Fax: +(81) 03 5652 4713

X-Ray Products
Corsa Susa, 299B
10098 Rivoli (Torino), Italy
Tel: +(39) 011 955 03 96
Fax: +(39) 011 953 62 59

X-Ray Products
P.O. Box 38
1714 Heitenried - Switzerland
Tel: +(41) 26-495 32 58
Fax: +(41) 26-495 32 59

X-Ray Products
B3-1801, Sunshine Plaza
68 Anli Road, Chaoyang District
Beijing 100101, P.R.China
Tel. +86-10-6496-1585
Fax.+86-10-6494-0743

www.varian.com

11/11/04

APPENDIX E – ADDITIONAL MATERIAL FOR CHAPTER 7

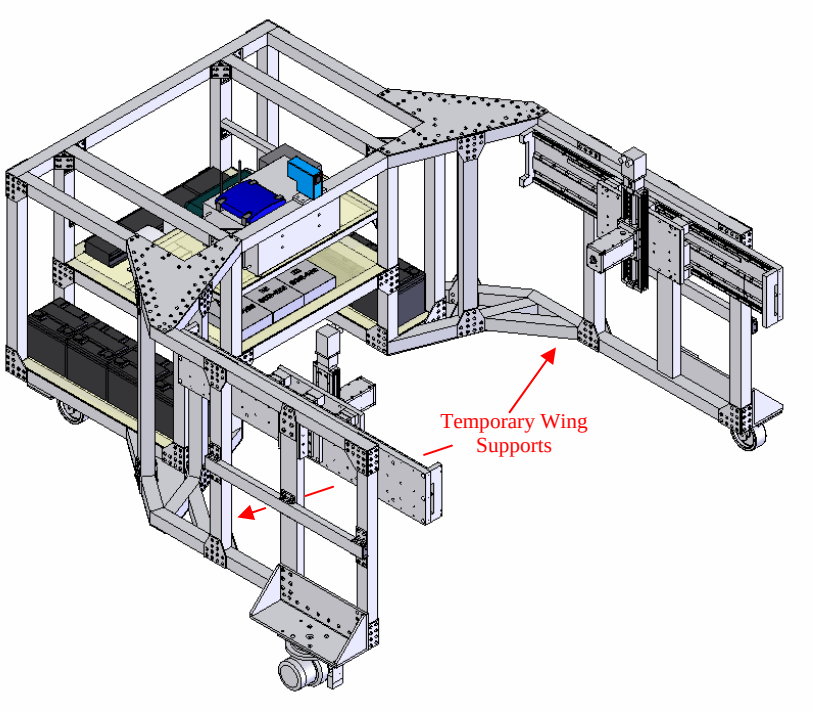


Figure E.1 Temporary wing support for hip configuration

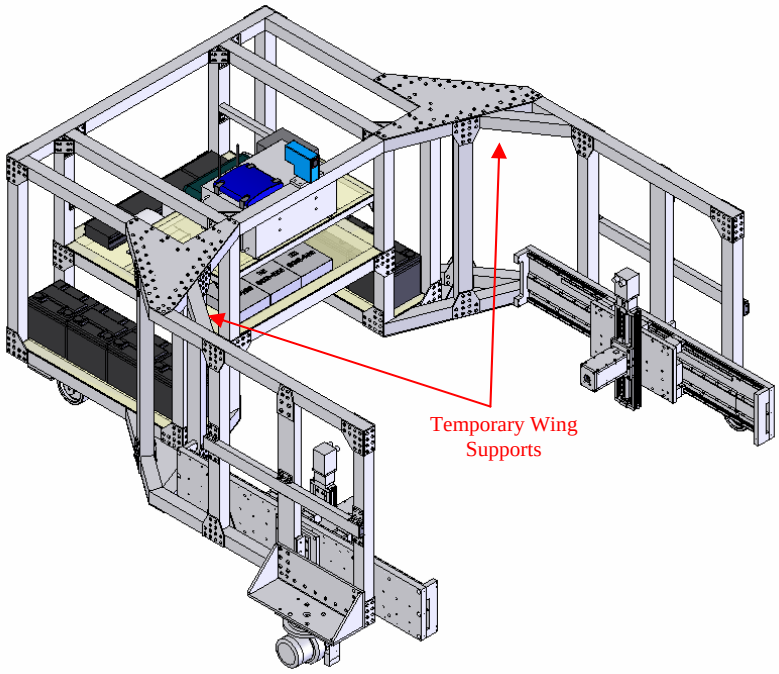


Figure E.2 Temporary wing support for ankle configuration

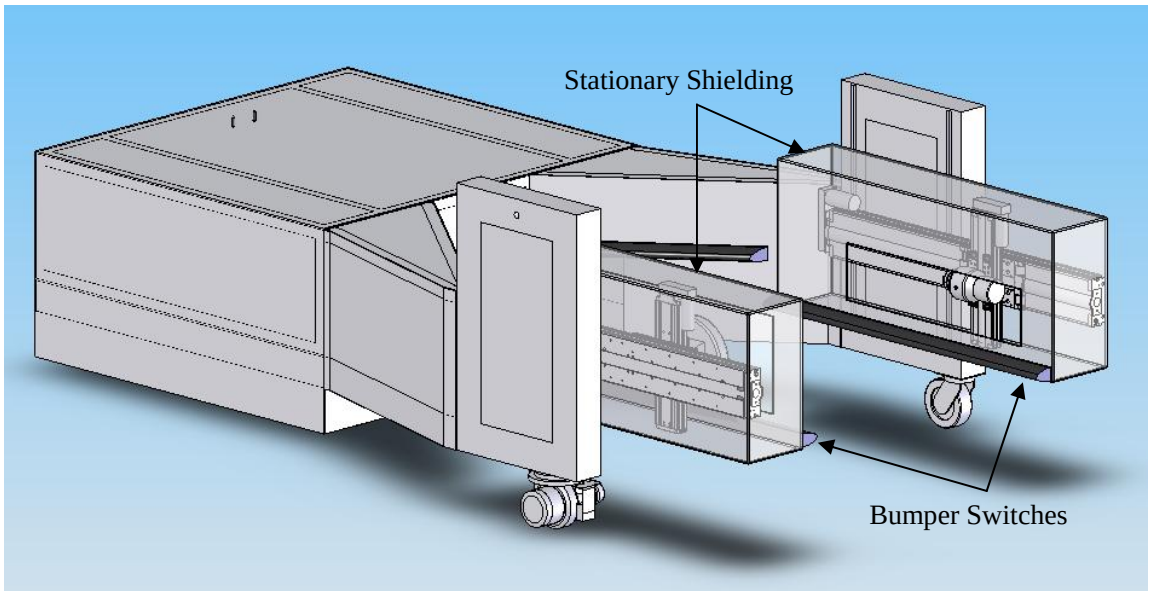


Figure E.3 Preliminary conceptual design with stationary lead shielding

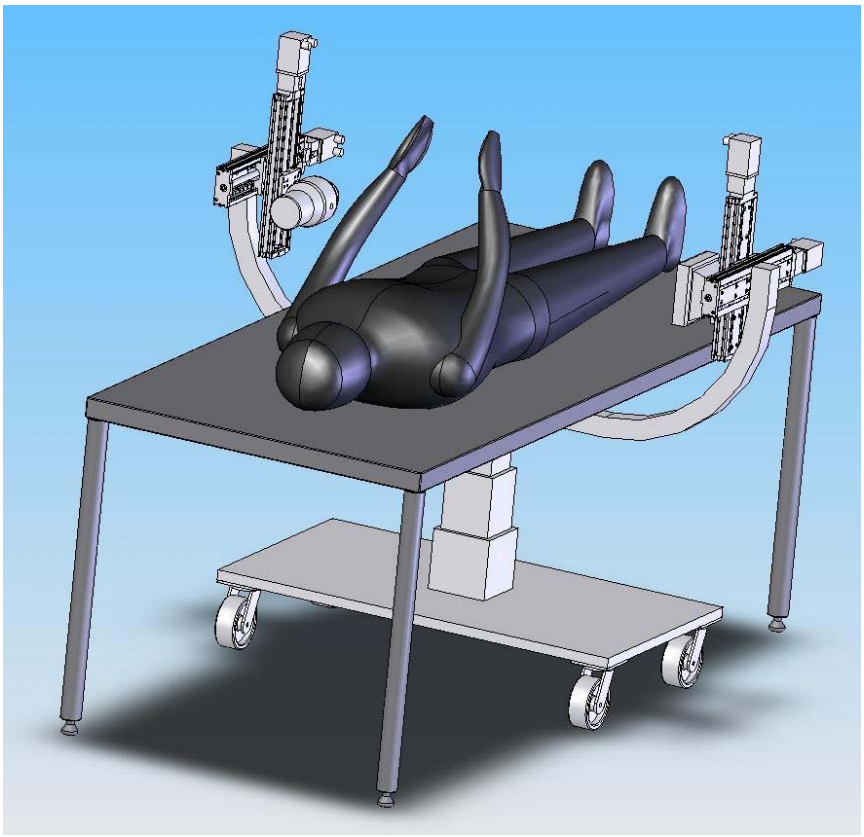


Figure E.4 TFS conceptual design for an operating table

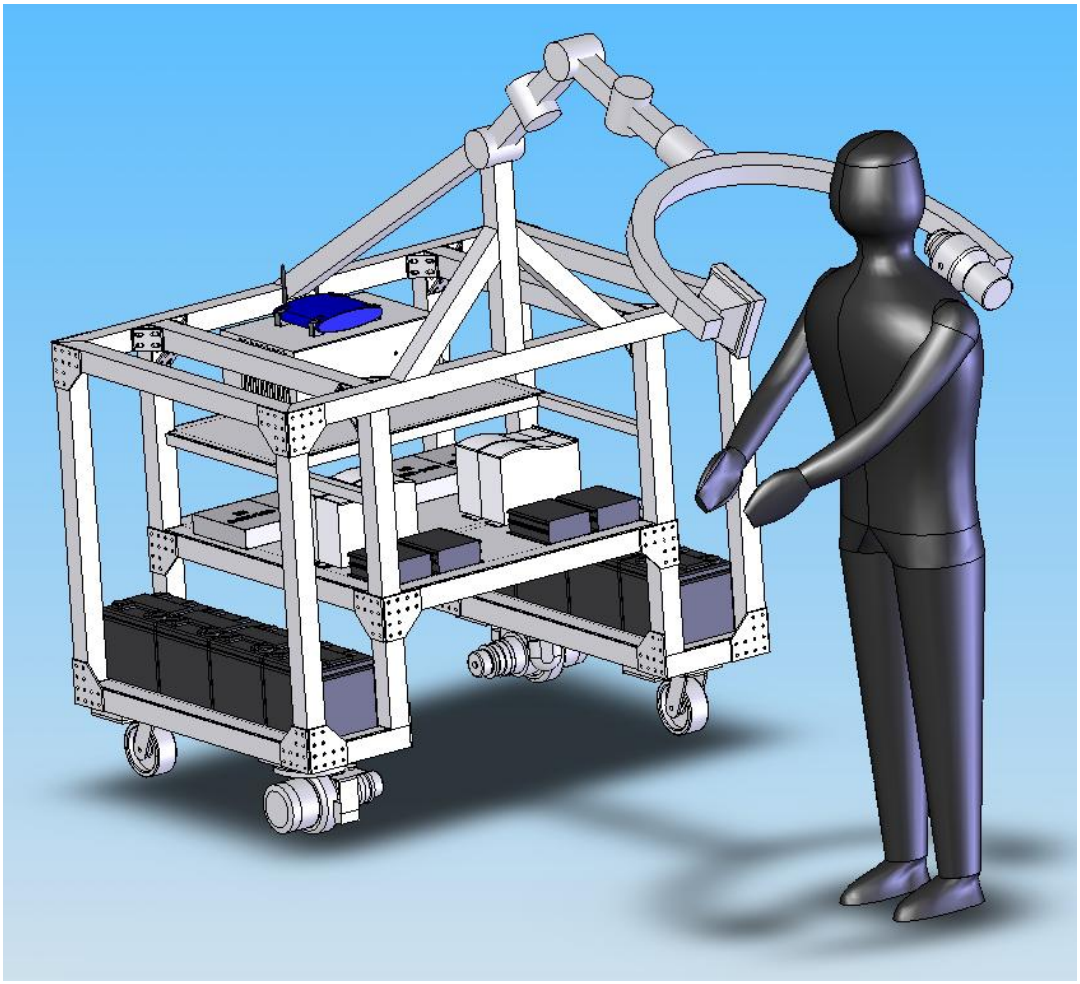


Figure E.5 TFS conceptual design for shoulder analysis

VITA

Robert Bradley Cunningham was born in Dallas, Texas and lived in the area through high school. He then attended Georgia Institute of Technology in Atlanta, Georgia from 1998-2003. While at Georgia Tech, he participated in a co-op program with Kimberly-Clark Corporation for four semesters and among other responsibilities, he designed inspection systems for medical products. His experience at Kimberly-Clark helped to develop a strong desire to work in the medical field. He graduated with high honors in August 2003 with a Bachelor of Science in Mechanical Engineering. In December of 2003 he was offered the perfect research opportunity combining Mechanical Engineering with cutting-edge medical research. He is currently finishing his requirements for a Master of Science degree in Mechanical Engineering at The University of Tennessee.